AD 739975

AFOSR - TR - 72 - 0608

6 MAR 1972

University of California, San Diego

Institute of Geophysics and Planetary Physics

FINAL REPORT
Contract F-44620-71-C-0128

sponsored by

Advanced Research Projects Agency
Air Force Office of Scientific Research
United States Air Force
Washington, D.C.

BROAD BAND ACCELEROMETERS AND THEIR DEPLOYMENT FOR SEISMIC STUDIES

ARPA Order No.	1618
Program Code No.	1F10
Contract Starting Date:	15 April 1971
Contract Expiration Date:	14 Nov. 1971
Amount of Contract	$121,592
Principal Investigator:	Barry Block
	453-2000, Ext. 1735

Reproduced by
NATIONAL TECHNICAL
INFORMATION SERVICE
Springfield, Va. 22151

D D C
APR 4 1972
C

February 22, 1972
La Jolla, California 92037

APPROVED FOR PUBLIC RELEASE: DISTRIBUTION UNLIMITED

DISCLAIMER NOTICE

THIS DOCUMENT IS THE BEST QUALITY AVAILABLE.

COPY FURNISHED CONTAINED A SIGNIFICANT NUMBER OF PAGES WHICH DO NOT REPRODUCE LEGIBLY.

UNCLASSIFIED

Security Classification

DOCUMENT CONTROL DATA - R & D

(Security classification of title, body of abstract and indexing annotation must be entered when the overall report is classified)

ORIGINATING ACTIVITY (Corporate author) University of California, San Diego La Jolla, CA 92037	2a. REPORT SECURITY CLASSIFICATION UNCLASSIFIED 2b. GROUP

3. REPORT TITLE

Broad Band Accelerometers and Their Deployment for Seismic Studies

4. DESCRIPTIVE NOTES (Type of report and inclusive dates)

Scientific.....Final

5. AUTHOR(S) (First name, middle initial, last name)

Dr. Barry Block

6. REPORT DATE 22 February 1972	7a. TOTAL NO. OF PAGES 23	7b. NO. OF REFS 3
8a. CONTRACT OR GRANT NO F44620-71-C-0128 b. PROJECT NO. AO 1618 c. 62701D d.	9a. ORIGINATOR'S REPORT NUMBER(S) 9b. OTHER REPORT NO(S) (Any other numbers that may be assigned this report) AFOSR - TR - 72 - 0603	

10. DISTRIBUTION STATEMENT

Approved for public release; distribution unlimited.

11. SUPPLEMENTARY NOTES TECH, OTHER	12. SPONSORING MILITARY ACTIVITY AF Office of Scientific Research/NPG 1400 Wilson Boulevard Arlington, VA 22209

13. ABSTRACT

The vertical accelerometers were used to make a six month (January to July 1971) data collection run which is being used to determine detection thresholds and azimuthal dependences. This run was made at a surface site at Camp Elliott, San Diego. The horizontal accelerometers were completed and placed in operation and data gathered simultaneously with the vertical accelerometers for several months at a surface site at Camp Elliott, San Diego. Both a vertical and horizontal were used in a mine test at 5300 and 6700 feet. The results showed that the major improvement came in the horizontal data which showed no diurnal effect as is seen in the surface data. The absolute values of the horizontal mine data taken at 5300 feet both for day and night in the seismic band (45 second period and shorter) were as good as the quiet night surface values at San Diego. There was not much difference in the vertical data taken at depth and at the surface.

DD FORM 1 NOV 65 1473

UNCLASSIFIED.

SUMMARY

The principal results of this contract are the following:

1. The vertical accelerometers were used to make a six month (January to July, 1971) data collection run which is being used to determine detection thresholds and asimuthal dependences. This run was made at a surface site at Camp Elliott, San Diego.

2. The horizontal accelerometers were completed and placed in operation and data gathered simultaneously with the vertical accelerometers for several months at a surface site at Camp Elliott, San Diego.

3. Both a vertical and horizontal were used in a mine test at 5300 and 6700 feet. The results showed that the major improvement came in the horizontal data which showed no diurnal effect as is seen in the surface data. The absolute values of the horizontal mine data taken at 5300 feet both for day and night in the seismic band (45 second period and shorter) were as good as the quiet night surface values at San Diego. There was not much difference in the vertical data taken at depth and at the surface.

Introduction

The Final report on ARPA Contract IGPP/AF/F-44620-71-C-0128 is divided into four sections. The first two will deal primarily with data taken at the Star Mine at Wallace, Idaho and at Camp Elliott, San Diego, California. The last two sections deal primarily with instrumental improvements in the vertical accelerometer and a first description of the horizontal accelerometer. These last two sections have been submitted for publication.

Section I. Operation of Vertical and Horizontal Accelerometers at Great Depth.

Section II. Teleseismic Signals Between and Below the Microseism Peaks. Bartholomew, B., Block, B. and Dratler, J., Jr.

Section III. Improvements in the Wide Band Vertical Quartz Accelerometer. Block, B. and Dratler, J., Jr.

Section IV. A Wide Band Horizontal Accelerometer with Preliminary Earth Normal Mode and Seismic Investigations. Dratler, J., Jr., and Block, B. (In press, Geophys. Jour. Roy. Astro. Soc.)

Section I. Operation of vertical and horizontal accelerometers at great depth.

Data was obtained in the Star Mine, Wallace, Idaho at depths of 5300 and 6700 feet for both vertical and horizontal broad band quartz torsional accelerometers. The experimental set-up will be described for the station at 5300 feet as it was typical.

The Star Mine is a zinc, lead and silver producing mine. The matrix rock is quartzite. The location of the seismic observatory was chosen to be as far as possible from the active excavation sites (unfortunately only a few hundred feet) and to be located in a tunnel which was not used in the mine ventilation system. The tunnel was closed off by means of metal doors at either end. At 5300 feet the temperature in the tunnel was 95° F with 100% humidity present. The tunnel showed relatively little rock damage compared to other possible sites investigated but every day in the 1000 feet from the shaft elevator to the instruments several small rockfalls were found. This mine has a history of rock bursts. In some locations the rock damage was so extensive that the walls had caved in two feet in a height of 10 feet even when held back by steel sheets and rock pins. The acceleration sensors were housed in a timber shack built in a bedbug. The shack was covered with burlap backed by polyethylene film. No temperature control was applied in the shack. The shack was used merely to keep drafts off the instrument and to protect against rockfalls.

A pier was installed by chipping away the shattered base rock and using a thinlayer of grout to lay a granite slab. A 100 feet of cable was installed to another bedbug where a similar shack was built to house the electronics and data logging equipment. This shack was cooled by an air conditioner and a dehumidifier operated continuously. This cooling and dehumidification was found necessary to keep the electronics and the data logger operating. A few words about the data logging system are in order. This is a twenty channel, 9 track 800 BPI system made by Monitor Laboratories, San Diego. The system operated successfully except for a power supply failure probably induced by the shack cooling system failing. Continued operation occurred after the mechanically traumatic move into the mine site at 6700 and 5300 feet. The tape deck stayed within specifications at all times and the digital electronics operated successfully. Loss of components occurred in the accelerometer electronics when the shack cooling and dehumidifying system failed. As soon as these systems were re-established giving a temperature of 80° F and a humidity level somewhat less than 100° the electronics problems ceased.

Both digital and analog records were taken over several weekends in the tidal, earth normal mode and seismic filter channels These channels are described in detail in Section III and IV. The sampling rate was once a second with a digitizer dynamic range of 10^4 in each filter channel.

Data in this mine can be taken only over the weekend from Saturday morning to Sunday night because the mine is on continuous three-shift operation throughout the remainder of the week. The data for the 5300 foot station will be discussed below. The data from the 6700 foot station was much noisier than that

obtained at 5300 feet. This is attributed to the massive rock damage and consequent motion at this depth in the mine. The walls were literally caving in at 6700 feet. This field operation could not have been carried out without the complete cooperation of personnel at the Star Mine site and the management of the Hecla Mining Company.

Figure 1 shows typical horizontal data obtained from the 5300 foot level of the Star Mine taken on a weekend. The seismic filter response functions of both a horizontal and vertical accelerometer are found in Sections (II-IV). For comparison, typical data taken at a surface site at Camp Elliott, San Diego are also given in Fig. 1. In essence, what Fig. 1 shows is that the vertical absolute noise at both sites is about the same through this seismic filter. The horizontal noise at Camp Elliott varies significantly from day to night. The daytime noise level is almost always being much larger than the nighttime noise level. However, the horizontal noise at the 5300 foot level does not show this diurnal change but remains appreciably constant throughout a weekend. The absolute noise level at 5300 is about the same size as an average day at Camp Elliott. But what happens at seismic frequencies (i.e., defined as a high pass filter with 6 db point at 45 seconds) is seen to be that the seismic horizontal noise level at 5300 feet is always about the amplitude of the best nighttime seismic horizontal noise level at Camp Elliott. For the daytime data, the 5300 foot horizontal noise level is considerably smaller than the daytime Camp Elliott data. (See Fig. 1 Caption) Two typical earthquakes taken at 5300 feet are shown in Fig. 2 for the vertical accelerometer along with their high pass filtered data. Information on these earthquakes is contained in the caption of Fig. 2. This data was hand digitized

from analog records when the data logger was down. It can be done to some extent but one experience convinces the author that this way of proceding is hard, costly and loses much dynamic range.

Figure 1 Caption

Data from the horizontal instrument showing day and night variations at the Camp Elliott Station (ground level) and the absence of such variations at Wallace, Idaho (5300 feet below the surface). The data are also shown after being convoluted with a hipass filter that cuts at 45 sec.

a) Raw data from Wallace: S.T. 13:29:10 local time.

b) Ras data from Elliott: S.T. 12:04:08 Local time.

c) Filtered data from Wallace: S.T. 13:29:10 local time.

d) Filtered data from Elliot: S.T. 12:04:08 local time.

e) Filtered data from Elliott: S.T. 00:04:08 local time.

f) Filtered data from Wallace: S.T. 01:29:10 local time.

g) Raw data from Elliott: S.T. 00:04:08 local time.

h) Raw data from Wallace: S.T. 01:29:10 local time.

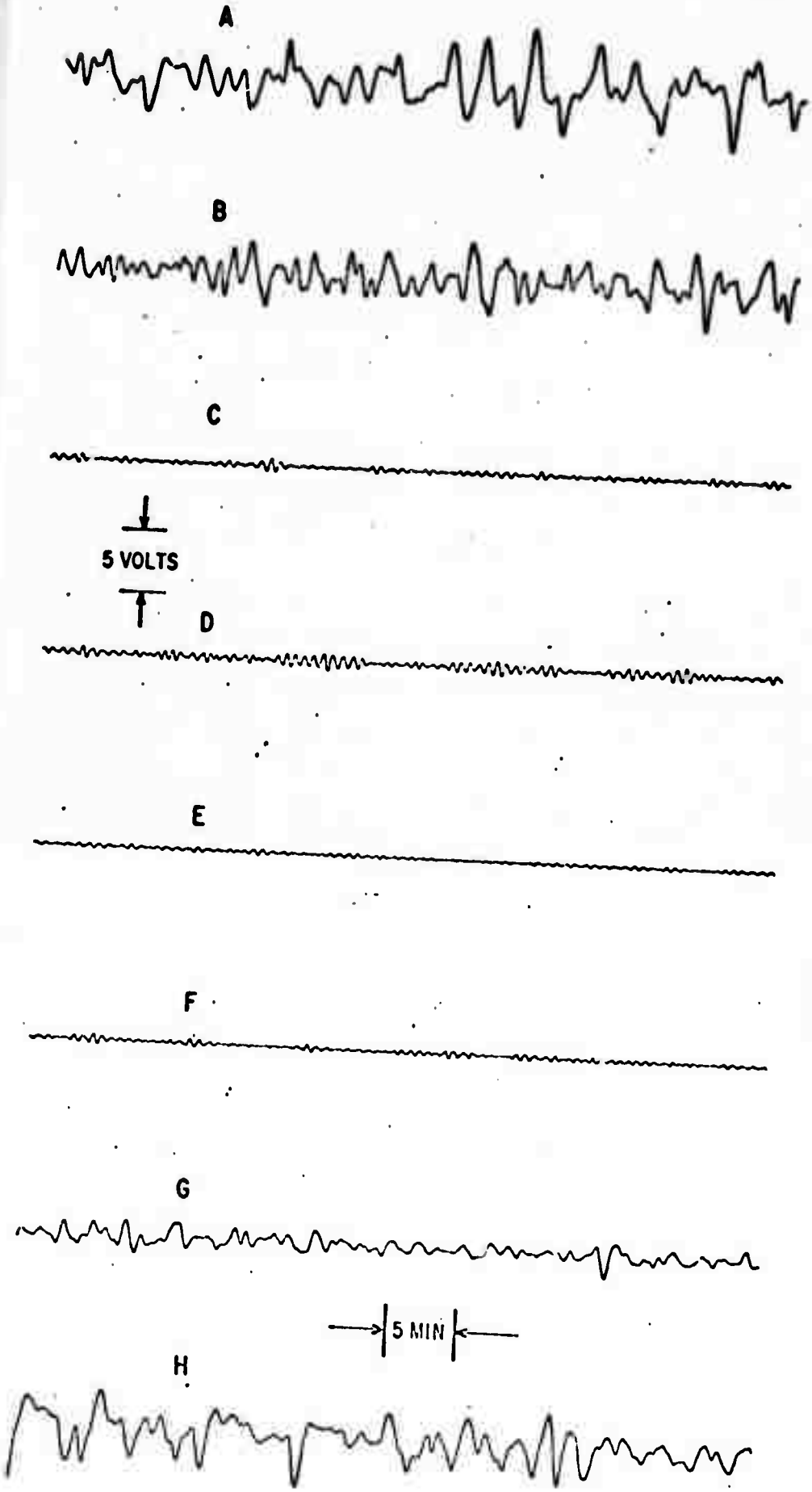

Figure 1

Reproduced from best available copy.

Data from the horizontal instrument showing day and night v
at the Camp Elliott Station (ground level) and the ambient
variations at Wallace, Idaho (5300 feet below the surface).
are also shown after being convoluted with a hipass filter
at 45 sec.

a) Raw data from Wallace: S.T. 13:09:10 local time.
b) Raw data from Elliott: S.T. 12:04:05 Local time.
c) Filtered data from Wallace: S.T. 13:23:10 local ti
d) Filtered data from Elliot: S.T. 12:04.03 local tim
e) Filtered data from Elliott: S.T. 00:04.03 local ti
f) Filtered data from Wallace: S.T. 01:23:10 local ti
g) Raw data from Elliott: S.T. 00:04:03 local time.
h) Raw data from Wallace: S.T. 01:23:10 local time.

Figure 2 Caption

Two earthquakes seen through the vertical seismic filter recorded on a stripchart at the 5300 foot level of the star mine are shown in A and C. The result of hand digitizing this data and subsequent high pass digital filtering (6 db point at 45 seconds) is seen in B. and D.

Event	Location	Origin Time (GMT)	Magnitude (M_B)	Distance
A	North Atlantic Ridge	17.05 9/4/71	4.6	66°
C	5.3°S, 153.0E New Ireland	04:35:35 9/5/71	4.5	95°

Figure 2

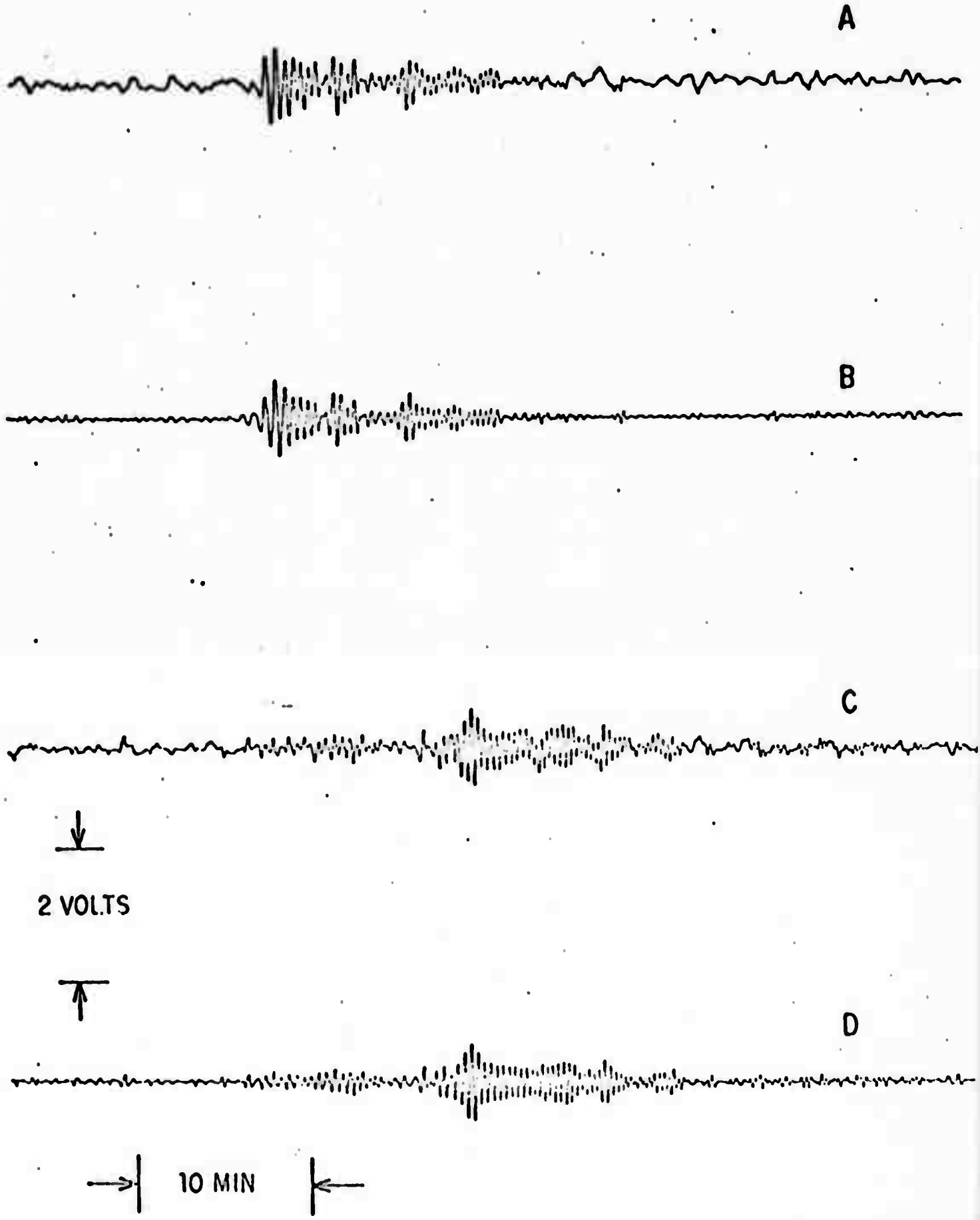

Section II.

TELESEISMIC DETECTION BETWEEN AND BELOW THE MICROSEISM PEAKS

Teleseismic signals and background noise will be examined in the frequency band .02 - .1 Hz (10-50 seconds) extending from the noise valley near 25 seconds to the noise minimum or crevice between the microseism peaks. Power spectra and digital band pass filtering of the background noise and two small events will be given by way of illustration.

The data from the broad band sensor (the Block-Moore quartz fibre accelerometer,[1,2,3] Camp Elliott, San Diego) are passed through an active seismic prefilter (the total transfer function of the system is shown in Fig. 1) and digitally recorded on magnetic tape, yielding a dynamic range of 10^4 with the seismic prefilter bandwidth. Other means of recording the data can cause a severe degradation of either dynamic range, band width, or both, leading to impaired detection capability. For instance, analogue recording (e.g. photographic) of seismic data using a notch filter to reduce the visual contribution of the large 6 second microseisms can degrade the dynamic range by a factor of 100 from this recording method alone. The effect of the wings of the notch filter in lowering the signal level below the recorder threshold will further degrade the data. The usefulness of the data between the microseism peaks, where both explosions and earthquakes possess high signal levels, is thus severely limited. Subsequent digitizing of such data cannot recover this loss in dynamic range and bandwidth.

The event in Figs. 2 and 3 was recorded simultaneously by a vertical and horizontal instrument in the surface vault at Camp Elliott. The data shown in Figs. 2 and 3, seen through the response function of Fig. 1, are

from an event near Oaxaca, Mexicc (N 15.1°, W 96.3°) of magnitude M_b = 4.7 on June 6, 1971 02:10:26.9 GMT at a depth of 33 km. The angular distance Δ from the sensor was 25.9°. The angle α between the great circle path connecting the epicenter with Camp Elliott and the axis of maximum sensitivity of the horizontal instrument was 83°.

In these figures the raw data, denoted by A, can be compared with the narrow band passed signals at 10 seconds (.05 Hz filter width), 15, 20, and 30 seconds (.01 Hz filter width), denoted by B, C, D, and E respectively. The power spectra of the event (dotted line) and background noise (solid line), computed from 20 minute intervals during and just before the earthquake, are shown in Figs. 4, 5. On this day, the 18 second microseism peak for vertical acceleration is low and the noise level in the crevice approaches the level of the noise valley between 20 - 50 seconds, presuming the least count noise of the digitizer is below the background level, a condition easily met with modern digitizers. The horizontal data (on Fig. 5) show a similar maximum in the signal to noise ratio near 15 seconds, but the signal degrades rapidly until there is no discernable signal at 30 seconds.

The noise crevice may vary in amplitude by a factor of 3 above the level shown in Fig. 4, although for a majority of the time it is clearly discernable, and the best place to take narrow band data.

The raw data from the vertical accelerometer for a second small earthquake near Oaxaca, Mexico (N 15.2°, W 94.6°) of magnitude

M_b = 5.2 on February 20, 1971 12:25:01.7 GMT appears in Fig. 6. The earthquake was 71 km. deep, the angular distance to the sensor $\Delta = 27.0°$ and $\alpha = 80°$. The power spectra for this event (Fig. 7) show that the crevice noise level is about 7 db above the crevice level in the previous example, but the signal to noise ratio between 12 - 15 seconds is still good.

The advantages of digital collection and processing of data compared to the irreversible losses inherent in analogue collection of data, even with subsequent digitization, can make the difference between detecting and missing an event.

Figure 1. The power spectra of the response functions for the vertical and horizontal accelerometers through the active seismic prefilter. The response functions in $(\text{Volts/Micron})^2$ are plotted in db (o db = 1(Volt/Micron) as a function of the period in seconds. The microns refer to microns of ground motion.

Figure 2. Data from the vertical instrument for the event on June 6, 1971. The raw digitized output from the accelerometer and active seismic prefilter is denoted by A. The narrow band filtered outputs at 10, 15, 20, and 30 seconds are denoted by B, C, D, and E respectively. The filter width is .05 Hz at 10 seconds and .01 Hz at 15, 20, and 30 seconds. The start time for all series is 02:14:49 GMT June 6, 1971.

Figure 3. Data from the horizontal instrument for the event on June 6, 1971. The raw digitized output from the accelerometer and active seismic prefilter is denoted by A. The narrow band filtered outputs at 10. 15, 20, and 30 seconds are denoted by B, C, D, and E respectively. The filter width is .05 Hz at 10 seconds and .01 Hz at 15, 20, and 30 seconds. The start time for all series is 02:14:49 GMT June 6, 1971.

Figure 4. Power spectra of the raw vertical data from Fig. 2 for the earthquake on June 6, 1971. The vertical scale is in db (o db = 1 $\text{micron}^2/\text{Hz}$) The microns refer to microns of ground motion. The dotted line was computed from a 20 minute interval during the earthquake, and the solid line is from a 20 minute interval just before the event.

Figure 5. Power spectra of the raw horizontal data from Fig. 3 for the earthquake on June 6, 1971. The vertical scale is in db (o db = 1 micron^2/Hz) The microns refer to microns of ground motion. The dotted line was computed from a 20 minute interval during the earthquake, and the solid line is from a 20 minute interval just before the event.

Figure 6. Output from the vertical accelerometer on February 20, 1971 showing the event near Oaxaca, Mexico, and the section of noise used to calculate the background noise power spectrum.

Figure 7. Power spectra for the raw vertical data from Figure 6 for the earthquake on February 20, 1971. The vertical scale is in db (o db = 1 micron^2/Hz). The dotted line was computed from a 30 minute interval during the earthquake, and the solid line is from a 30 minute interval just before the event.

REFERENCES

1) Block, B. and J. Dratler, Jr. Improvements in the Wide Band Vertical Torsion Accelerometer.

2) Block, B. and J. Dratler, Jr. Teleseismic Detection with Wide Band Vertical and Horizontal Accelerometers, Nature Phys. Sci., 232, No. 28, 33-37, July 12, 1971.

3) Dratler, J., Jr. and B. Block. A Wide Band Horizontal Accelerometer with Preliminary Earth Normal Mode and Seismic Investigations, in print. Geophys. Jour. Roy. Astron. Soc.

This work was supported under ARPA Contract AF/F-44620-71-C-0128.

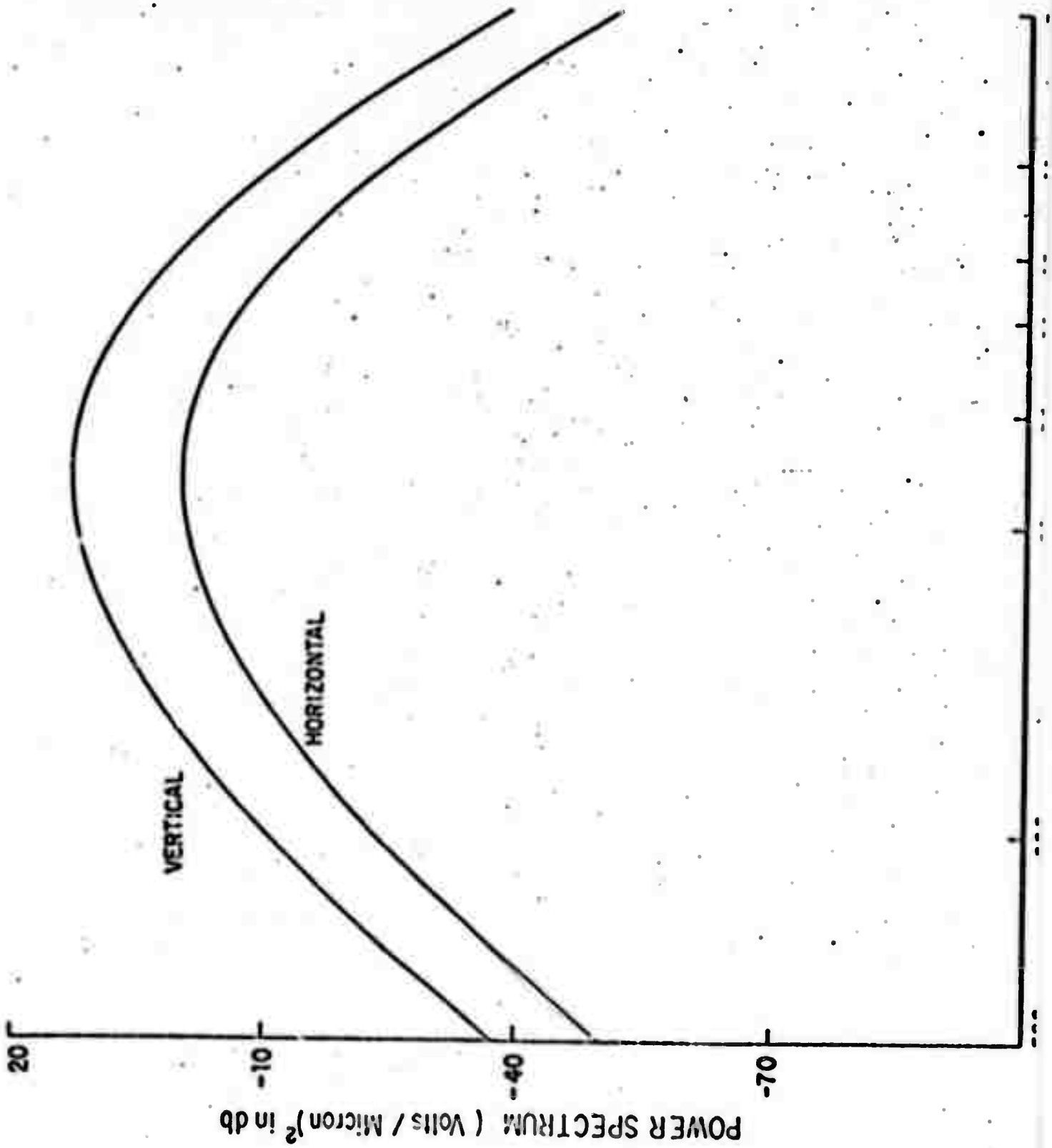
VERTICAL
HORIZONTAL
20
-10
-40
-70
POWER SPECTRUM (Volts / Micron)^2 in db

Figure 1

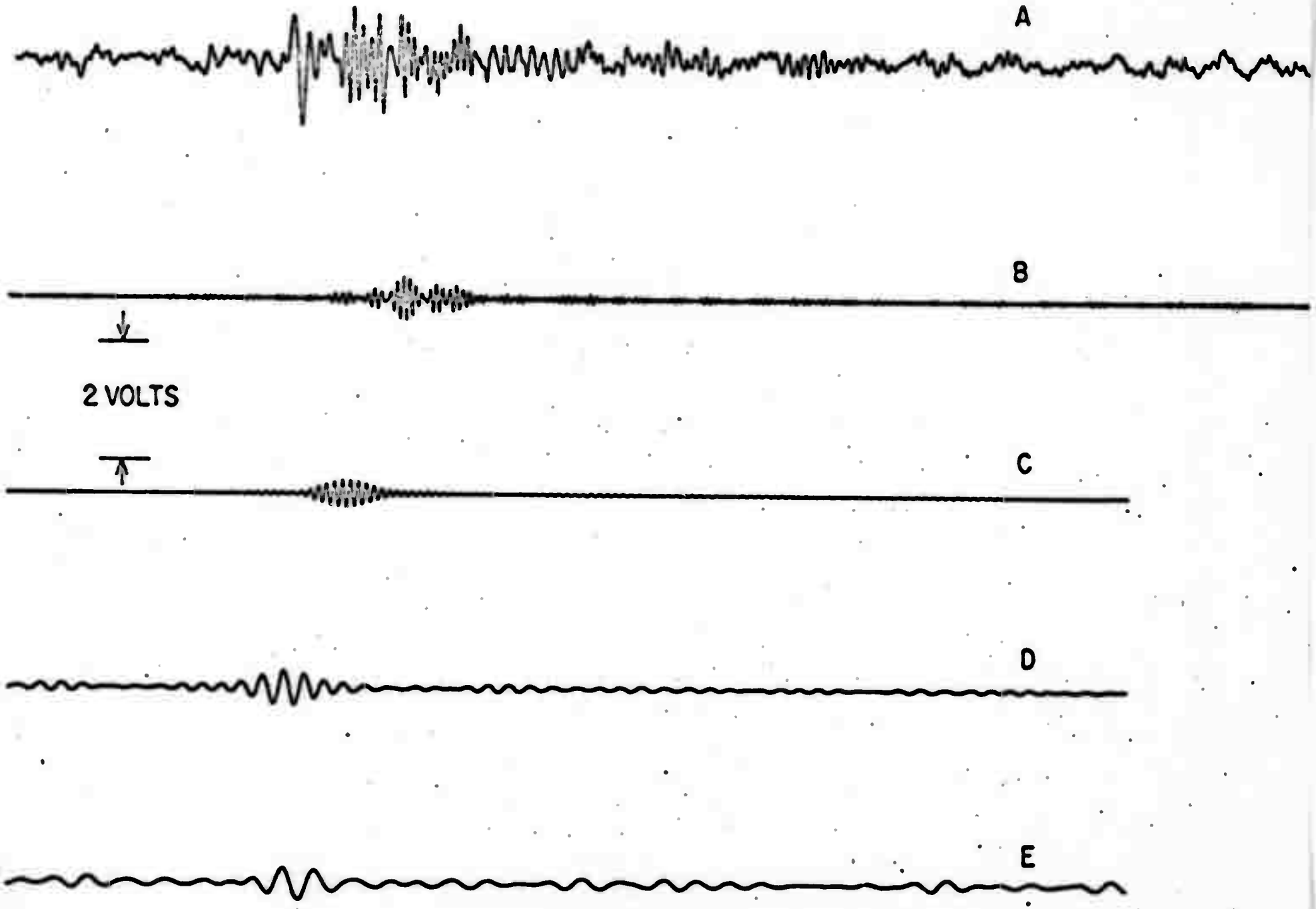

Figure 2

19

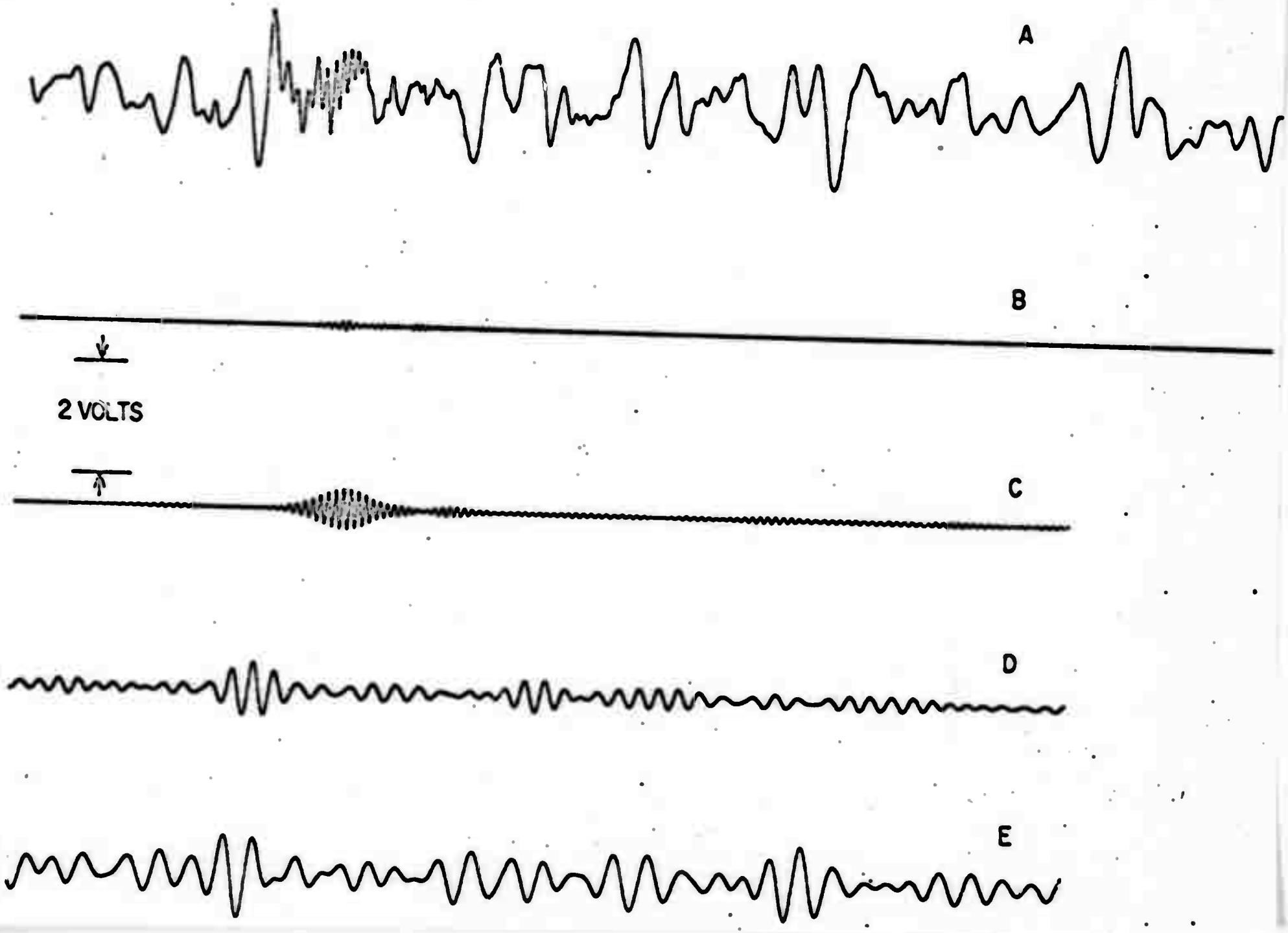

Figure 3

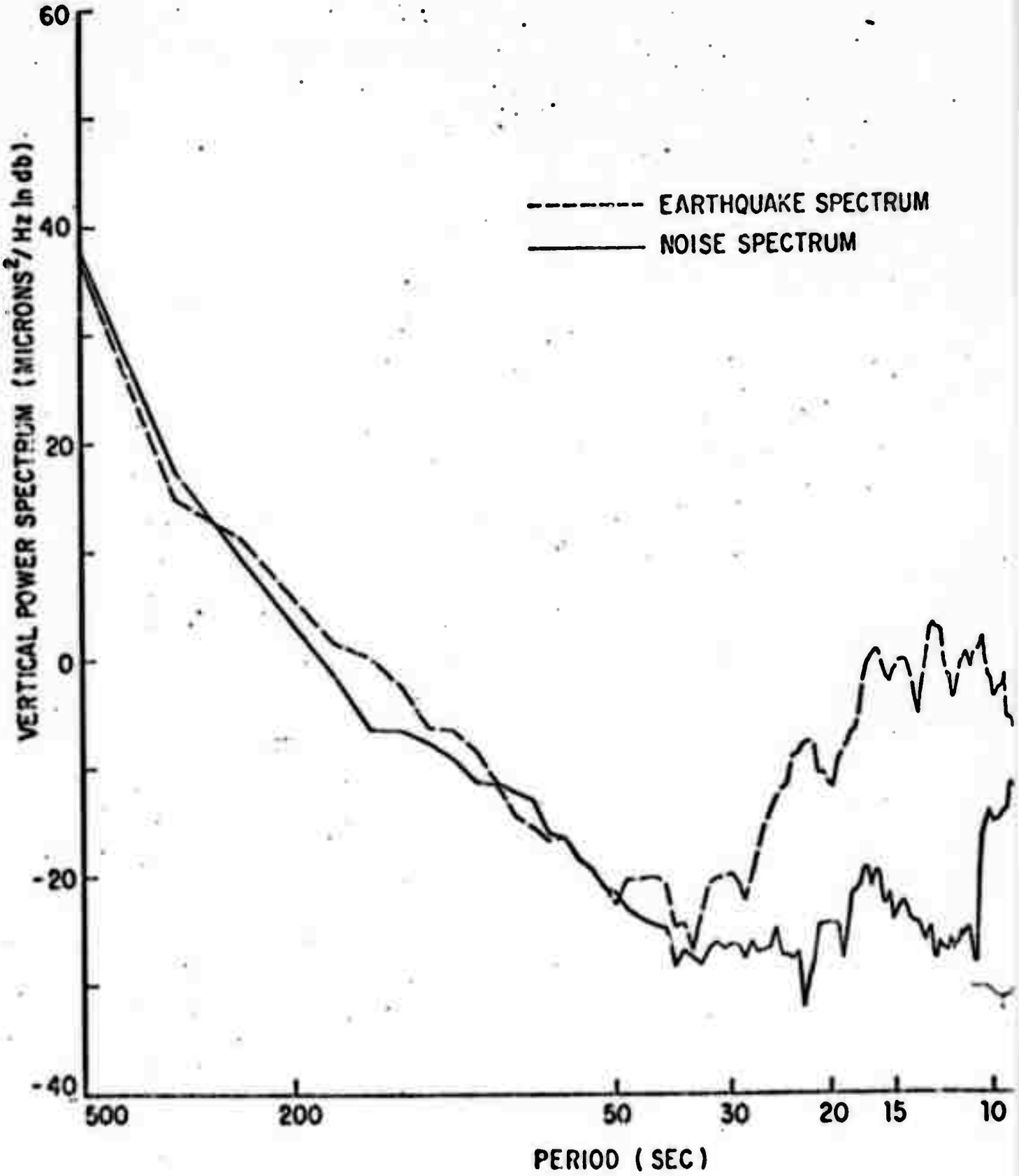
60
40
20
0
-20
-40
VERTICAL POWER SPECTRUM (MICRONS²/Hz in db)
EARTHQUAKE SPECTRUM
NOISE SPECTRUM
500
200
50
30
20
15
10
PERIOD (SEC)

Figure 4

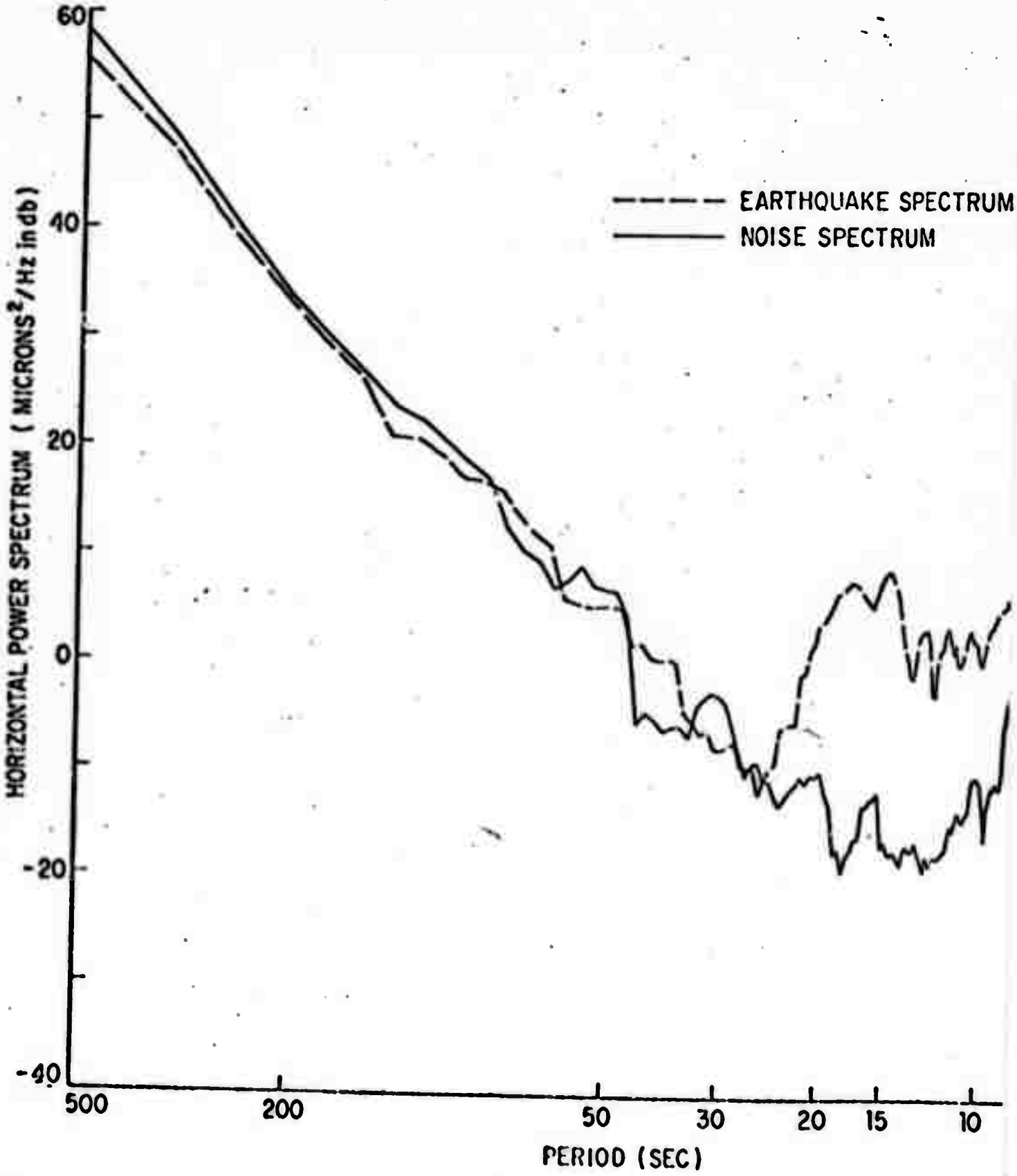
60
40
20
0
-20
-40
HORIZONTAL POWER SPECTRUM (MICRONS²/Hz in db)
EARTHQUAKE SPECTRUM
NOISE SPECTRUM
500
200
50
30
20
15
10
PERIOD (SEC)

Figure 5

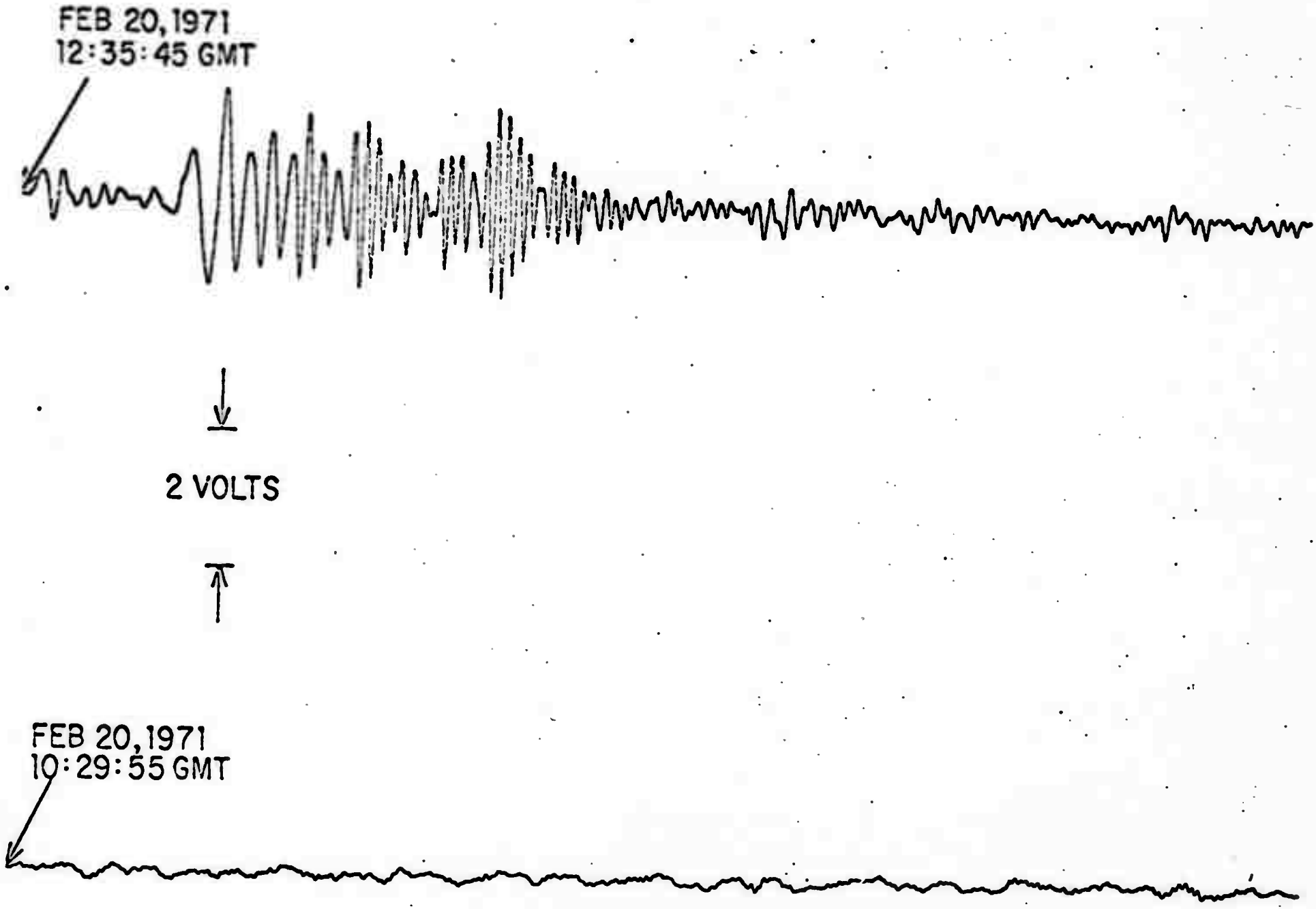

Figure 6

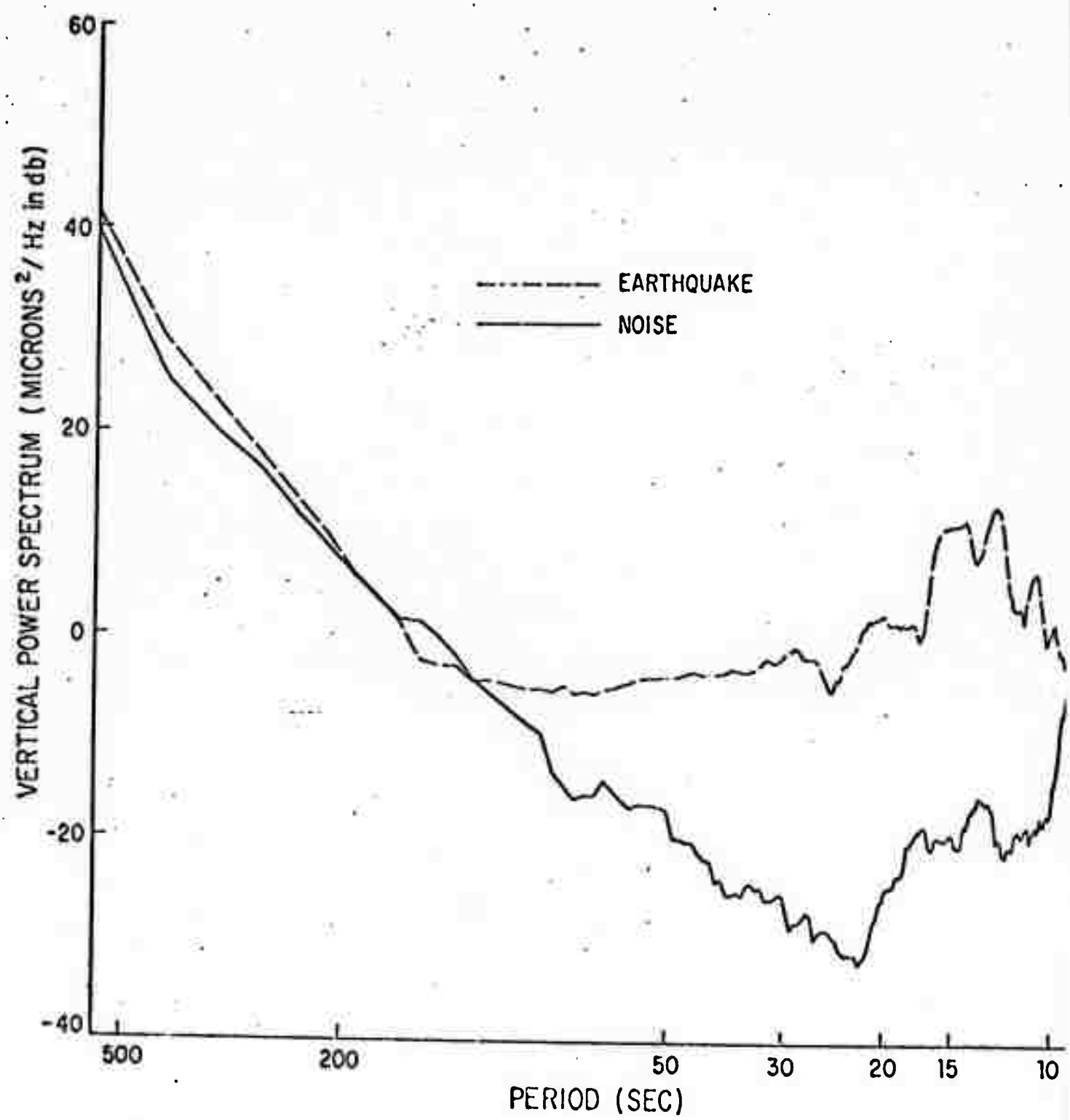
60
40
20
0
-20
-40
VERTICAL POWER SPECTRUM (MICRONS²/ Hz in db)
EARTHQUAKE
NOISE
500
200
50
30
20
15
10
PERIOD (SEC)

Figure 7

AFOSR - TR - 72 - 0603

IMPROVEMENTS IN THE WIDE BAND VERTICAL TORSION ACCELEROMETER

by

Barry Block
and
Jay Dratler, Jr.

Institute of Geophysics and Planetary Physics
University of California, San Diego

IMPROVEMENTS IN THE WIDE BAND VERTICAL TORSION ACCELEROMETER

Significant improvements have been made in the wide band vertical torsion accelerometer since the original design and operation were reported upon.[1,2]

In this paper, these improvements are outlined and some typical data taken with the modified instrument are shown.

Instrumental Improvements

The vertical accelerometer is composed of a horizontally stretched fiber in torsion which supports a mass on a moment arm against gravity. The mass in the shape of a flat plate forms the center element in a balanced parallel plate capacitance position sensor. The position sensor uses a phase sensitive detector.[3] The mechanical Q of the instrument is high so as to lower the Brownian noise in the bandwidth of interest, since the mass used (approximately 10 grams) is small.

The instrument is small (8 inches OD) and comes with its own pressure and temperature controlled environment. It is suitable for borehole use.

Several modifications were made in the capacitance position sensor to improve the signal-to-noise ratio directly. The capacitor plate area (Fig. 1) was increased from 9.5cm^2 to 19.5cm^2 and the spacing from the position detector mass plate to either capacitor plate was decreased from 1.5mm to 0.5mm. These changes result in an overall increase in signal level of 6.1 without change in any noise level. The free period has been lengthened to a

typical value of 0.8 second from the previous value of about 0.6 second. This was made possible by increasing the fiber pulling speed which allows a more uniform diameter fiber to be pulled from the matrix rod while keeping the overall length constant.

In the new models, the drive voltage has been reduced from 40 volts peak to peak at the capacitor plates to 15 volts peak to peak. This reduction in drive voltage diminishes the non-linear destabilizing force by a factor of 7. The increase in plate area and the decrease in plate separation together increase the destabilizing force by about a factor of 18. The net increase in destabilizing force is then a factor of 2.5, which has not been found troublesome. The net increase in signal level from the above sources is a factor of 2.3.

The capacity-to-ground C_{DG} of the position detector plate (Fig. 2, D1 and Fig. 3) was reduced by modifying the center plate clamping assembly (Fig. 2, D4) with an insulating quartz flat (Fig. 2, D2) upon which the detector plate is clamped. A 1 mill tungsten wire is used as the signal lead directly from the detector plate. Another 1 mill tungsten wire is used to ground the remainder of the center plate clamping assembly. The capacity C_{DG} in the new version of the instrument would have been large compared to that in the published version[1] because of the introduction of eddy current damping ears (Fig. 2, D3). The use of these damping ears in controlling the Q's of unwanted modes is discussed below. As a general practice, the reduction of C_{DG} from whatever source is advisable as C_{DG} acts as a voltage divider to reduce the signal level at the preamplifier. To this end, the

preamplifier (PAR Model 112) is built so that its input FET is mounted directly onto the seal-through in the outer vacuum can of the instrument. The protective diodes at the input FET are removed to reduce C_{DG}. Modifications suggested by the manufacturer were made to the mixer of the phase sensitive detector (PAR Model 120) to reduce its noise level.

For damping certain modes of the mass-torsion fiber system, it was found that the damping ears (Fig. 2, D3) were necessary. The small magnets (Fig. 4) provide a field which is perpendicular to the plane of the damping ears. This configuration damps out the twisting mode whose axis is along the arm which supports the mass and also the translational modes which are perpendicular to the mass arm axis. The Q's of the other modes are damped by the magnets mounted with opposite poles facing on the two detector plates. In practice, the Q's of the modes are determined by the magnetic fields present and not by the residual atmosphere in the inner high vacuum can. The Q of the fundamental mode was varied from 20 to 200 in various models. No effects in the earth normal mode or seismic channels described below were seen coming from instrument mode excitation and nonlinear coupling to the fundamental when the ambient acceleration field was produced by nearby jets at Miramar Naval Air Station and could even be felt causing ground vibration.

All stainless steel parts in the center clamp assembly were replaced by beryllium copper parts. This was to ensure that no effect would come from local changing magnetic fields or magnetic storms. The mass was made of OFHC copper. A magnetic field with

a 60 second period having an amplitude of 10^3 gamma at the accelerometer produced no visible effect on the seismic channel which has the highest gain at the 60 second period of any output channel.

The improvements in the temperature control system involve both the passive and active parts of the system. The accelerometer (Fig. 5) is housed in a hard vacuum ($<10^{-7}$mmHg) stainless steel can sealed with a gold O-ring. This in turn is housed in an aluminum vacuum can (<1mmHg) sealed with a rubber O-ring. This outer vacuum can is hung from a rigid thermal insulating structure made from fiber glass (Fig. 5). An outer aluminum surface,called the control surface,and open on the top supports the fiber glass structure. This control surface has the heater winding and sensing thermistor (Figs. 5 and 6) on its outer surface. The control surface along with the fiber glass structure forms an additional thermal filter from the outside world. The control surface sits upon legs made of thin wall stainless steel tubing for thermal isolation from the tilting platform. The control surface is nested inside a container and all spaces are filled with polystyrene balls. In practice, the tilting platform is covered with insulation.

An alternate heat path to that through the nested series of thermal filters described above is through the electrical cables to the accelerometer and temperature sensor.

In order to maximize the effective thermal resistance of these cables, lengths of them are coiled inside the thermal enclosure before they emerge into the outside world. In addition, lightweight cables are used to connect the mechanical system to the external electronics. The coaxial cables are teflon-insulated RG187/U, while the other conductors are part of a 30AWG ribbon cable. After emerging from the thermal enclosure, these cables are connected to heavier standard cables (RG2/U and 18AWG multi-conductor), which connect the deployable unit to the electronics panel.

With the thermal insulation constructed as outlined above, the time constant for heat transfer between the outside world and the fiber is several hours. The thermal filtering drastically reduces the effects of external temperature fluctuations with periods of a few minutes or less. However, the high DC gain of the temperature controller eliminates the low frequency temperature variations.

The fedback temperature contoller is a proportional control system with extremely high DC gain. A thermistor measures the temperature at a point on the control surface (Fig. 5). The temperature sensor bridge and preamplifier compare the thermistor resistance to that of a standard. An error signal is produced proportional to their difference. This error signal is sent to the fedback power amplifier whose output determines the current in the resistive heater wound around the control surface. The error signal changes the heater current to bring the control surface temperature back to the null point. Since the null point, which is determined by the resistance of the standard in the sensor, exceeds room temperature, there is always current in the heater winding. This mean current compensates for thermal leakage through the insulation. Fluctuations in the heater current maintain the temperature at the thermistor fixed within 4×10^{-6}°C per 100 sec and 4×10^{-8}°C per day. These limits are obtained by assuming the output in the seismic filter and the drift in the tidal channel are caused by temperature fluctuations alone.

All models of these instruments have extremely low drift. The first one was operated continuously for a year and has shown less than 10^{-8}g drift during this time. A conservative upper bound to the drift rate is thus 10^{-10} g/day.

In practice, the active temperature controller and the passive thermal insulation interact considerably. Not only does the insulation determine the mean heater current needed to maintain a given temperature, but it also affects the stability of the temperature controller. For small fluctuations in the heater current, the insulation helps to control the heat loss from the control surface and thus

limits the thermal lag between the heater and thermistor. This thermal lag is primarily responsible for difficulties in stabilizing recalcitrant control systems. As in the case of the design of the insulation itself, calculations of the stabilizing effects are made prohibitively difficult by the fact that the parameters are distributed. Such improvements are most quickly made by trial and error.

The temperature controller can increase the need for thermal insulation by providing small thermal fluctuations of its own. The thermal insulation between the control surface and the outer aluminum can forestalls this problem. Being a lon-linear system, the thermal controller is subject to marginal instabilities. Usually, these are at rather high frequencies where the controller loop gain is low. In the presence of strong environmental temperature drift, however, the controller sometimes cycles at the higher teleseismic frequencies. To reduce the effect of these low-level thermal oscillations, the control surface is placed on the outside of the soft vacuum can and is itself insulated from direct external temperature variations. The heat capacity of the control surface is significantly lower than that of the soft vacuum can, thus making the temperature controller easier to stabilize. The present isolated control surface is open at the top. At low frequencies, thermal gradients can exist between the control surface and the soft vacuum can. Normally, this is unimportant, as long as the isolated control surface is not used for accurate observations of earth tides. This problem can be eliminated by making the isolated control surface completely closed except for thermally insulated electrical feed thrus.

The open loop gain of the temperature control system extremely high below 10^{-4} H_z and falls 20 db/dec above this frequency. This active device provides good regulation where the passive insulation is ineffective. Conversely, the insulation attenuates temperature fluctuations at higher frequencies, where the low loop gain reduces the effectiveness of the temperature controller. A phase lead compensator is used to stabilize the system if needed. A series of tests of the temperature controller with varying thermal time constants between the control heater and the outer aluminum can show that from approximately 5 cph to the seismic band, no appreciable noise comes from the controller.

One possible source of thermally induced noise within the mechanical instrument itself is ohmic heating in the center transducer plate and auxiliary damping paddles due to the eddy currents which provide the damping. If unwanted modes are variably excited, this heating could conceivably cause fluctuations in the fiber temperature. A worst case analysis of this effect proceeds as follows. Suppose that one of the unwanted modes of vibration in the vertical accelerometer is continually excited by site noise to an amplitude corresponding to full scale open loop output. Then the energy in the mode is approximately

$$\epsilon = \frac{1}{2} m\omega^2 \delta_{fs}^{\ 2} \qquad (1)$$

where m is the accelerometer mass, $\omega=2\pi f$ is the angular frequency of the mode, and δ_{fs} is the full scale displacement of the mass.

If Q is the quality factor for the mode, the amount of energy dissipated per cycle is $\frac{2\pi\omega}{Q}$, by definition of Q. Thus, the power lost to heating can be written as

$$P = \frac{2\pi c}{Q} f = \frac{c\omega}{Q} = \frac{1}{2Q} m\omega^3 \delta_{fs}^{\ 2} \qquad (2)$$

with the help of equation (1).

Frequencies and Q's for typical unwanted modes in the vertical accelerometer have been estimated as follows:

$$f = 40\text{Hz}, \qquad Q = 30 \qquad (3)$$

The parameters m and δ_{fs} are roughly 10g and 5×10^{-6}cm, respectively. Hence, the rate of heat production in the damping plates due to continuous excitation of an unwanted mode is

$$P \approx 6\times10^{-5}\ \text{erg/sec} = 1.5\times10^{-12}\ \text{cal/sec} \qquad (4)$$

Since the power (equation 2) depends on the cube of the modal frequency ω, the heating due to continual excitation of the fundamental mode would be considerably less than this.

Now the heat capacity of the entire mass assembly is roughly that of the copper mass itself, or about $C_h = 2\text{cal}/^\circ\text{C}$. If all the energy dissipated in damping is assumed to heat this assembly, then the rate of change of its temperature is

$$\frac{\Delta T}{\Delta t} = P/C_h \approx 10^{-12}\,^\circ\text{C/sec} \qquad (5)$$

This rate is just large enough to cause a barely perceptible temperature change of $10^{-7}\,^\circ$C in one day of continuous excitation of an unwanted mode. Moreover, heating due to damping of the

fundamental mode is much slower. Obviously, the effect of heating in the damping assemblies is negligible as far as the accelerometer output is concerned.

Filtering and Recording of Data

The quartz fiber accelerometers in the open loop system have broadband response from DC to the resonance frequency of about 1 Hz. With this bandwidth, simultaneous investigations of earth tides, free oscillations of the earth, and long period teleseisms can be carried out. Tidal data is more easily analyzed when earthquakes are removed from it. Teleseismic records[4,5] can be obtained at a higher gain when the tidal signals are removed. Earth normal mode studies[6] are conveniently studied through a band pass gainful filter. The raw output of the accelerometer is thus modified by three active analog filters called prefilters, which respond preferentially to tides, free oscillations, and teleseisms. The resultant total response functions are plotted along the accelerometer response for the open loop system in Figure 6.

Each of the three prefilters is an electronic circuit which uses fedback operational amplifiers to set its response and the full scale output of $\pm$ 10V. The tidal prefilter simply attenuates high frequency signals, while the normal mode and seismic prefilters both have gainful response at certain frequencies.

The tidal prefilter is a double-pole lowpass filter with a cutoff frequency of 5.75 cph (slow) or 57.5 cph (fast). For tidal investigations, the lower cutoff frequency is used. Since the highest tidal frequency of usual interest is that of the triurnal tide, or 0.125 cph, the slow cutoff frequency gives the tidal prefilter nearly unity gain and zero phase shift over the entire tidal band.

The response near DC is used for calibration of the instrument. The tidal prefilter is used during calibration to observe DC levels while averaging out fluctuations due to microseismic ground noise. To avoid long waiting periods, the time constant is set to fast for such work.

Normal mode oscillations of the earth are best investigated using a gainful bandpass filter. Its passband is variable, with a lower knee frequency of 1 cph and an upper knee frequency of 30, 60, 120 or 180 cph. The gain in the passband is 40db above the DC level. On the high side of the passband, the response falls 40 db/dec. On the low side, it falls 40db/dec to 0.1 cph and is constant at lower frequencies. An input attenuator sets the DC level. When the attenuation is zero, the gain at DC is unity.

The normal mode prefilter is usually run with no input attenuation and the upper knee frequency set at 30 cph. This configuration provides sufficient gain and bandpass for studies of the lower frequency normal modes. Increasing the upper knee frequency includes more of the normal mode band in the gainful region. At the highest setting, long period seismic signals are included in the bandpass. This setting allows all seismic signals with periods greater than 20 sec to be observed with nearly the same gain. Unfortunately, large Rayleigh waves and ground noise tend to saturate the prefilter electronics when its bandwidth is this large. This is the reason the input attenuator is provided. It allows a compromise between gain and bandwidth to be made. The nature of this compromise depends on the size of events to be observed and the level of ground noise at the instrument site.

The normal mode prefilter attenuates the tidal signals which allows more gain to be used in the bandpass. Peak-to-peak tidal accelera-

tions can be as high as 3×10^{-7}g, while normal modes and seismic waves typically produce accelerations of order 10^{-9}g. Tidal signals at the lock-in amplifier output are thus near 1V peak-to-peak. If amplified significantly, these signals saturate the prefilter. Phase shifts due to the changing gain of the prefilter near tidal frequencies distort the tidal signals. This precludes use of the normal mode prefilter output for tidal studies or tidal calibration.

The seismic prefilter is a peaked bandpass filter. Its peak is fixed at 100 second periods, while its half power points are at 60 and 200 second periods. At high frequencies, its response falls as ω^{-7}, or 140db/dec, while at low frequencies its response dies as ω^{2}, or 40db/dec. The peak gain is set by the input attenuator, which has six positions, and can be varied from 60 to 5830. Normally, the attenuator is set for a peak gain of 621.

The high peak gain and the rather narrow bandwidth of the seismic prefilter are quite useful in observing long period teleseisms. They permit measurement of seismic signals as low as 10^{-10}g in amplitude. The sharp rolloff of the response at high frequencies reduces interference due to microseismic signals, while the rolloff at low frequencies eliminates the tides. The seismic prefilter is used primarily for detection of distant teleseismic events.

The accelerometers have flat responses to acceleration over the bandpasses of the prefilters. Thus, the shape of the composite response at the output of each prefilter is determined by the response of the prefilter itself. The

gain level is determined by the DC gain of the accelerometer. The exact form of the response to acceleration at each prefilter output is calculated by multiplying the prefilter response function by the appropriate accelerometer response.

The output of each prefilter is recorded digitally on magnetic tape with a resolution of ±16384 digitizer counts per ±10 volts. In the cases of the normal mode and seismic prefilters, the outputs with ±10V full scale, are used for digitizing. The typical sampling interval is 1 second, giving a digitizer Nyquist frequency of 1/2 Hz. Part of the function of the prefilters is to provide large attenuation above the Nyquist frequency to eliminate aliasing of energy in the digitizing process. As Figure 6 shows, the response of each prefilter at the Nyquist frequency is down at least 80 db from its peak response. Such attenuation is sufficient to eliminate aliasing for all practical purposes.

Noise

Measurements of the full electronic system noise will be presented below and compared with calculated Brownian motion noise and measured ambient site noise. This will be done for the normal mode and seismic prefilter channels. The calculated Brownian noise of the mass-torsion fiber system, with appropriate measured gain factors and measured prefilter response functions is contained in Table I as an equivalent output voltage. The electronics is assumed to produce no noise in these calculations.

The full electronic system noise is measured with the instrument in thermal control and with the synchronous detector drive voltage set to zero. The measured values are contained in Table II for the normal mode prefilter and the seismic prefilter outputs. Comparison of the values in Tables I and II show that the noise in the normal mode prefilter output from both sources is about equal and the electronic noise is lower than the Brownian noise in the seismic prefilter output.

A typical ambient output in the seismic filter is shown in Fig. 7 for both day and night. It should be noted that there is little difference in these levels. The peak to peak output voltage is about 500 mv which is considerably larger than the combined Brownian and electronic noise levels. The microseisms[7] are visible in both traces of Fig. 7 as high frequency hash. The largest amplitude wiggles are at about 100 seconds, the period at which the seismic prefilter response is peaked. Recent studies[8,9,10] have shown that the effects of propagation of pressure cells in the atmosphere become important at periods greater than 60 seconds. These wiggles are probably due to

local ground motion induced by these pressure cells. The presence of this noise just below the seismic band (20 - 50 second periods) makes the use of digital filtering[5] an important technique to improve the signal to noise ratio for teleseismic events. The ambient noise in the normal mode prefilter with the upper knee frequency of 30 cph and no input attenuator was between 50 and 100 mv peak to peak. A comparison of Tables I and II show that the ambient noise is larger than the combined electronic and Brownian noise.

The improvement in noise performance of the present instrument compared to the first model of the vertical accelerometer is between 6 to 10 db in the normal mode (1-30 cph) prefilter band. The decrease in noise for the seismic prefilter band is about a factor of three in amplitude.

Data

The modified instrument described above has been in operation since February 1971. During this time a continuous digitally recorded run was made at Camp Elliott, San Diego from February to July inclusive to obtain data from a sizable number of earthquakes. This data was taken with the prefilters described in the section Filtering and Recording of Data. A complete catalogue of the events detected is in progress by T. Whorf at IGPP.

Selected examples of earthquakes as seen through the normal mode prefilter and seismic prefilter are given below. Fig. 8 shows the normal mode prefilter record of an earthquake (M_b = 6.3) in the Southern Shetland Islands (63.5°S, 61.2°W) on February 8, 1971, origin time 21:04 GMT at a depth of 33 km. The ambient noise through the prefilter before the earthquake is also seen in Fig. 8. The power spectrum of this earthquake from 15 hours of data is plotted in Fig. 9 where zero db corresponds to $1 \times 10^{-24} g^2$/cph. The mean of the ambient noise power spectrum is also plotted on Fig. 9. The ambient noise and its mean are shown displaced downward from their true values by 10 db on Fig 9 so as not to be confused with the earthquake power spectrum. The ambient noise power spectrum is derived from the same length of record used in the earthquake power spectrum and is processed by the same program. In this case, data from the 15 hours preceeding the earthquake was used.

The time record of this earthquake (Fig. 8) shows several passes of the Rayleigh waves and commensurately the power spectrum shows clearly defined normal mode excitation with a 20 db or larger signal to noise ratio above 6 cph. Unfortunately this fine record was interrupted by the

San Fernando earthquake (M_b = 6.2) on February 9, 1971, origin time 14:01 GMT. Figs. 10 and 11 show the normal mode prefilter record of this event. Since the accelerometer was essentially at the epicenter, instrumental saturation occurred at the primary event and for the larger aftershocks. There are two main features to be noted in Figs. 10 and 11. Being at the epicenter means that both Rayleigh wave packets arrive simultaneously and the long wave length, high velocity Rayleigh waves[11] can be seen with minimal interference from the Rayleigh wave packets. The aftershocks seen in Figs. 10 and 11 should, by their form and magnitude, yield information on the moment of the event and its source structure. An investigation of the aftershocks will be made for this purpose. The tidal prefilter shows less saturation than the earth mode prefilter because of its lower gain. The tidal prefilter can provide better information on the aftershocks for this reason. No net DC displacement in the tidal channel was observed larger than 3×10^{-10} g or an equivalent vertical motion of 1 mm relative to the center of mass of the earth. This estimate is an upper bound only owing to difficulties in matching the endpoints of the tidal signal because of saturation problems.

Fig. 12 shows an earthquake (M_b = 6.0) in Adak (51.4°N, 177.2°W) on May 2, 1971 origin time 06:08 GMT at a depth of 43 km. The power spectrum of this earthquake from 18 hours of data is plotted in Fig 14. The ambient noise and its mean are plotted as in Fig. 9. The ambient noise is obtained from the previous 18 hours of normal mode prefilter data. The power spectrum of this earthquake is quite different from that of the Shetland Island event. The underlying reasons for the general features of these power spectra is still not clearly understood although computation of excitation spectra from earth-

quake models is now possible.[12] A spectrum similar to those shown in Figs. 9 and 11 is obtained somewhat more than once a month on an average.

Seismic prefilter data is contained in Figs. 13 and 14 where a typical series of small teleseismic events taken over several days are shown. Table II contains identifications and pertinent data on the events. Event 17 has been previously published[4] and is omitted. The salient feature of this data is the low ambient noise level through the seismic prefilter and the consequent low magnitude threshold for visual detection of events. The visual detection threshold can be greatly improved by digital high pass or band pass filtering.[4,5] The seismic prefilter data shown is typical in its noise performance for the entire body of data taken from February to July.

A paper on the horizontal analogue of this vertical accelerometer design with preliminary data is in progress.

ACKNOWLEDGEMENTS

This research was supported by the Advanced Research Projects Agency of the Department of Defense and was monitored by the Air Force Office of Scientific Research under Contract No. F44620-71-C-0128.

The authors wish to thank Bruce Bartholomew for his help in analyzing the data shown.

REFERENCES

1. Block, B. and R. D. Moore. Tidal to seismic frequency investigations with a quartz accelerometer of new geometry, *J. Geophys. Res.*, *75*, No 8, 1493-1505, March 10, 1970.

2. Dratler, J., Jr. *Quartz Fiber Accelerometers and some Geophysical Applications*, doctoral thesis, IGPP, University of California, San Diego, September, 1971.

3. Hoffman, W. F. *A Pendulum Gravimeter for Measurement of Periodic Annual Variations in the Gravitational Constant*, Appendix 1, doctoral thesis, Palmer Physical Laboratory, Princeton University, January 1962.

4. Prothero, W., J. Dratler, Jr., J. Brune and B. Block. Surface wave detection with a broad band accelerometer, *Nature*, *231*, No. 80, May 24, 1971.

5. Block, B. and J. Dratler, Jr. Teleseismic detection with wide band vertical and horizontal accelerometers, *Nature Phys. Sci.*, *232*, No. 28, 33-37, July 12, 1971.

6. Block, B., J. Dratler, Jr., and R. D. Moore. Earth normal modes from a 6.5 magnitude earthquake, *Nature*, *226*, No. 5423, 343-344, April 25, 1970.

7. Haubrich, R. A. and K. McCamy. Microseisms: coastal and pelagic sources, *Reviews of Geophys.* *7*, No. 3, 539-571, August, 1969.

8. Haubrich, R. A. and G. S. MacKenzie. Earth noise, 5 to 500 millicycles per second, *J. Geophys. Res.*, *70*, 1429-1440, 1965.

9. Sorrells, G. G. and Z. A. Der. Long period seismic noise and atmospheric pressure variations, Teledyne Geotech Technical Report Number 70-12, Garland, Texas, 1970.

10. Sorrells, G. G. A preliminary investigation into the relationship between long period seismic noise and local fluctuations in the atmospheric pressure field, *Geophys. J. Roy. Astr. Soc.*, in press.

11. Brune, J., M. Ewing and J. Kuo, Group and phase velocities for Rayleigh waves of period greater than 380 seconds. *Science*, *No 3455*, 757, 133, March 17, 1961.

12. Gilbert, Freeman, Private communication.

TABLE I

Fluctuations at Prefilter Outputs Due to [redacted]

	Tidal Prefilter FAST T_t=10sec	Tidal Prefilter SLOW T_t=100sec	Normal Mode Prefilter with No Input Attenuation Upper Knee Frequency 30 cph	Seismic Prefilter with Peak Gain at 621
Vertical Accelerometer				
$\langle V^2 \rangle$ $(volts)^2$	3.63×10^{-9}	3.63×10^{-10}	1.65×10^{-5}	1.48×10^{-3}
V_{RMS} mv	.06	.019	4.1	38

TABLE II

	Normal Mode Prefilter with no input attenuation Upper Knee Frequency 30 cph	Seismic Prefilter with peak gain at 621
V_{RMS} (mv)	5.0	18.0

46

TABLE II

Event	Location	Date (1971)	Origin Time	Δ°cpe	H	(PDE) M_b	(LASA) M_b
12	New Ireland	2 Feb	22:16:28:4	93°	100	4.5	--
13	Andreanof Island	8 Feb	00:01:47	45°	48	--	4.0
	Andreanof Island	8 Feb	00:04:31	45°	48	4.3	--
	Andreanof Island	8 Feb	00:04:42	45°	33	--	4.2
	Fox Island	8 Feb	00:15:55	45°	48	--	4.3
14	Andreanof Island	8 Feb	01:03:14	45°	64	4.6	4.7
15	Andreanof Island	8 Feb	02:29:11	47°	44	5.2	5.4
16	Sunda Arc	8 Feb	04:25:16.9	132°	33	4.9	--
18	New Ireland (PDE)	8 Feb	08:03:29.5	95°	43	--	--
19	LR arrival = 14:00						
20	LR arrival = 14:44						
21	LR arrival = 15:38		Not listed in PDE or LASA				
22	LR arrival = 19:09						
23	LR arrival = 09:03	9 Feb	Not listed in PDE or LASA				
24	Near Coast of Honshu	9 Feb	09:44:20.8	81°	41	4.8	5.2
25	LR arrival = 13:00	9 Feb	Not listed in PDE or LASA				
26	E. Coast of N. Island New Zealand	9 Feb	12:48:08	92°	33	5.2	--

FIGURE CAPTIONS

Figure 1 Assembly of the mass-torsion fiber system with the drive capacitor plates in place.

Figure 2 Exploded view of the fiber center clamp assembly with mass.

Figure 3 Assembled fiber center clamp assembly with mass.

Figure 4 Assembled mass-torsion fiber system with assembly of mode damping magnets. The pitted surface of the aluminum frame comes from chemical cleaning.

Figure 5 Thermal insulation system for the vertical accelerometer. Note the temperature controller heater windings on control surface.

Figure 6 Composite responses to acceleration of open loop instrument and three prefilters, with response at position sensor output shown for comparison. All response magnitudes are plotted relative to open loop DC gain of accelerometer which is 6.24×10^6 volts/g.

Figure 7 Daytime and nighttime vertical noise in seismic band at Elliott Station. Records are computer plots of digitized output of seismic prefilter for open loop vertical accelerometer. Input attenuator of prefilter is set at a gain of 621. Scales apply to both traces. Calibration in terms of ground acceleration can be made using Figure 7 with DC gain taken as 6.24×10^6 volts/g.

Figure 8 Computer plot of normal mode prefilter data for Southern Shetland Island earthquake (M_b = 6.3). Vertical scale corresponds only to signals in 1-30 cph band-pass, not to tides. The epicenter was (63.5°S, 61.2°W), origin time 21:04 GMT, February 8, 1971 at a depth of 33 km.

Figure 9 Spectra of the Southern Shetland Island earthquake (Fig. 8) from 2 to 30 cph. Absolute spectral density of 0 db point is $1 \times 10^{-24} g^2$/cph. Earth normal mode spectrum is derived from 15 hours of data shown in Fig. 8. Ambient spectrum is derived from 15 hours of data just previous to the earthquake. The running mean of ambient spectrum is average over 1 cph. The ambient spectrum and running mean are displaced downward by 10 db in Fig. 9. Approximate level of Brownian noise at input of accelerometer is indicated by heavy line. Selected modal lines are identified from theoretical calculations of eigenfrequencies.

Figure 10 Computer plot of normal mode prefilter data for the San Fernando earthquake (M_b = 6.2). Vertical scale corresponds only to signals in 1-30 cph bandpass, not to tides. The origin time was 14:01 GMT, February 9, 1971, and the epicenter was (34.4°N, 118.4°W) at a depth of 13 km.

Figure 11 Continuation of Figure 10.

Figure 12 Computer plot of normal mode prefilter data for the Adak earthquake (M_b = 6.0). Vertical scale corresponds only to signals in 1-30 cph bandpass, not to tides. The epicenter was (51.4°N, 177.2°W), origin time 06:08, May 2, 1971 at a depth of 43 km.

Figure 13 Spectra of the Adak earthquake (Fig. 12) from 2 to 30 cph. Earth normal mode spectrum is derived from 18 hours of data shown in Fig. 12. The ambient spectrum is derived from 18 hours of data just previous to the earthquake. See caption for Fig. 9 for explanation of ambient and mean spectra.

Figure 14 Computer plot of seismic prefilter data for a series of small teleseismic events. (See Table II for pertinent data.) Event 17 has been published (see text).

Figure 15 See caption Figure 14

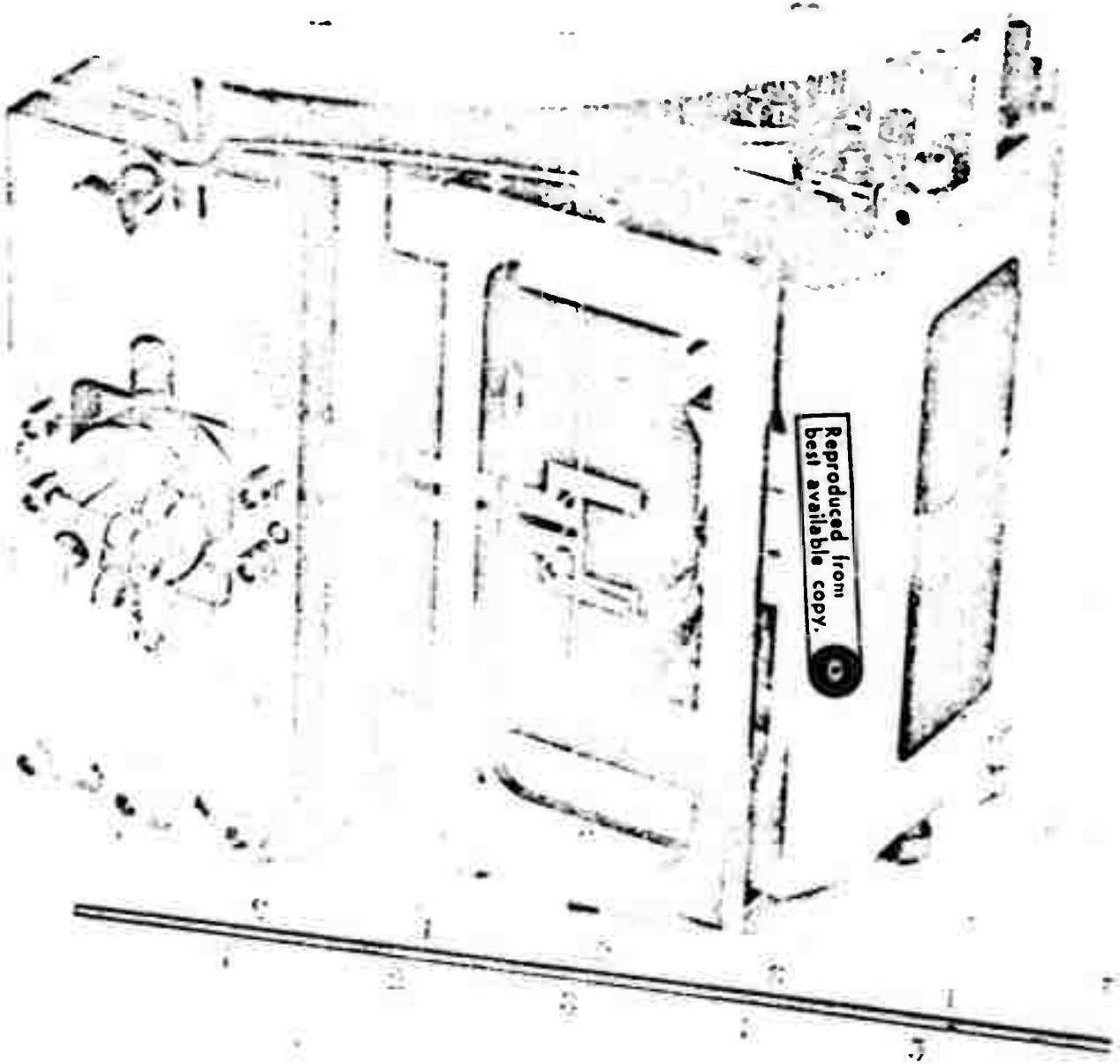

Reproduced from best available copy.

Figure 1

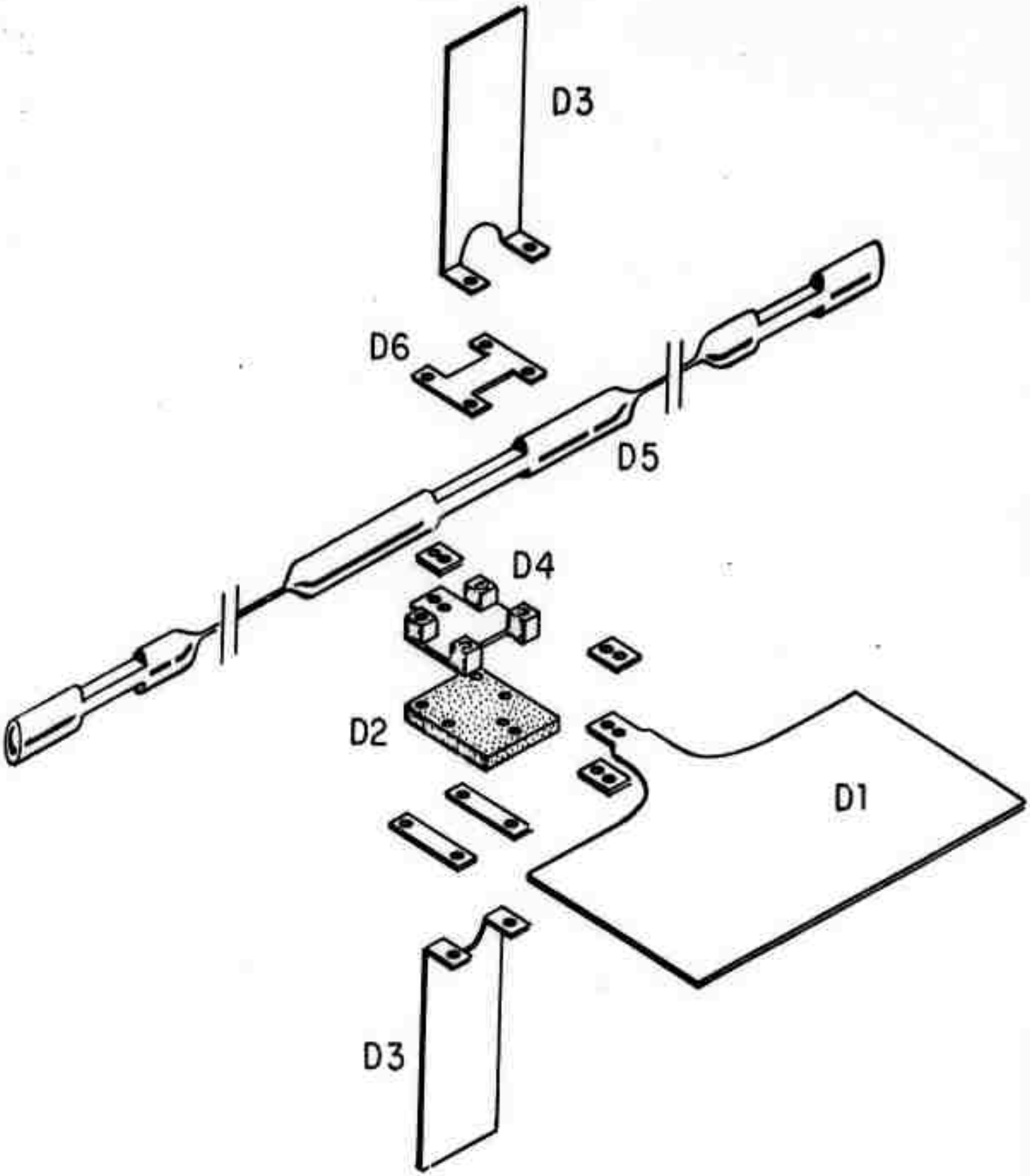

Figure 2

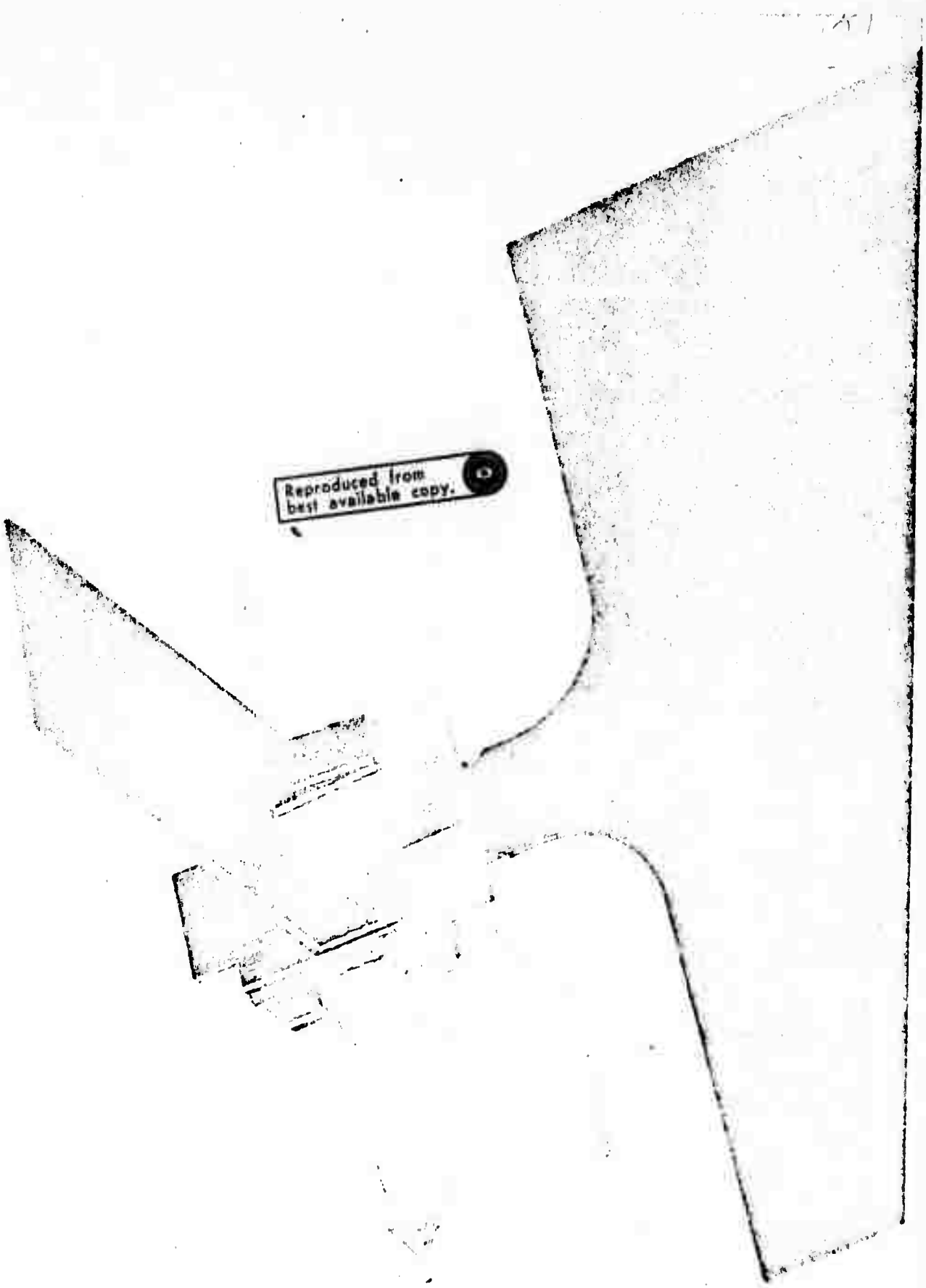

Reproduced from best available copy.

Figure 3

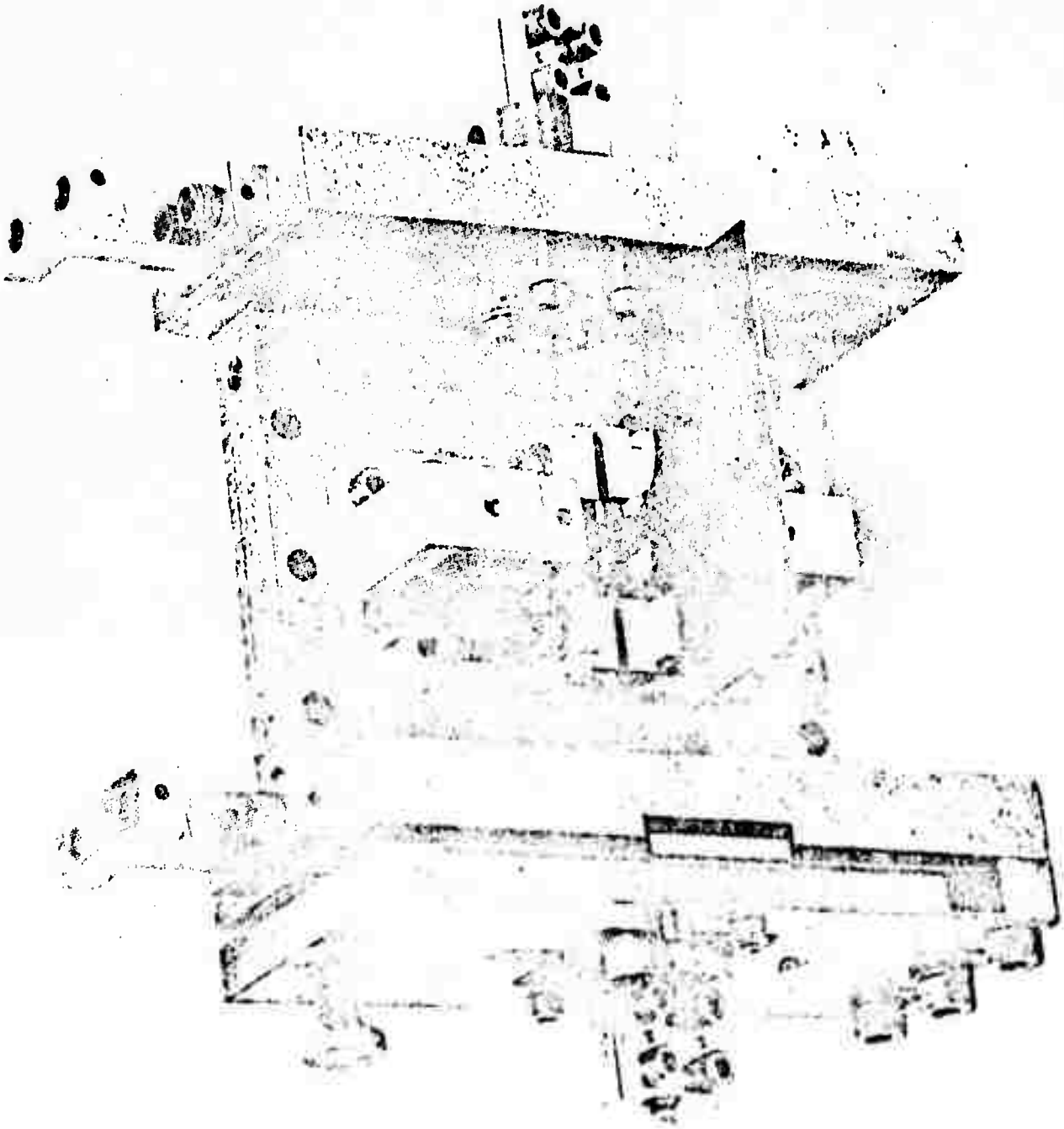

Reproduced from best available copy.

Figure 4

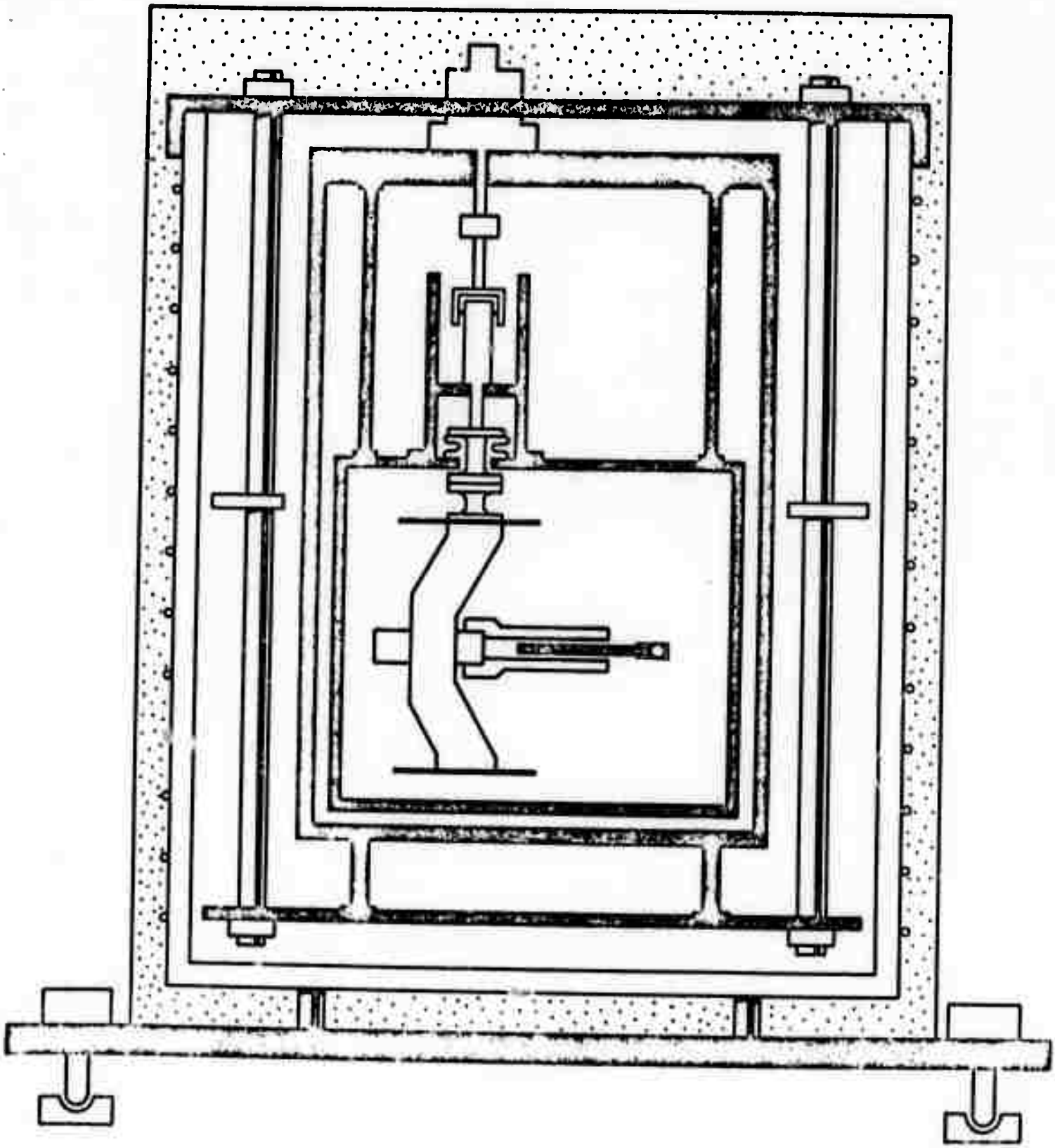

Figure 5

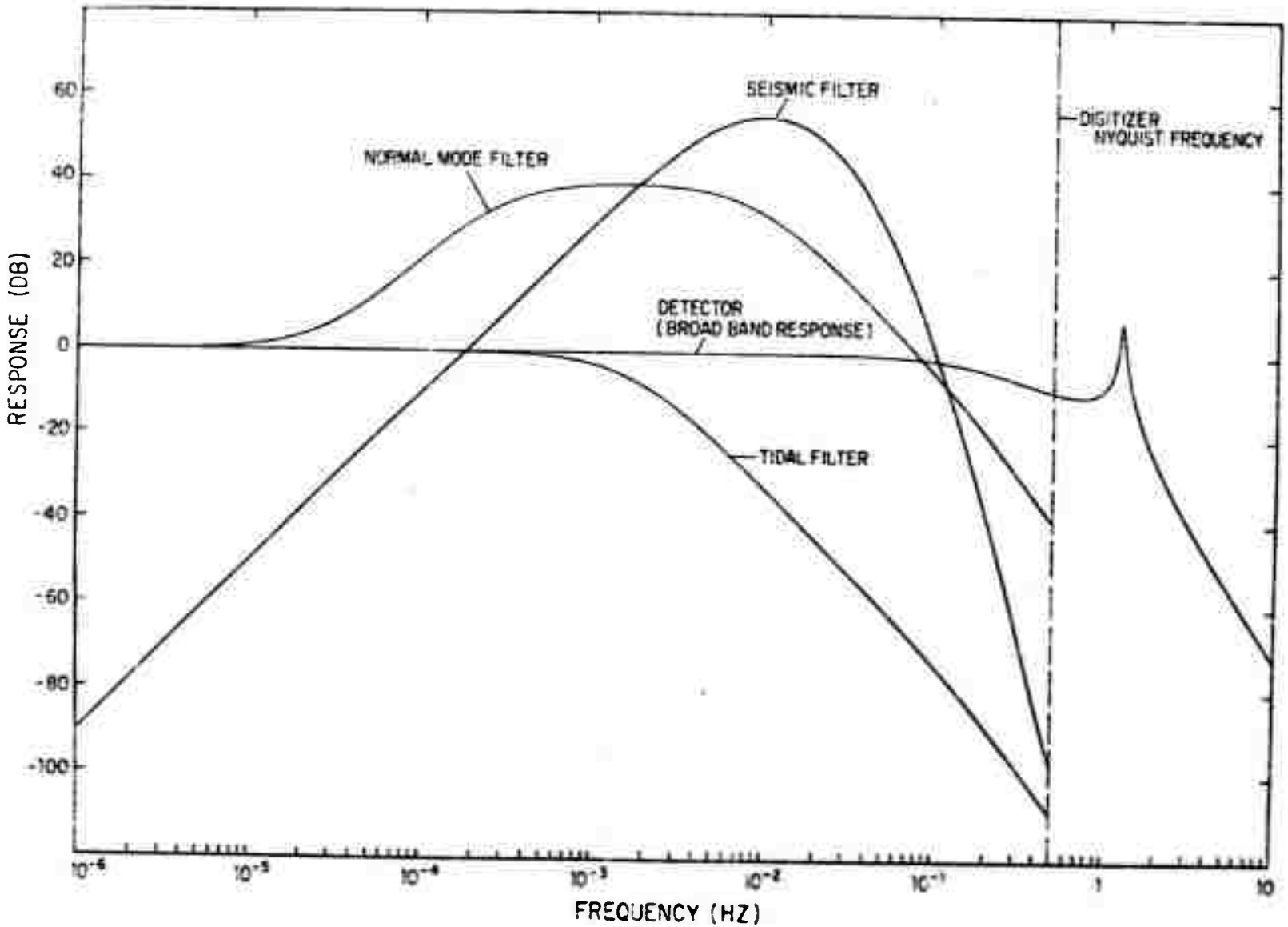
SEISMIC FILTER
NORMAL MODE FILTER
DIGITIZER
NYQUIST FREQUENCY
DETECTOR
(BROAD BAND RESPONSE)
TIDAL FILTER
RESPONSE (DB)
60
40
20
0
-20
-40
-60
-80
-100
10^{-6}
10^{-5}
10^{-4}
10^{-3}
10^{-2}
10^{-1}
1
10
FREQUENCY (HZ)

Figure 6

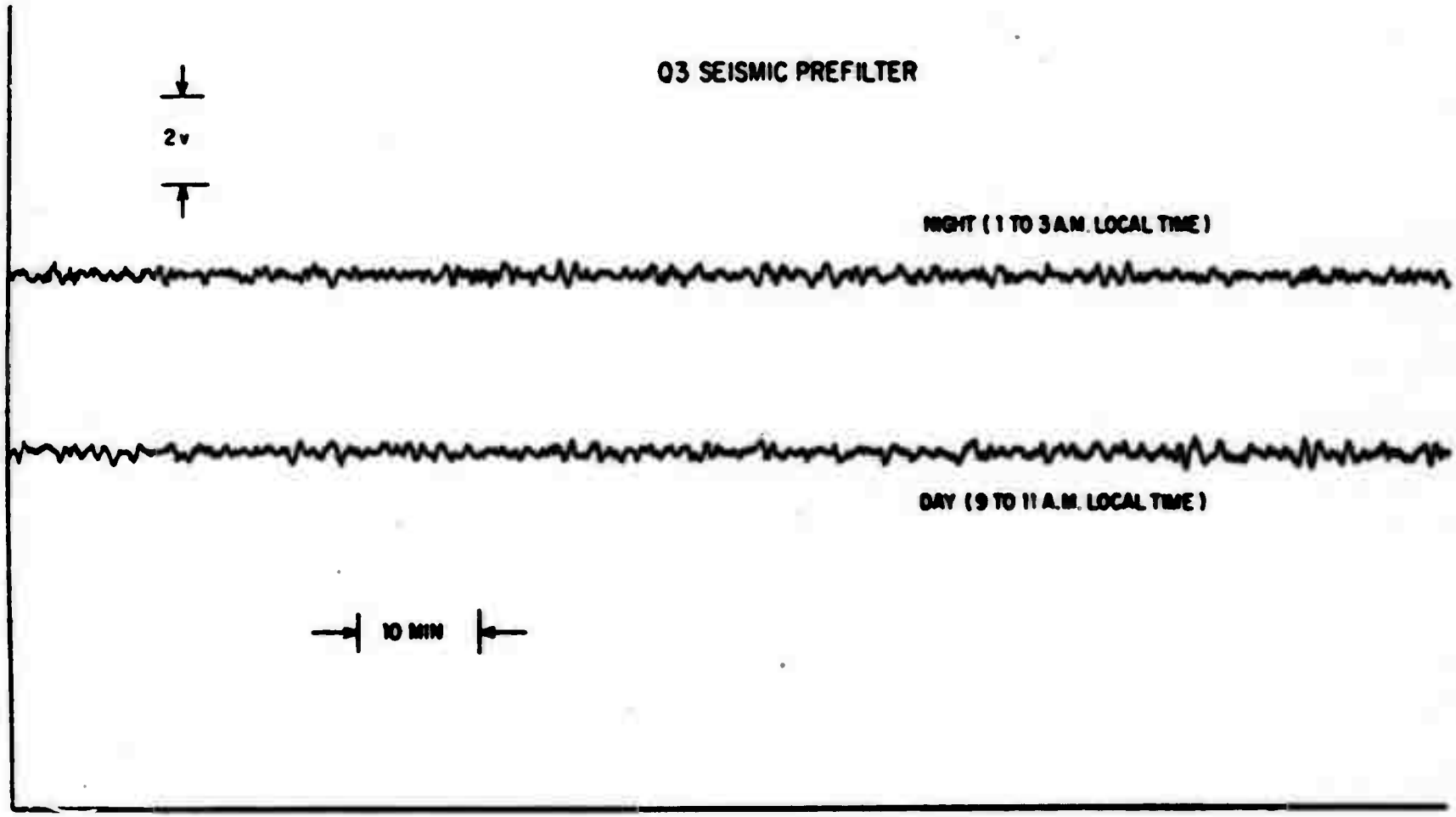
03 SEISMIC PREFILTER
2v
NIGHT (1 TO 3 A.M. LOCAL TIME)
DAY (9 TO 11 A.M. LOCAL TIME)
10 MIN

Figure 7

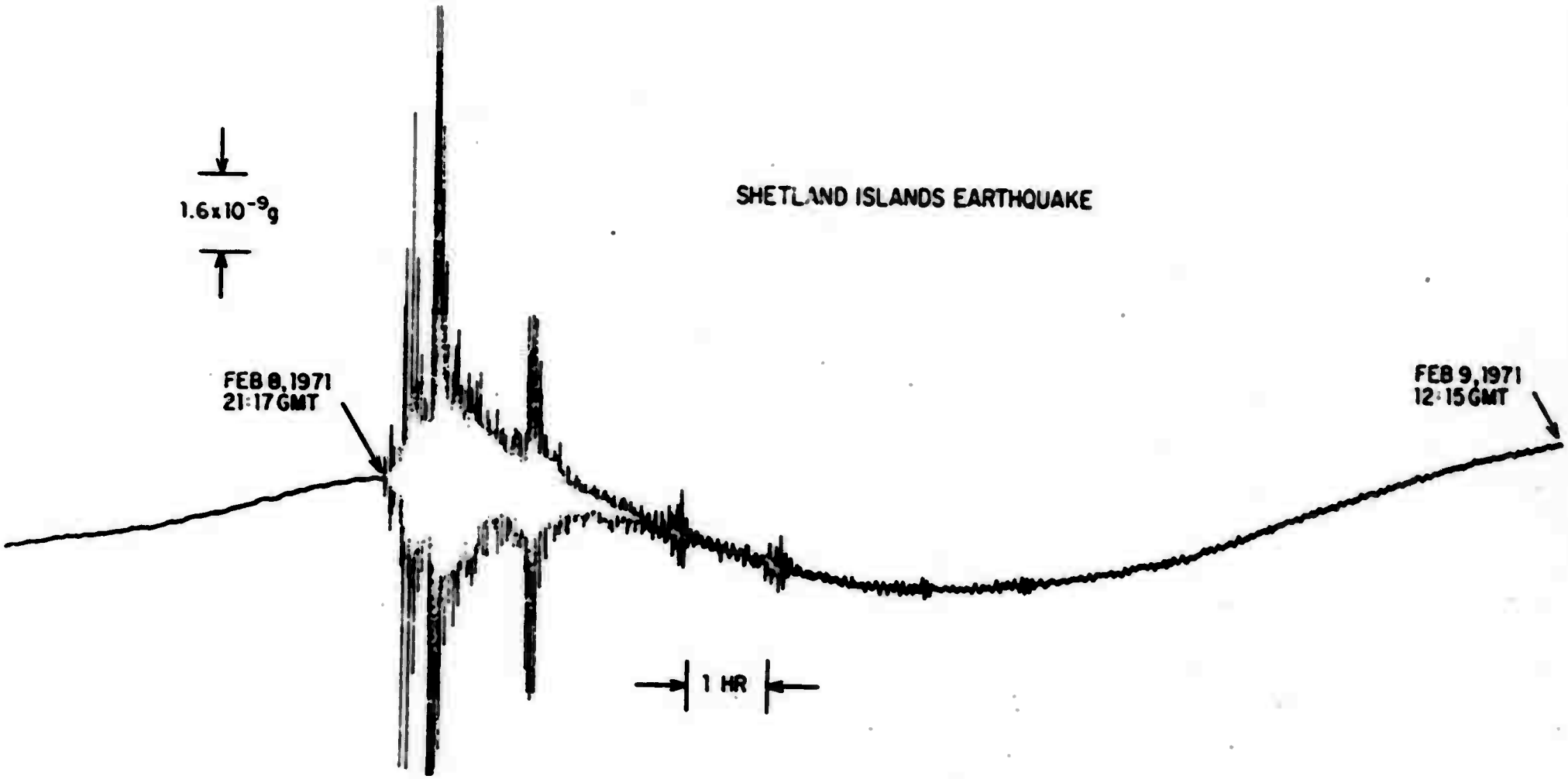
SHETLAND ISLANDS EARTHQUAKE
1.6x10^{-9}g
FEB 8, 1971
21:17 GMT
FEB 9, 1971
12:15 GMT
1 HR

Figure 8

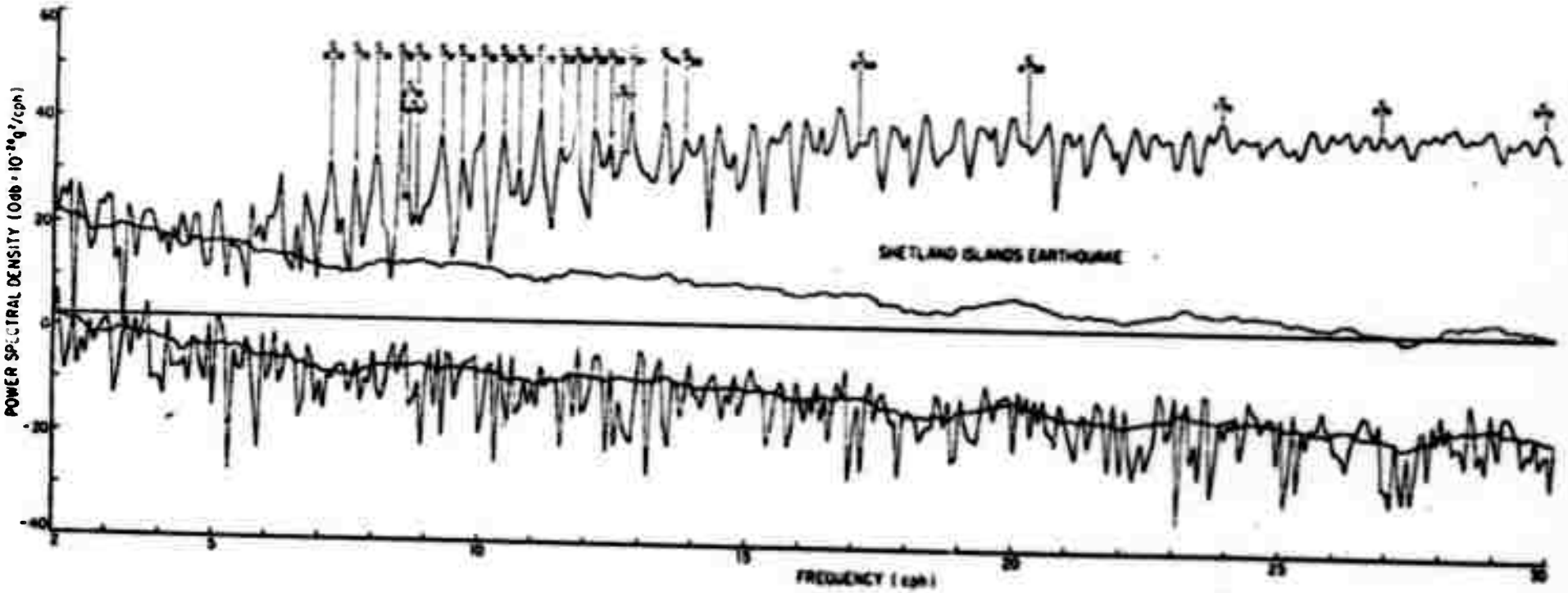
POWER SPECTRAL DENSITY (0db = 10⁻²⁰g²/cph)
60
40
20
0
-20
-40
2
5
10
15
20
25
30
FREQUENCY (cph)
SHETLAND ISLANDS EARTHQUAKE

Figure 9

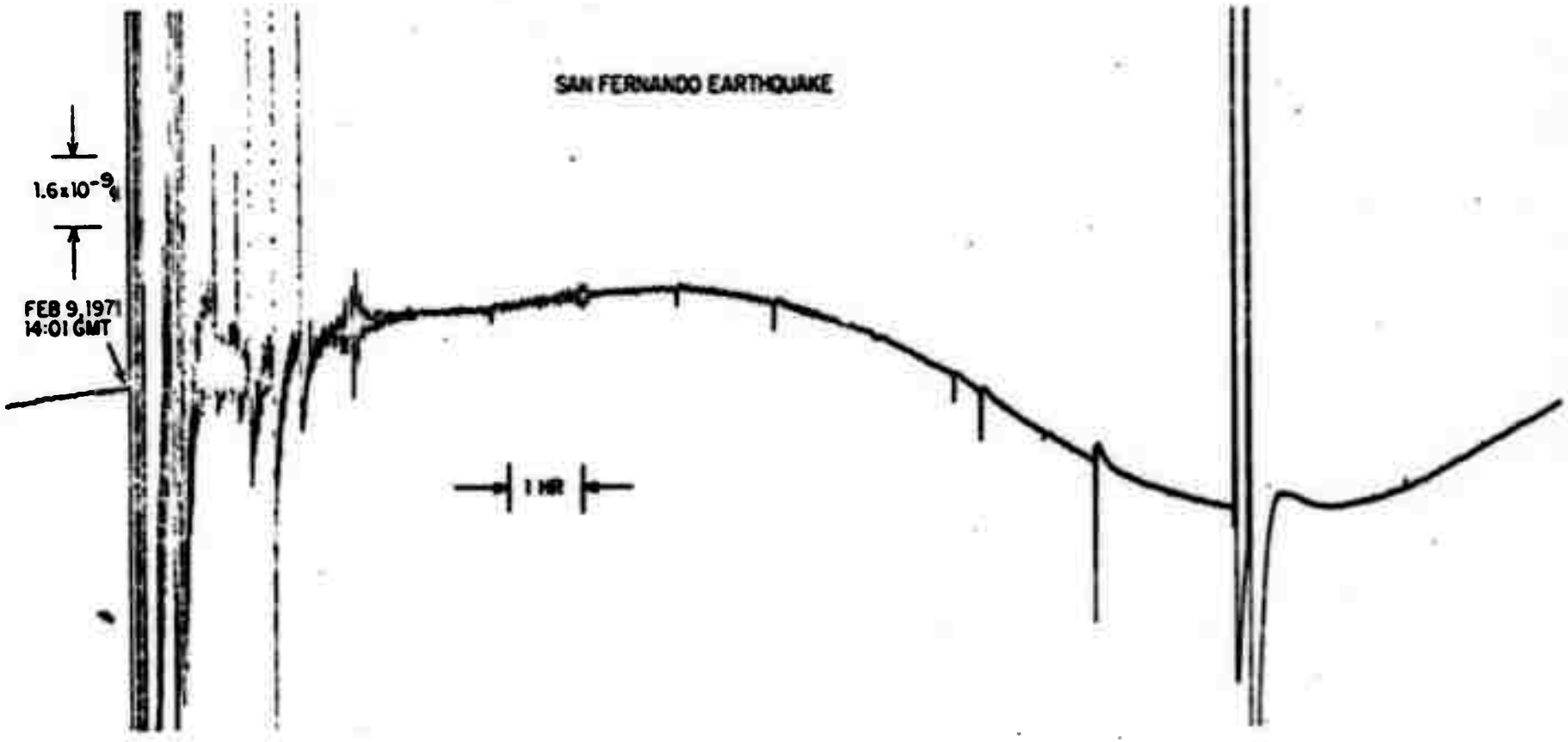

Figure 10

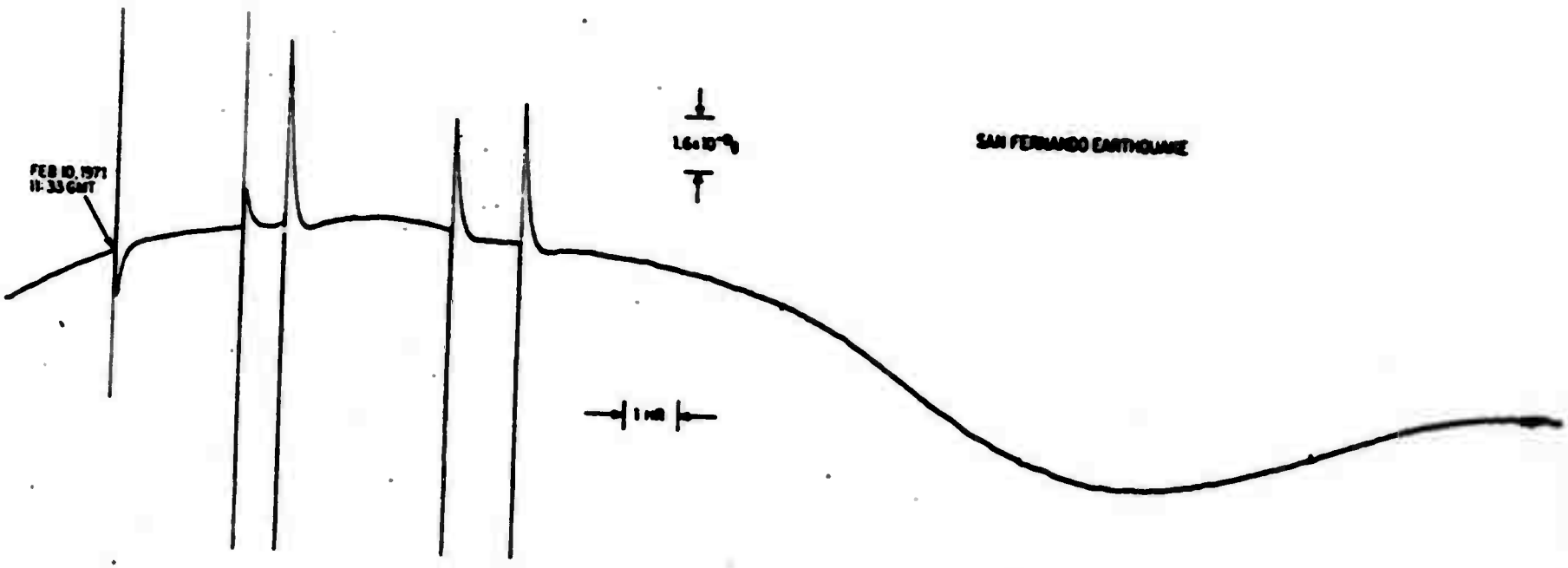

Figure 11

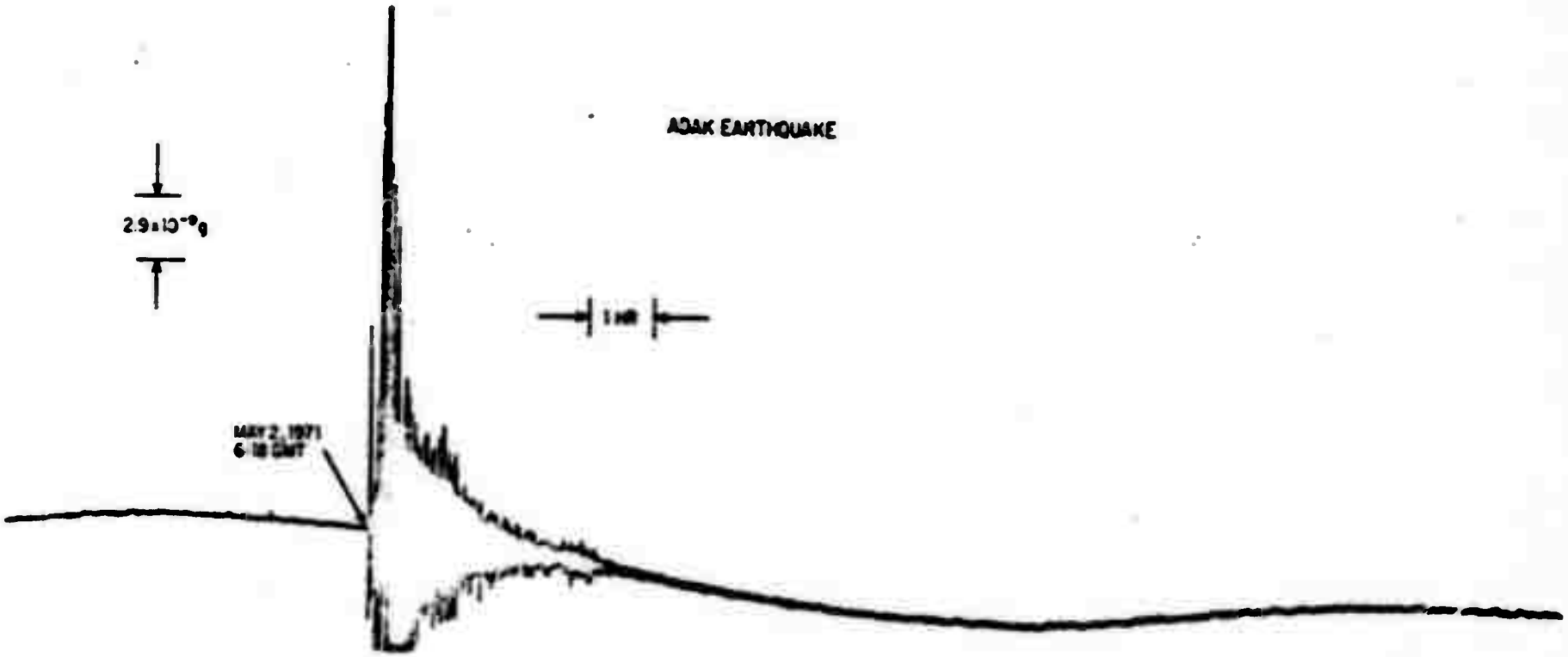

Figure 12

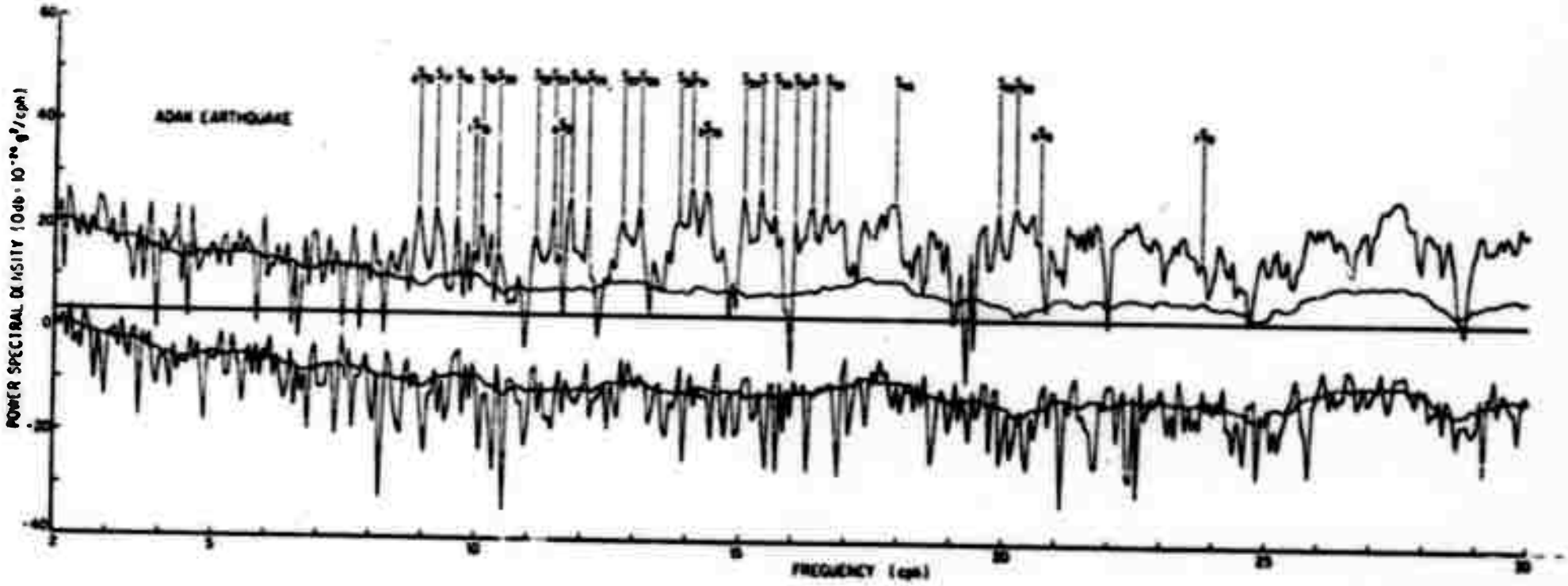
ADAK EARTHQUAKE
POWER SPECTRAL DENSITY (10db = 10⁻¹⁰ g²/cps)
FREQUENCY (cps)

Figure 13

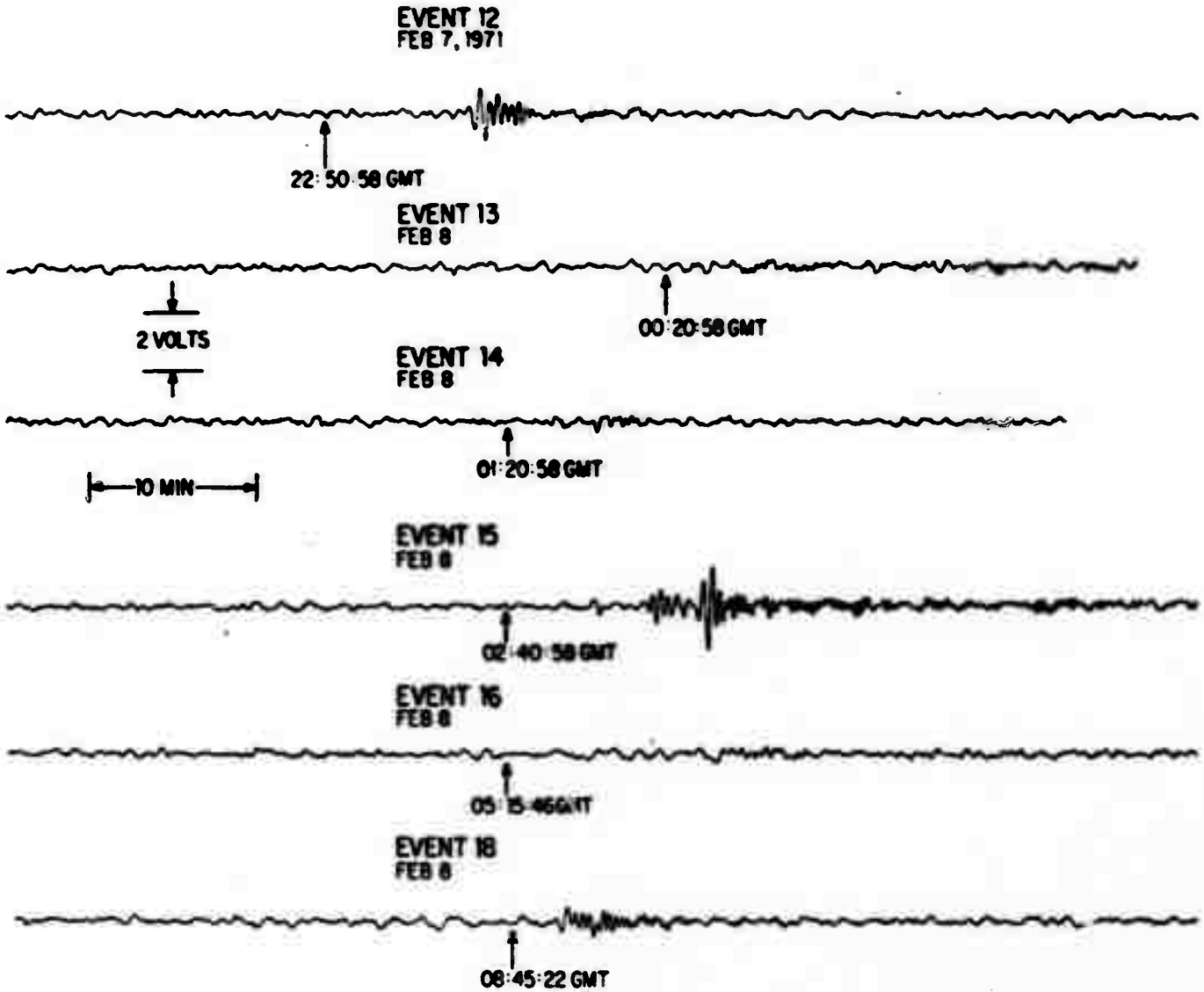
EVENT 12
FEB 7, 1971
22:50:58 GMT
EVENT 13
FEB 8
2 VOLTS
00:20:58 GMT
EVENT 14
FEB 8
01:20:58 GMT
10 MIN
EVENT 15
FEB 8
02:40:58 GMT
EVENT 16
FEB 8
05:15:46 GMT
EVENT 18
FEB 8
08:45:22 GMT

Figure 14

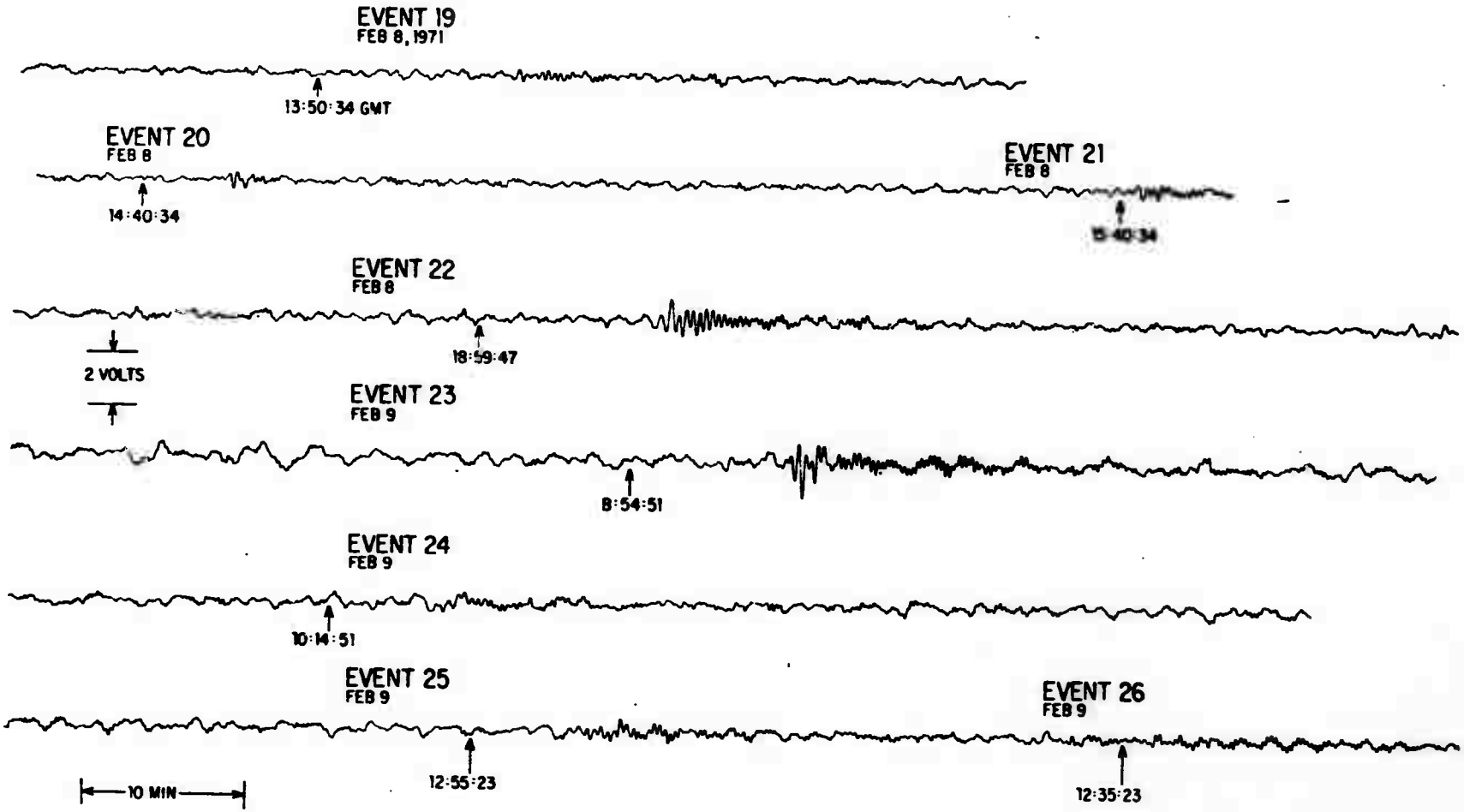
EVENT 19
FEB 8, 1971
13:50:34 GMT
EVENT 20
FEB 8
14:40:34
EVENT 21
FEB 8
15:40:34
EVENT 22
FEB 8
18:59:47
2 VOLTS
EVENT 23
FEB 9
8:54:51
EVENT 24
FEB 9
10:14:51
EVENT 25
FEB 9
12:55:23
EVENT 26
FEB 9
12:35:23
10 MIN

Figure 15

AFOSR - TR - 72 - 0608

A WIDE BAND HORIZONTAL ACCELEROMETER WITH PRELIMINARY EARTH NORMAL MODE AND SEISMIC INVESTIGATIONS

Jay Dratler, Jr.

and

Barry Block

Institute of Geophysics and Planetary Physics

University of California, San Diego

ABSTRACT

A wide band horizontal accelerometer using a quartz torsional pivot and capacitative position sensing with phase-sensitive detection is described. Devices for magnetic damping of unwanted modes of vibration and internal stabilization of temperature and pressure are discussed in detail. The accelerometer is small enough in size and weight to allow deployment in bore holes. Data from the earth normal mode band and the seismic band are shown. Although horizontal noise due to surface tilting is high for periods greater than 50 seconds, noise in the seismic band can be reduced by as much as an order of magnitude by digital high pass filtering. The resulting horizontal signal-to-noise ratio for teleseismic events is comparable to that for the vertical signals.

1. The Pendulum

Due to the presence of gravity, sensitive vertical accelerometers are in general harder to make than their horizontal counterparts. In vertical instruments, some spring device must precisely cancel the acceleration of gravity. Since the residual after cancellation must be below the desired level of measurement, stringent stability requirements are imposed on the spring device. Any changes in the spring force which opposes gravity appear as spurious output. Fortunately, this problem does not occur in horizontal measurements. Nearly all horizontal accelerometers are variants of two basic devices: the pendulum and the "swinging gate." Stability problems do occur in these systems, as the pivots or supports must work smoothly and consistently over long time periods. However, the problem here is not one of stability under stress.

Many different suspension systems have been used in horizontal accelerometers. Among them are knife edges, cross-spring pivots, and magnetic supports.[11,16,17] At the infinitesimal levels of motion and force involved in geophysical work, most of these devices have instabilities. They often pop or creak, and pivots made of metal tend to drift. The present design takes advantage of the excellent stability of a quartz fiber suspension developed for use in a vertical accelerometer.[6] The fiber suspension is made from a fused quartz rod 0.19 inches in diameter with ground

clamping flats at its center and ends. Two active sections, more than ten times smaller in diameter and each about 2.5 cm long, are drawn between the center and end sections. This design eliminates instabilities in the clamps, a common source of trouble in fiber suspensions, by providing large flats for positive contact.

At the fiber's center, a pendulum assembly is suspended. The pendulum is preferred to the "swinging gate" design, as the latter has a fundamental asymmetry with respect to gravity. The mass of the pendulum is a flat plate which aids in the magnetic damping of unwanted modes of vibration. It is sufficiently large, and the fiber is sufficiently weak, so that gravitational restoring forces predominate. Thus the fiber serves only as a stable loss-free pivot, and the free period of the device is its pendulum period. Motion of the pendulum is detected by means of a three-plate capacitative position sensor, whose center plate is attached to the pendulum assembly. The pendulum length is 25 cm. During construction, the fiber is rotated so that it is free of torsion when the pendulum hangs vertically. However, the fiber is kept under tension by means of an elinvar parallel-motion spring. The position sensor and the mechanisms for tensioning and rotating the fiber are the same as those in the vertical accelerometer.[6] Figure 1 shows the fiber suspension and pendulum assembly.

To avoid direct magnetic forces on the moving parts, all materials used in the pendulum assembly are free from magnetic contamination. Where strength is necessary, beryllium copper is

FIGURE 1

Photograph of fiber suspension and pendulum assembly for horizontal accelerometer. Fiber center section and active sections are visible in center of frame. Large detector plate serves as center element of three plate capacitative position sensor. Small plates attached a' fiber clamp are auxiliary damping paddles, which serve to reduce excitation of unwanted vibrations. One of lower auxiliary damping magnets is visible below paddle. Plate at right, in conjunction with elinvar parallel motion spring, maintains tension in fiber, which is set with large bolt at right. Slip rings under fiber end clamps allow rotation of fiber during assembly. Frame housing assembly mates wit', similar frame supporting outer plates of position sensor (*cf.* Figure 2). Tripod is not part of instrument.

FIGURE 2

Position Sensor Assembly. Note the damping magnets on the capacitor plates and plink stoppers in the arc of the magnets. Plates shown are from prototype vertical accelerometer. Those actually used for horizontal are twice as wide.

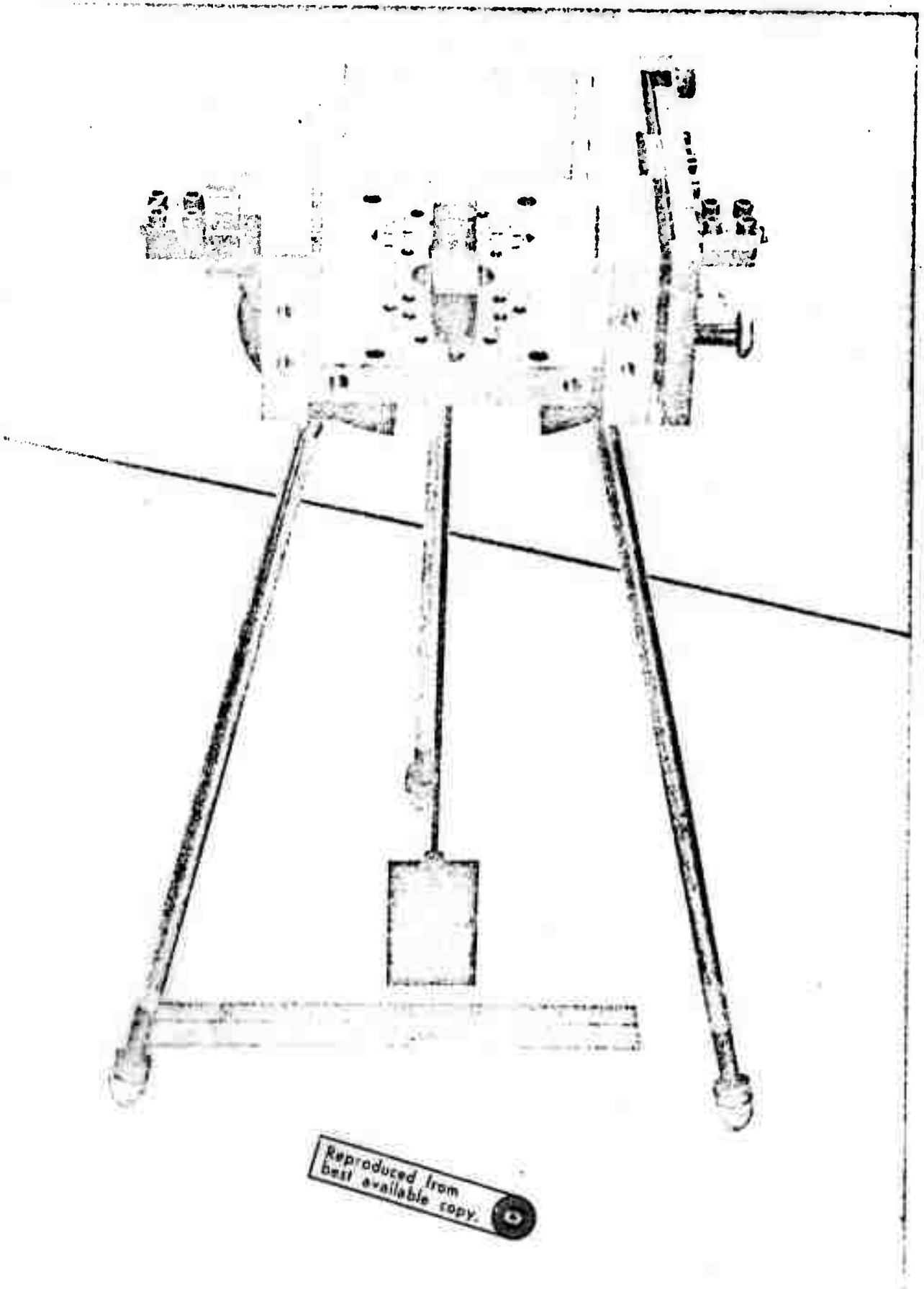

Reproduced from best available copy.

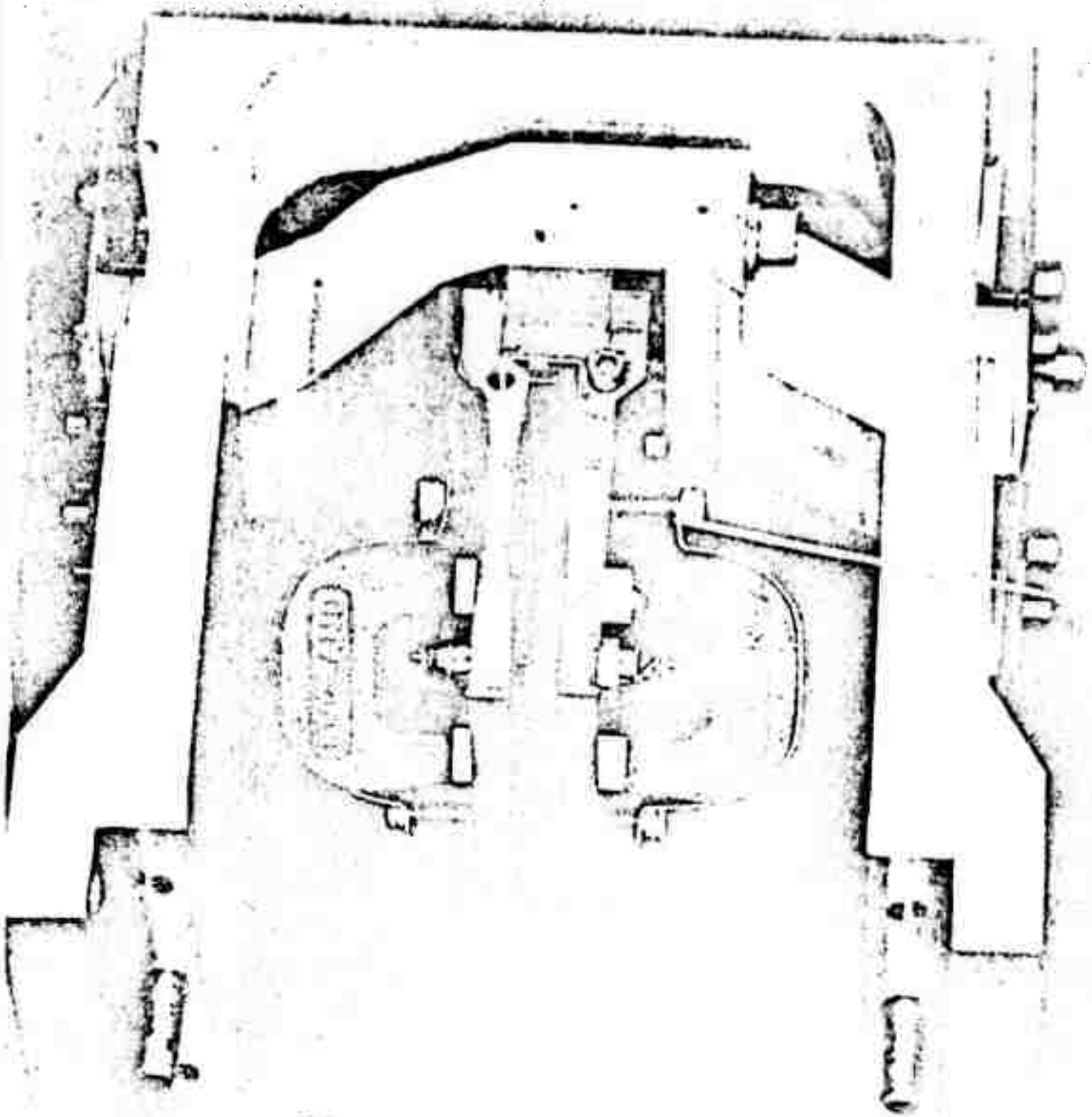

Reproduced from best available copy.

used. Otherwise, nearly pure (1100 series) aluminum or OFHC copper is used. Even the tiny 0-80 screws in the assembly are non-magnetic, being fashioned from beryllium copper.

Figure 3 shows an exploded drawing of the pendulum assembly. Beryllium copper clamps B6 and B9 mate with the ground flats on fiber center section B7. Pendulum mass B12, of OFHC copper, is supported by beryllium copper rod B11, which is contracted in the drawing. Aluminum detector plate B1, part of the position sensor, is attached to clamp B6 by means of quartz insulator B5 and beryllium copper clamping bars B2-B4. The purpose of aluminum auxiliary damping paddles B8 and B10 and pendulum damping magnets B13 and B14 is to aid in reducing excitation of unwanted modes.

In the fundamental mode of vibration, the pendulum executes small rotational oscillations about the fiber axis. For a small rotation θ away from the vertical, the restoring torque due to gravity has the form

$$\tau_g = -mL_m g \sin\theta = -mL_m g\theta \qquad (1.1)$$

where m is the mass of the entire pendulum assembly, including the support and clamps, and L_m is the distance of its center of mass from the fiber axis. This restoring torque corresponds to an effective gravitational torsion constant $mL_m g$. If the fiber has a torsion constant K and the pendulum assembly has a moment of inertia I about the fiber axis, the equation of undamped

FIGURE 3

Exploded diagram of pendulum assembly for horizontal accelerometer. Fiber center section B7 is held by fiber clamps B6 and B9 , and pendulum mass B12 is supported by rod B11. Detector plate B1 is is electrically insulated from rest of assembly by quartz insulator B5. Permanent magnets B13 and B14 damp unwanted vibrations by inducing eddy currents in pendulum mass B12. They are supported by sleeve (not shown) surrounding rod B11. Plates B8 and B10 are auxiliary damping paddles. Auxiliary damping magnets are not shown.

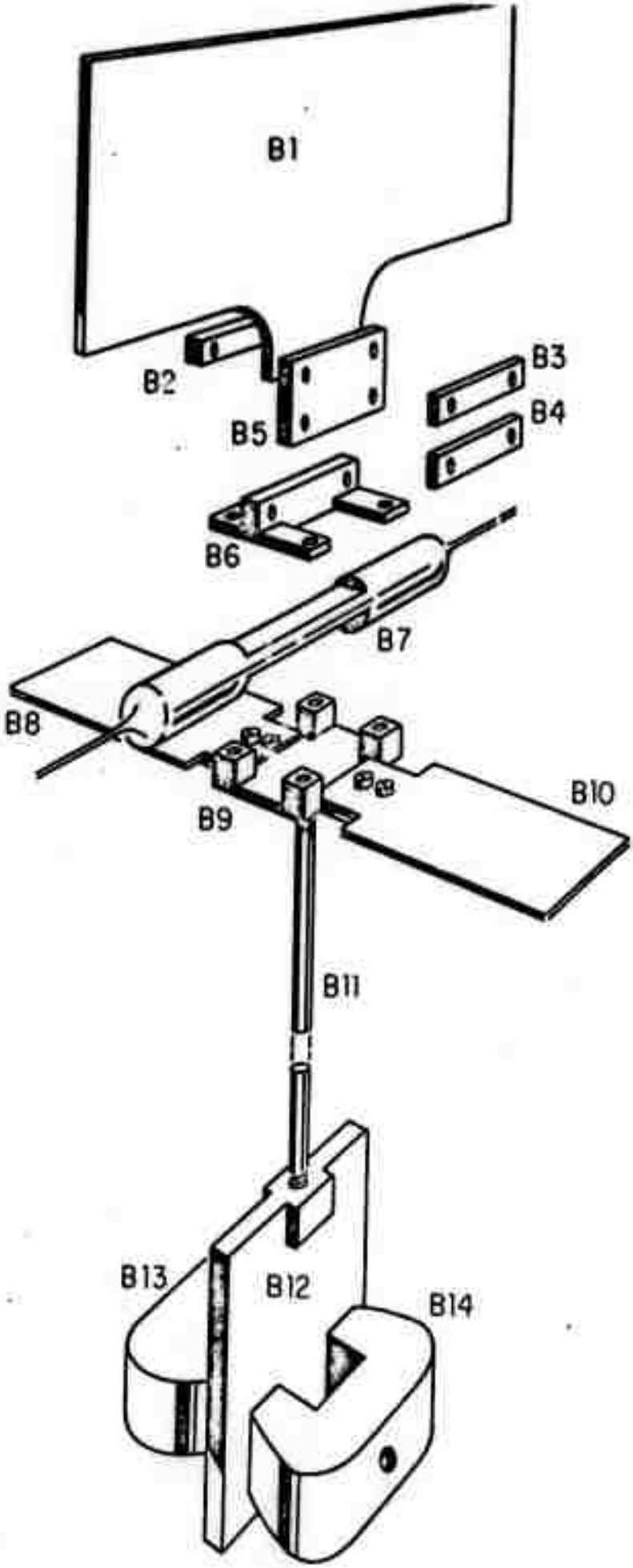
B1
B2
B3
B4
B5
B6
B7
B8
B9
B10
B11
B12
B13
B14

motion is

$$
\begin{aligned}
I\ddot{\theta} &= \tau_g - K\theta \\
\text{or} \quad I\ddot{\theta} &= -(mL_m g + K)\theta \qquad (1.2) \\
\text{or} \quad \ddot{\theta} + \omega_o^2\theta &= 0 \\
\text{where} \quad \omega_o^2 &\equiv \frac{mL_m g + K}{I}
\end{aligned}
$$

Equation (1.1) has been used for the gravitational restoring torque. Thus for small amplitude θ the fundamental mode is an harmonic oscillation with a free period

$$T_0 = \frac{2\pi}{\omega_0} = 2\pi\sqrt{\frac{I}{mL_m g + K}} \qquad (1.3)$$

The mechanical parameters of the instruments have the following approximate values

$$
\begin{aligned}
m &= 35 \text{ g} \\
L_m &= 15 \text{ cm} \qquad (1.4) \\
I &= 1.36 \times 10^4 \text{ g-cm}^2
\end{aligned}
$$

With these parameters, the effective torsion constant of gravity is $mL_m g \approx 5.1 \times 10^5 \ \frac{\text{dyne-cm}}{\text{rad}}$.

In the vertical instrument,[6,7] the fiber, which is torsionally stressed

to support the weight of the mass, has a torsion constant of $7.5 \times 10^3 \frac{\text{dyne-cm}}{\text{rad}}$. The torsion constant of the unstressed fiber in the horizontal must be even less. Thus, the fiber in the horizontal supplies at most 1.5% of the restoring torsion. As stated above, the horizontal accelerometer acts like a simple pendulum. Its free period is given by equation (1.3), with K being ignored as a small quantity. Substitution of the parameters (1.4) yields $T_0 = 1.0$ sec. The measured natural period is

$$T_0 = 0.910 \text{ sec} \tag{1.5}$$

2. Unwanted Modes of Vibration

The ideal mechanical system for an accelerometer is one with strictly a single degree of freedom. Unfortunately, this ideal cannot be physically realized, as every real system is three-dimensional and so has more than one mode of vibration. Residual non-linearities transfer energy from the unwanted modes to the fundamental mode. This coupling can be a major source of noise when the unwanted modes are highly excited.[6]

The fiber suspension has two advantages over other elastic supports in this respect. It has a high degree of symmetry, and it has an extra variable, the fiber tension, with which to control the unwanted modes. In the limit of infinite tension, the unwanted modes are absent and the fiber can only rotate. As shown by equations (1.2), the undamped frequency of the fundamental mode is independent of the fiber tension. All of the unwanted modes, however, have frequencies which increase as the fiber tension is raised. The fiber tension is adjusted so that the frequencies of the unwanted modes are separated from that of the fundamental and placed in regions of low seismic noise. This protects the fundamental mode from non-linear coupling. Additional protection is provided by magnetic damping assemblies which affect the unwanted modes preferentially.

Besides the fundamental mode, the fiber-pendulum system has four significant normal modes of oscillation, two translational modes and two twisting modes. The translational modes involve

horizontal and vertical motion of the fiber center perpendicular to the fiber axis, while the twisting modes involve rotation of the pendulum assembly. In one twisting mode the assembly rotates about its vertical axis of symmetry. In the other, it rotates about a horizontal axis perpendicular to the fiber. Together with the fundamental, the four modes comprise the three principal rotations and two of the principal translations of the system. Translation along the fiber axis is precluded by the supporting structure.

Crude estimates of the frequencies of the unwanted modes can be made from simple physical reasoning. For this purpose the pendulum assembly is characterized by its total mass m and its moments of inertia I_1 and I_2 about the two twist axes. It rests on the fiber center section of length ℓ_o, which is supported by the two active sections of length ℓ under tension T. Figure 4 illustrates the type of motion involved in each mode.

The two translational modes are functionally identical. As the center section of the fiber translates a small amount x, the active fiber sections make angles $\theta = x/\ell$ with their relaxed directions. The active sections are assumed to remain straight and unchanged in length, and their stiffness is neglected. Under these assumptions, the restoring force is provided by the component of the tension in the direction of the translation. Since there are two active fiber sections, the restoring force is

FIGURE 4

Schematic illustration of unwanted modes of vibration of pendulum assembly in horizontal accelerometer. Active fiber sections of length ℓ are assumed neither to stretch nor to flex. Fiber center section has length ℓ_0. Entire pendulum assembly has mass m and moments of inertia I_1, I_2 about two twist axes

(a) Vertical translation mode.

(b) Horizontal translation mode.

(c) First twisting mode. Rotation is about vertical axis of symmetry of pendulum assembly.

(d) Second twisting mode. Rotation is about horizontal axis perpendicular to fiber (out of paper in drawing).

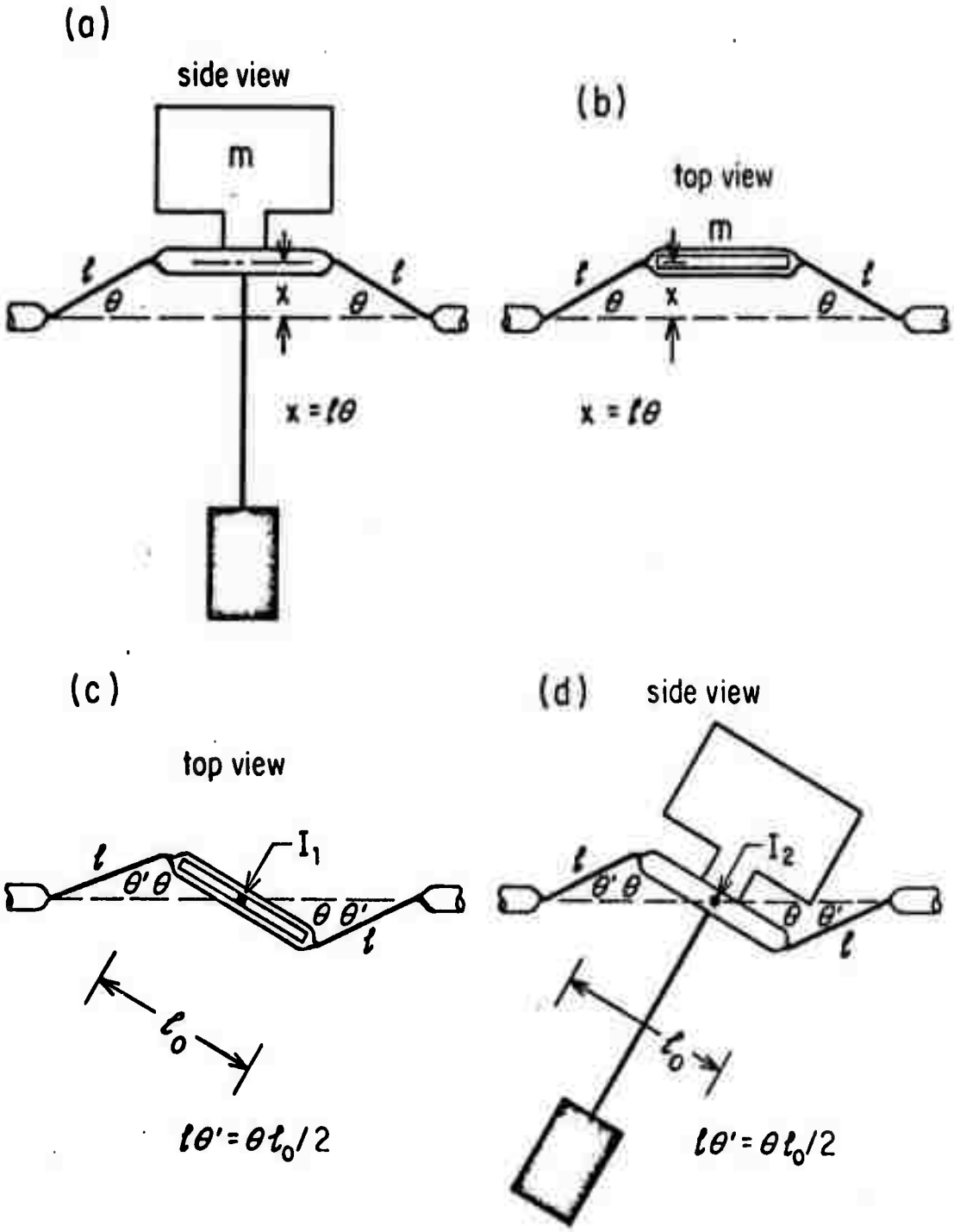
(a)
side view
m
ℓ
θ
x
θ
ℓ
x = ℓθ
(b)
top view
m
ℓ
θ
x
θ
ℓ
x = ℓθ
(c)
top view
ℓ
θ' θ
I1
θ θ'
ℓ
ℓ0
ℓθ' = θℓ0/2
(d)
side view
ℓ
θ' θ
I2
θ θ'
ℓ
ℓ0
ℓθ' = θℓ0/2

$$F = -2T \sin\theta = -2T\theta = -\frac{2Tx}{\ell} \qquad (2.1)$$

The equation of motion for the translations is

$$m\ddot{x} = F = -2T\frac{x}{\ell} \qquad (2.2)$$

or $\ddot{x} + \omega_t^2 x = 0$ where

$$\omega_t^2 = \frac{2T}{m\ell}$$

Thus the translational modes have a common frequency

$$f_t = \frac{\omega_t}{2\pi} = \frac{1}{2\pi}\sqrt{\frac{2T}{m\ell}} \qquad (2.3)$$

As promised, this frequency increases with the tension in the fiber, although only as its square root.

The two twisting modes are nearly alike, their only difference being in the moments of inertia. As the pendulum assembly twists through a small angle θ, the two active fiber sections make angles θ' with their original directions. Again their lengths are assumed to remain unchanged and their stiffness and bending is ignored. From the geometry shown in Figure 4, the following relation between the two small angles θ and θ' is obtained:

$$\frac{\theta \ell_0}{2} = \theta' \ell \tag{2.4}$$

A restoring couple is provided by the tension in the two active sections, which make angles $\theta+\theta'$ with respect to the center section. For small θ and θ', the restoring torque is

$$\tau = -2T \left(\frac{\ell_o}{2} \right) \sin(\theta + \theta')$$

$$= -T\ell_o (\theta + \theta') \tag{2.5}$$

$$= -T\ell_o \left(1 + \frac{\ell_o}{2\ell} \right) \theta$$

In the last expression, equation (2.4) has been used to eliminate θ'. Thus the equation of motion for a twisting mode is

$$I_r \ddot{\theta} = \tau = -T\ell_0 \left(1 + \frac{\ell_0}{2\ell} \right) \theta \tag{2.6}$$

or $\ddot{\theta} + \omega_r^2 \theta = 0$, where $\omega_r^2 = \frac{T\ell_0}{I_r} \left(1 + \frac{\ell_0}{2\ell} \right)$

Here I_r denotes the moment of inertia appropriate for the particular mode. The frequency of oscillation is

$$f_r = \frac{\omega_r}{2\pi} = \frac{1}{2\pi} \sqrt{\frac{T}{I_r} \left[\ell_o + \frac{\ell_o^2}{2\ell} \right]} \tag{2.7}$$

Like the frequency of the translational modes, it increases as the square root of T.

Typically, the parameters of the pendulum-fiber system have the following values:

$m = 35$ g	$\ell = 2.5$ cm
$T = 1\times10^6$ dynes	$\ell_0 = 7$ cm

From equation (2.3) the frequency of the translational modes is estimated as 24 Hz. The frequency of each twisting mode depends on the moment of inertia involved. About the vertical axis of symmetry, the moment is $I_1 = 35$g-cm^2, so the frequency is roughly 110 Hz, according to equation (2.7). The moment of inertia about the horizontal axis perpendicular to the fiber at its center is $I_2 = 1.36\times10^4$g-cm^2, so that the estimated frequency of twisting about this axis is 5.6 Hz.

Owing to the relatively large mass and length of the pendulum, the second twisting mode has quite a low frequency. Observations of the fiber pendulum-system in air indicate a frequency lower than the calculated value, about 3 Hz. Crude estimates for the frequencies of the translational modes from equation (2.3) are also in error. The frequency of the horizontal translation has been measured as 42 Hz in the completed instrument. The first twisting mode has never been observed.

Although in the vertical accelerometer one of the unwanted modes couples directly to the fundamental,[6] this is not the case in the horizontal instrument. In first order, the unwanted modes are relatively innocuous in the horizontal instrument. However, non-linear processes in the fiber can still cause coupling of energy when the unwanted modes are highly excited. This is particularly true for the second twisting mode, due to its low frequency. For this reason, magnetic damping is used to control the excitation of the unwanted modes.

The apparatus for damping the troublesome second twisting mode is shown in Figure 3. Pendulum damping magnets B13 and B14 produce a magnetic field which passes perpendicularly through copper pendulum mass B12. Motion perpendicular to the field lines causes eddy currents which dissipate energy by ohmic heating in the mass, while motion along the field lines is unaffected in first order. Hence the twisting mode, but not the fundamental mode, is damped. The vertical translation mode is also damped. In order to maximize eddy currents, the mass is made of copper. The magnets used, which have six pound pull, are mounted in a cylindrical sleeve not shown in the figure.

Preferential damping of the twisting mode depends critically on the shape and thickness of the mass and the positions of the magnets. Although the field of the magnets is primarily perpendicular to the pole faces, fringe fields are appreciable. Use of a thin, flat mass in the region of the most linear field minimizes

the effect of the fringe fields in damping the fundamental mode. Spacing of the magnets is determined by a compromise between the strength of the linear field at the center and the volume of copper affected by fringing fields. Optimum damping is obtained when a flat mass 0.1 inch thick is used and the separation between the pole faces and the surface of the mass is 0.05 in.

Other magnetic damping assemblies similar to those used in the vertical accelerometer aid in the elimination of unwanted modes. Two magnets similar to B13 and B14 are mounted on either side of the position sensor so that their fields pass perpendicularly through detector plate B1. These magnets, which are shown in Figure 2 , have the same effect as the pendulum damping magnets: they damp the vertical translation and second twisting modes. With the two systems working together, the Q of the twisting mode is reduced to less than 5, while the Q of the fundamental mode is 20. Auxiliary damping paddles B8 and B10, together with sixteen small magnets not shown, reduce excitation of the horizontal translation mode and the first twisting mode. With this auxiliary damping assembly, the Q of the horizontal translation is about 30.

3. The Position Sensor

The position sensor used to detect motion of the pendulum is identical to that in the vertical accelerometer. It is described in detail elsewhere.[7] The essential component is a three-element parallel plate capacitor whose center element is aluminum detector plate B_1 in Figure 3. The stainless steel outer plates of this capacitor are stationary, being separated by a stable quartz spacer. They are shown in Figure 2.

The outer plates of the sensing capacitor are driven out of phase at a frequency of 16kHz by precisely matched secondaries of a toroidal transformer. The resulting signal on the detector plate is proportional in amplitude to the displacement of the center plate from the null position. After preamplification, the center plate signal is synchronously detected with respect to the original drive signal. The output of the phase sensitive detector is then a measure of the position of the detector plate. As a whole, the position sensor is quite linear if fringing fields in the capacitor are neglected.[12] Its sensitivity is high enough to permit detection of .05Å displacements over averaging times of the order of 1 sec.[7]

Placement of the detector plate is dictated by the requirements of ease of design. Although the gain of the sensing system is obviously greater if the sensor center plate is the pendulum mass itself, the sensitivity of the sensor is sufficient to allow detection at the present position without serious loss of

gain. The advantage accruing from such a design is that the proven structure of the sensor, fiber, clamps and frame from the vertical accelerometer are employed without alteration. The gain loss is recovered simply by increasing the electronic amplification. The end clamps and tensioning mechanism for the fiber, the position sensor plates and their mounting and adjusting apparatus, and the supporting frames are the same as in the vertical instrument. There is, however, no need for external adjustment of the sensor null position, as the horizontal instrument can be zeroed by tilting. Thus, the parallel motion springs upon which the outer sensor plate assembly rides[6] are locked under tension at the time of construction and no mechanical coupling is necessary. The assembled accelerometer is shown in Figure 5.

Though it is possible to apply electrostatic feedback to the detector plate to close the accelerometer loop, all the preliminary data have been taken in the open loop configuration. Feedback operation is accomplished in exactly the same way as in the vertical instrument.[7] Inverted and non-inverted outputs from the lock-in-amplifier are applied to the outer plates of the position sensor. In conjunction with a small bias voltage on the detector plate, these equal and opposite feedback voltages produce a linear electrostatic force on the center plate. A feedback network, consisting of an integrator and compensator, tailors the gain and phase of the loop to make the system stable. The integrator provides high loop gain for

FIGURE 5

Photograph of assembled horizontal accelerometer, showing mating frames for fiber-pendulum assembly and outer transducer plates. Fiber tensioning plate of Figure 1 is facing camera. Insulated plink stoppers in center of outer transducer plates are visible inside mode damping magnets. Quartz spacer supporting outer plates is attached to yoke which rides on parallel-motion springs (not visible) at right and left. Since transducer zero is adjustable by tilting, bolt in bracket under thumb at left locks yoke in position under tension of springs. Supports at top of upper frame attach to top of hard vacuum can. At right is C. William Van Sice, who assembles instruments, and at left is Jay Dratler, Jr. Barry Block is taking picture.

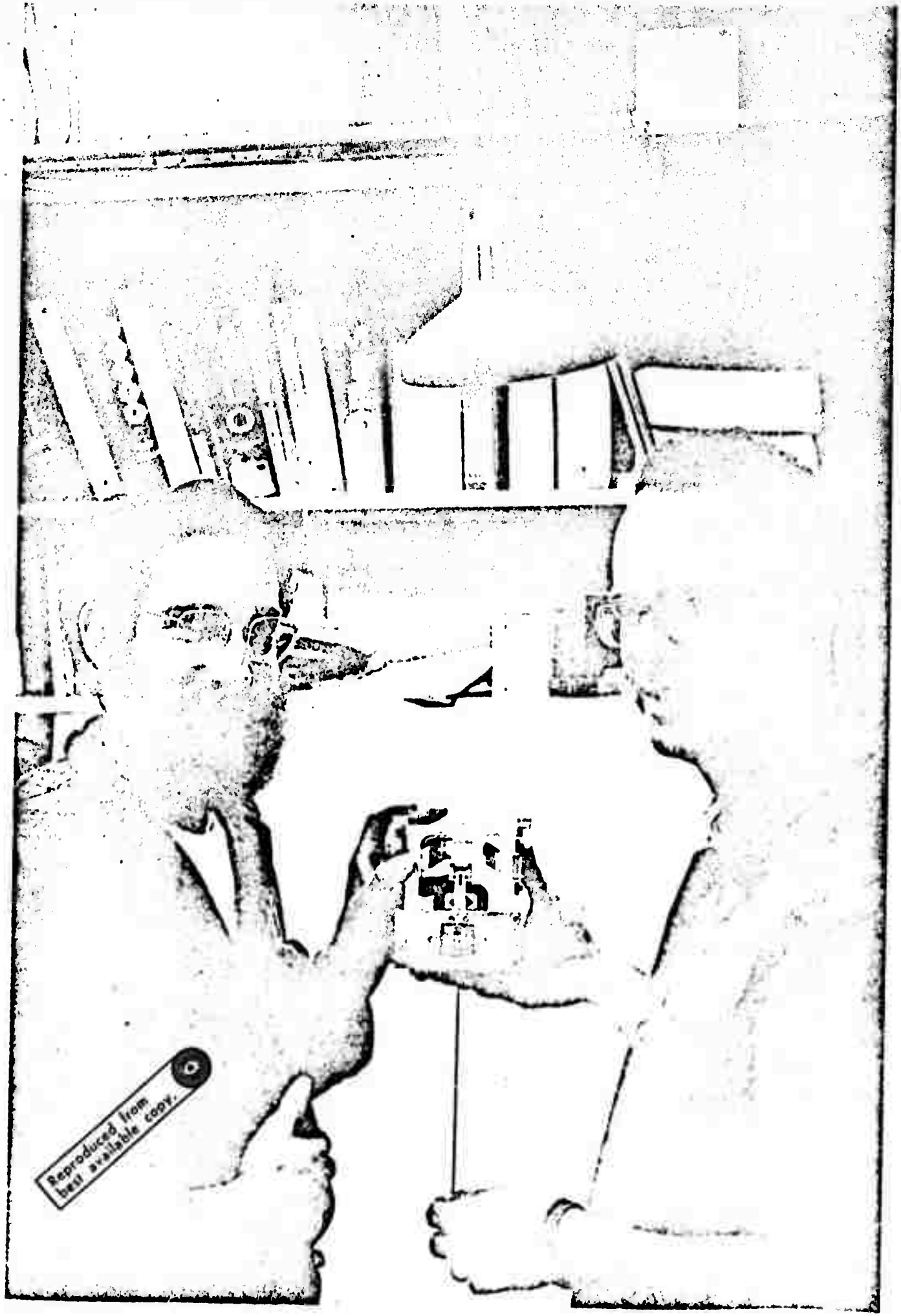

Reproduced from best available copy.

stability at low frequencies, while the compensator reduces the resonance peak of the pendulum. In fedback operation, the instrument output is taken from the integrator.

The advantages of fedback operation are stabilization of response at low frequencies and reduction of actual pendulum motion, which results in greater linearity. Because the fiber is torsionally unstressed, the open-loop linearity of the horizontal accelerometer is *a priori* far greater than that of the open-loop vertical instrument. For investigations of teleseisms, long term stability of response is not important, so feedback is of little value.

4. Environmental Control

Like its vertical counterpart,[6] the horizontal instrument features precise internal control of the mechanical system's environment. Pressure is maintained by a system of sealed containers, while temperature is regulated by a fedback temperature controller in conjunction with elaborate thermal insulation. The pendulum assembly, fiber, transducer, and supporting frames are enclosed in a stainless steel hard vacuum can sealed with a gold O-ring. Pressure in the can is 10^{-7} torr. During evacuation, the can and its contents are baked at 400°C for 48 hours, so that complete stress relief of metal parts and a stable high vacuum are assured.

Several purposes are served by sealing the basic accelerometer in a high vacuum environment. First, isolation from external pressure fluctuations is obtained. In the absence of such isolation, changes in buoyant forces on the pendulum and in the dielectric of the position sensor constitute sources of noise. Second, the mean free path for molecules in the dilute gas is made larger than a typical dimension of the space inside the container. Thus, convection and its attendant problems are precluded. Third, the low thermal conductity of the high vacuum provides

thermal isolation which aids in stabilizing the temperature of the fiber.

With the exception of part of the temperature control system, the hard vacuum can and its contents constitute the deployable part of the accelerometer. The small diameter (8 inches) and light weight (20 lbs) of this unit make it suitable for deployment in bore holes to escape the effects of local surface tilting. Such tilting, which is the most formidable source of earth noise, has been observed to decrease with depth of deployment.[19] For bore hole use, redesign of the temperature control system for compactness is necessary. No effort has yet been made to minimize either the size or weight of the accelerometer or the temperature controller.

For deployment in vaults, where space is plentiful, the environmental control is completed as follows. The hard vacuum can is enclosed in a thick-walled aluminum soft vacuum can sealed with a standard rubber O-ring. Evacuated to a pressure of 1 torr, this can provides additional pressure and temperature isolation. The temperature of the can is maintained precisely at 40°C by ohmic heating in a bifilar wire wound on its surface, the current in which is supplied by a remote power amplifier. A bifilar winding is used to eliminate inductive effects. Heater current is controlled by the error signal from a precision thermistor bridge and high gain preamplifier. The thermistor is mounted directly on the heater winding with thermally conducting epoxy. Phase compensation

and response-tailoring feedback at the power amplifier insure that the thermistor bridge, preamplifier, power amplifier and heater form a stable closed loop.[7] For further thermal isolation, the soft vacuum can with its heater winding is surrounded by several inches of polystyrene balls in a thermal insulation can. Long lightweight cables (RG/187/U coaxial cable and 30AWG ribbon cable), coiled in the thermal insulation, provide connections between the soft vacuum can and the cables leading out of the vault while maintaining a high resistence to heat flow. The soft vacuum can and thermal insulation can are mounted on a remotely controlled tilting platform used to level and calibrate the instrument. Long legs made from thin-walled stainless steel tubing support the soft vacuum can without ruining the thermal isolation. The soft vacuum can, thermal insulation, temperature controller, and tilting platform are the same as in the vertical instrument.[6,7] The only difference is that the soft vacuum can in the horizontal has longer legs and a snoot to house the protuberance on the hard vacuum can.

5. Temperature Stabilization

In the vertical accelerometer, precise temperature control is needed because the torsion in the fiber, which has a large temperature coefficient, balances the entire force of gravity. This difficulty does not occur in the horizontal instrument, where quiescent torsion in the fiber is small (See section 1). Theoretically, the horizontal accelerometer has zero temperature coefficient. In practice, however, a temperature dependence arises from errors in setting the fiber at its torsionally unstressed position during

assembly. Due to such errors, there is some small torsion in the fiber when the instrument is level. Changes in this torsion with temperature produce spurious output.

A worst-case analysis proceeds as follows. The maximum error in installing the fiber is $\theta_e \approx 0.1$ radian of rotation. The tortion constant for the fiber in the vertical accelerometer is given in Section 1. Since the initial rotation of the fiber in the vertical is considerable, the torsion constant for small additional rotations must be larger than the torsion constant of the nearly unstressed fiber in the horizontal. Thus, a reasonable upper bound for the torsion constant in the horizontal is

$$K_h \approx 7.5\times10^3 \ \frac{\text{dyne-cm}}{\text{rad}} \tag{4.1}$$

The corresponding upper limit for the quiescent fiber torsion in the levelled horizontal instrument is $K_h\theta_e \approx 7.5\times10^2$ dyne-cm. Using the values of the mass m and effective torsional lever arm L_m of the pendulum assembly given in equations (1.4), the equivalent horizontal acceleration is estimated as

$$a_h = \frac{K_h\theta_e}{mL_m} \approx 1.4\text{cm/sec}^2 \approx 10^{-3}g \tag{4.2}$$

The fiber positioning error in the horizontal produces a maximum effective acceleration of $10^{-3}g$. The temperature coefficient

of the torsion constant of the quartz fiber is[6]

$$\Delta K_h/K_h = 1.2\times10^{-4}/^\circ C \qquad (4.3)$$

This results in a temperature-induced input to the horizontal accelerometer of

$$\Delta a_h/a_h = 1.2\times10^{-4}/^\circ C \qquad (4.4)$$

$$\text{or} \qquad \Delta a_h = 1.2\times10^{-7} g/^\circ C$$

Since the fiber torsion in the vertical accelerometer balances the entire force of gravity, temperature induced noise in the horizontal is 1000 times less than that in the vertical.

Although the horizontal accelerometer is far less susceptible to temperature fluctuations than the vertical, fairly precise temperature control is needed for accurate geophysical measurements. To measure teleseismic accelerations of 10^{-10}g, for instance, the fiber temperature must be stable at the millidegree level. This temperature regulation is accomplished in two ways. First, the mechanical system is isolated from environmental temperature changes by the system of passive thermal insulation consisting of the hard and soft vacuum cans and the polystyrene balls. Second, the temperature of the control surface surrounding the soft vacuum can is held fixed by the fedback temperature controller. The vacuum cans provide thermal filtering between the fiber and the control surface, while the polystyrene balls isolate the control surface from the outside world.

In considering the thermal insulation, an analogy with RC lowpass filters in electronics is useful. A system with a large heat capacity is contained in a can with low thermal conductivity, i.e., high thermal resistance. Temperature fluctuations in the external environment create a temperature difference between the inside and outside of the can. This difference drives a thermal current, namely a heat flow, into the inner system. The heat flow is related to the temperature difference by the integrated thermal resistance of the outer can, which is analogous to the resistance in Ohm's Law. As the thermal current heats the inner system, it causes a temperature rise proportional to its integral over time and inversely proportional to the system's heat capacity. This is analogous to the charging of a capacitor. Taken as a whole, the thermal system is like an RC lowpass filter. When a temperature step is generated outside the can, some time elapses before enough heat can flow through the can's resistance to "charge" the inner system to a higher temperature. The time required for 1/e of the external temperature step to appear at the inner system is the thermal time constant. It increases directly as the thermal resistance of the container and the thermal capacitance of the inner system. As in the electronic lowpass filter, any sinusoidal fluctuation in external temperature whose period is appreciably shorter than the time constant is considerably attenuated at the inner system.

This analogy between thermal and electronic filters, however, cannot be carried too far. The parameters of the electronic circuit are localized in discrete components, while the thermal resistance and capacitance are mixed and distributed over space. The outer container, which acts as the thermal resistor, has a fair amount of heat capacity, and the thermal capacitor has some thermal resistance. Both the thermal resistance and capacitance depend on the details of construction, materials, and parts placement. For this reason, such thermal systems are quite difficult to analyze mathematically. The general idea of a lowpass filter with a characteristic time constant is useful in estimating the effectiveness of thermal insulation.

In the quartz fiber accelerometer, there are three stages of thermal filtering. The high thermal resistance of the polystyrene balls, followed by the large heat capacity of the soft vacuum can, constitutes one stage of filtering. The next stage relies on the thermal resistance of the soft vacuum and the thermal capacity of the hard vaccum can. Finally, the thermal resistance of the hard vacuum, coupled with the thermal capacity of the mechanical system and its frame, provide the third stage of filtering.

Reductions in the effective thermal resistances due to alternate paths of heat flow are quite important. The polystyrene insulation, for instance, is bypassed by a thermal path through the tilting platform and up the three legs which support the soft vacuum can. These legs are made of thin-walled stainless steel tubing to maximize the thermal resistance of this path. Similarly,

heat can flow through the legs on which the hard vacuum can is suspended inside the soft vacuum can and thus bypass the soft vacuum itself. Mica sheets between these legs and the top of the soft vacuum can increase the thermal resistance of this path. The hard vacuum is bypassed by the short legs with which the mechanical system and its frame are suspended. Since these legs are not insulated, the final stage of thermal filtering is not as effective as the others. Another important thermal path is through the tilting platform, which is a large, thick plate of aluminum. To protect it from direct exposure to the thermal environment, it is usually surrounded by polystyrene balls contained in a circular layer of foam rubber on the vault floor.

Perhaps the most damaging alternate path of heat flow is through the electrical cables to the mechanical system and temperature sensor. In order to maximize the effective thermal resistance of these cables, lengths of them are coiled inside the thermal insulation can. In addition, lightweight cables are used to connect the mechanical system to the external electronics. The coaxial cables are teflon-insulated RG187/U , while the other conductors are part of a 30AWG ribbon cable. After emerging from the thermal insulation can, these cables are connected to heavier standard cables (RG62/U and 18AWG multiconductor), which connect the deployable unit to the electronics panel. With the thermal insulation constructed as outlined , the time constant for heat transfer between the outside world and the fiber is several hours. Thus,

the thermal filtering drastically reduces the effects of external temperature fluctuations with periods of a few minutes or less. Lower frequency variations are eliminated by the temperature controller.

Figure 6 shows a flow chart of the fedback temperature controller. The thermistor measures the temperature at a point on the control surface. The temperature sensor and preamplifier compares the termistor resistance to that of a standard. When the two differ, it produces an error signal proportional to the difference. This temperature error signal is sent to the fedback power amplifier, whose output determines the current in the resistive heater wound around the control surface. The error signal changes the heater current to bring the control surface temperature back to the null point. Since the null point, which is determined by the resistance of the standard in the sensor, exceeds room temperature, there is always current in the heater winding. This mean current compensates for thermal leakage through the insulation. Fluctuations in the heater current maintain the thermistor temperature fixed within 4×10^{-6}°C per 100 sec and 4×10^{-8}°C per day.[7]

FIGURE 6

Flow chart of fedback temperature controller for accelerometer. Control surface is metallic cylinder surrounding mechanical instrument. It is thermally insulated from both fiber and external environment.

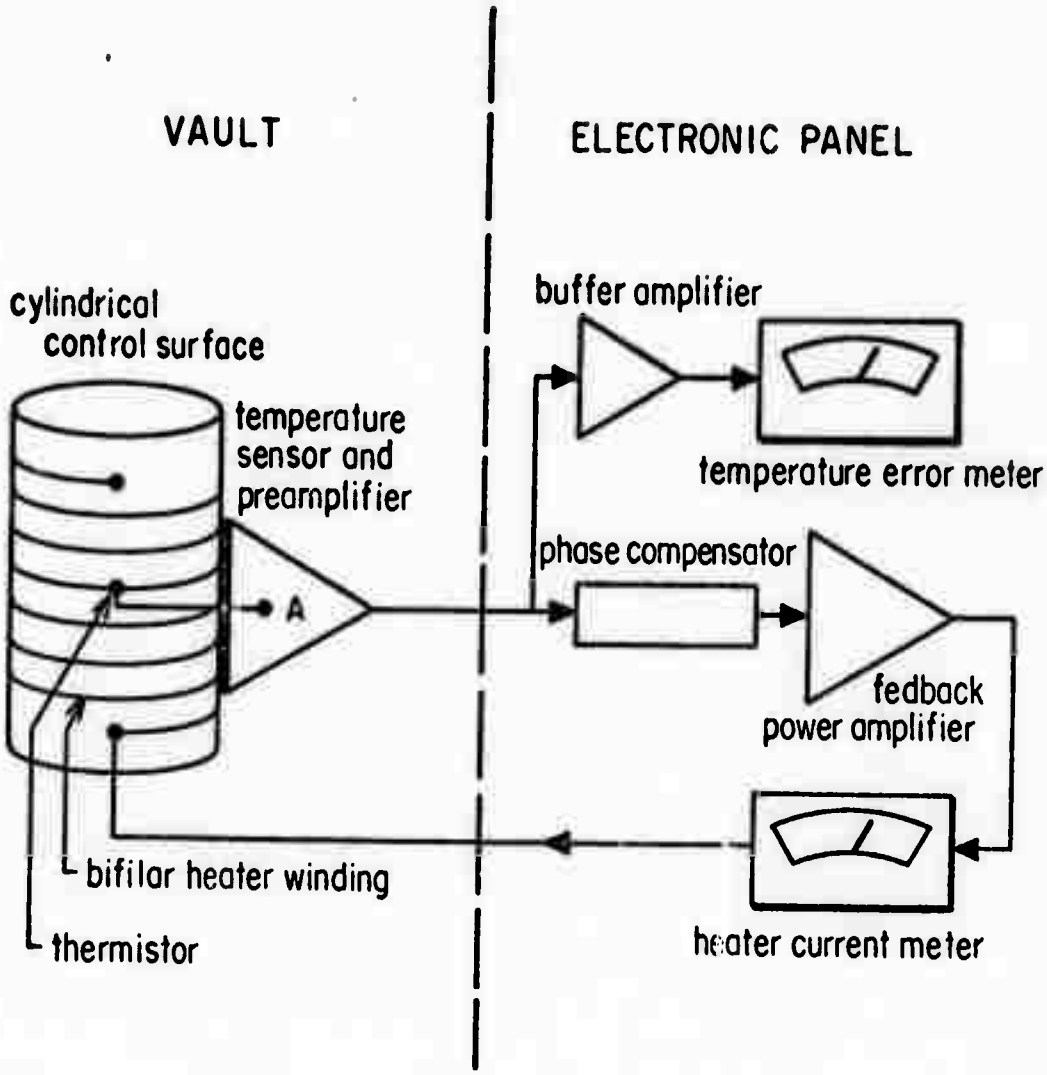
VAULT
ELECTRONIC PANEL
cylindrical
control surface
temperature
sensor and
preamplifier
A
buffer amplifier
temperature error meter
phase compensator
fedback
power amplifier
bifilar heater winding
thermistor
heater current meter

In practice, the active temperature controller and the passive thermal insulation interact considerably. Not only does the insulation determine the mean heater current needed to maintain a given temperature, but it also affects the stability of the temperature controller. For small fluctuations in the heater current, it controls the loss of heat from the surface and thus limits the thermal lag between the heater and thermistor.

Since this thermal lag is primarily responsible for difficulties in stabilizing the fedback controller, improvement in the thermal insulation is thus one of the expedients to be used in stabilizing recalcitrant control systems. As in the case of the design of the insulation itself, calculations of the stabilizing effects are made prohibitively difficult by the fact that the parameters are distributed. Such improvements are most quickly made by trial and error.

The temperature controller can increase the need for thermal insulation by providing small thermal fluctuations of its own. As heating depends on the square of the current, the controller as a whole is a non-linear system. It is subject to marginal instabilities. Usually, these are at rather high frequencies where the controller loop gain is low. In the presence of strong environmental temperature drift, however, the controller sometimes cycles at the higher teleseismic frequencies. To reduce the effect of these low-level thermal oscillations, the control surface is placed on

the outside of the soft vacuum can, where it is better insulated from the fiber.

When the temperature controller is working properly, it complements the thermal insulation by providing regulation for periods longer than the time constant of the thermal filtering. The loop gain of the temperature controller is quite high below 10^{-4} Hz and falls 20 db/dec above this frequency.

The active device thus provides good regulation where the passive insulation is ineffective. Conversely, the insulation attenuates temperature fluctuations at higher frequencies, where the low loop gain reduces the effectiveness of the temperature controller. The frequency region of worst temperature regulation is in the neighborhood of 100 sec periods, where neither the active nor the passive system is optimally effective.

The overall effectiveness of the temperature regulation is best measured by the quality of the accelerometer output. In the seismic spectral region, data from the vertical accelerometer indicate that the total instrumental noise level is below ground noise levels, which are of the order of 10^{-10}g. Thus stabilization of the fiber temperature over teleseismic periods (20-50 sec) is good to a microdegree. As for vertical tidal observations, they agree with theory to better than 1%. This implies fiber temperature control of the order of 10^{-5}°C over half-day periods. The only exception to the generally high degree of stability is in the neighborhood of 100 sec periods. Some unexplained noise has been observed in this region. However, the origin of this noise is not known, since ground noise levels at these frequencies have not been accurately determined.

6. Response and Gain

In open-loop operation, the response of the horizontal instrument is determined primarily by the pendulum assembly. There is a well determined DC gain, and the response is flat from DC to the neighborhood of the natural resonance frequency. To derive the transfer function of the pendulum assembly, consider the pendulum subject to a possibly time dependent horizontal acceleration a_h. There are three pertinent torques: the inertial torque, the gravitational restoring torque, and the damping torque. Since it is small compared to the gravitational restoring torque, the fiber torsion is neglected. Let θ be the angle the pendulum makes with the instrumental vertical, and assume $\theta \ll 1$. The instrumental and local gravitational vertical are assumed to coincide. The inertial force acts at the center of mass, and has magnitude ma_h. Since its lever arm is L_m, the torque is

$$\tau_i = ma_h L_m \cos\theta = mL_m a_h \tag{6.1}$$

The restoring torque due to gravity is given in equation (1.1). The damping torque is simply given by

$$\tau_d = -b\dot{\theta} \tag{6.2}$$

where b is some damping constant with dimensions of torque times time and the dot denotes a time derivative. The rotational equation of motion of the pendulum can be written

$$\ddot{\theta} + \frac{\omega_0}{Q}\dot{\theta} + \omega_0^2\theta = \frac{mL_m}{I} a_h \tag{6.3}$$

where $Q = \frac{I\omega_0}{b}$ and $\omega_0^2 = \frac{mL_m g}{I}$

The position sensor does not measure θ, but the displacement δ of the geometrical center of the detector plate with respect to its null position. Let L be the distance between the fiber axis and this geometrical center. Since the sensor geometry is unchanged, L is the same as in the vertical instrument. Use of the relation $\delta = L$ yields the following equation of motion for δ:

$$\ddot{\delta} + \frac{\omega_0}{Q}\dot{\delta} + \omega_0^2\delta = C_m a_h \tag{6.4}$$

where $C_m = \frac{mL_m L}{I}$

The transfer function is obtained by assuming a steady state solution $\delta(\omega)e^{i\omega t}$ for a driving acceleration of the form $a_h(\omega)e^{i\omega t}$ and solving equation of motion (6.4) for $\delta(\omega)$. In terms of the displacement amplitude $\delta(\omega)$ the response of the pendulum assembly to horizontal acceleration is

$$S_p(\omega) = \frac{\delta(\omega)}{a_h(\omega)} = \frac{C_m/\omega_0^2}{\left[1 + \frac{i\omega}{\omega_0 Q} - \frac{\omega^2}{\omega_0^2}\right]} \qquad (6.5)$$

This is of the same form as the response of the mass-fiber system in the vertical accelerometer.

As in the vertical, the DC gain depends on the dimensionless constant C_m and the square of the free period. The constant C_m depends only on mechanical parameters: the total mass m, the center-of-mass distance L_m, and the moment of inertia I. The damping of the pendulum system is described in terms of a Q. Since the position sensing and feedback electronics are the same for both the vertical and horizontal instruments, the general shapes of the open and closed loop response functions are the same. The only substantial difference between the two instruments lies in the dependence of the pendulum frequency on the acceleration of gravity, rather than fiber torsion constant.

It is of interest to calculate the ratio of the DC open loop gains of the horizontal and vertical instruments. According to equations 6.4 and 6.5, the DC response of the pendulum system is given by the expression

$$S_p(0) = C_m/\omega_0^2 = \frac{mL_m L}{I\omega_0^2} = \frac{mL_m L\, T_0^2}{4\pi^2 I} \qquad (6.6)$$

where $T_0 = \frac{2\pi}{\omega_0}$ is the free period.

This gain has the same form as that for the vertical accelerometer's mass-fiber system. Since L is made the same in both instruments, the horizontal-to-vertical DC gain ratio is given by

$$\frac{S_p(0)}{S_m(0)} = \frac{m_h}{m_v}\,\frac{L_{mh}}{L_{mv}}\,\frac{I_v}{I_h}\,\frac{T_{0h}^2}{T_{0v}^2} \qquad (6.7)$$

where the subscripts v and h denote the obvious.

Numerical values of the quantities in expression (6.7) are obtained by a combination of calculation and measurement. The masses are determined by direct weighing of parts, while the moments of inertia are calculated from the known weights and dimensions. Moment arm L_{mh} is determined by balancing the pendulum assembly, and L_{mv} is calculated from part weights and blueprint dimensions. The free periods are measured from chart recordings of the decaying fundamental mode oscillations. In Table 1, parameter values for a typical vertical instrument and the prototype horizontal instrument are listed. The gain ratio (6.7) is computed as

$$\frac{S_p(0)}{S_m(0)} = 0.18 \qquad (6.9)$$

TABLE 1

Comparison of Mechanical Parameters of Vertical and Horizontal Accelerometers

Parameter	Units	Vertical (Q3)	Horizontal (H1)
m	gram	9.47	35
L_m	cm	3.5	15.0
L	cm	3.5	3.5
I	g-cm^2	124	13,600
$C_m = \frac{mL_mL}{I}$	none	0.94	0.14
T_o	sec	0.807	0.910
Q	none	21.2	20.1

The DC open loop gains have been measured for both instruments. Their ratio is 0.13, which is 26% below the value calculated from crude measurements of the moments.

There is one important difference between the vertical and horizontal instruments which is not illuminated by response calculations. Below the resonance frequency, the horizontal is a tiltmeter, while the vertical measures tilt only in second order. In deriving the response 6.5 for the horizontal, it was assumed that the instrumental and local gravitational verticals were coincident. If this is not true, there may be a non-zero component of the acceleration of gravity along the degree of freedom of the accelerometer. Such a component of gravity along the instrumental horizontal depends on the sine of the tilt angle, so there is a linear relationship between tilt and accelerometer output for small DC tilts. The output of the horizontal accelerometer can thus be calibrated in terms of volts/g of acceleration or volts/radian of tilt. For small tilts, these units are equivalent, as the effects on the instrument of tilt and kinematic horizontal acceleration are physically indistinguishable. As for the vertical instrument, the component of gravitational acceleration along its degree of freedom depends on the cosine of the tilt angle, so that it responds in second order to small tilts. The DC responses of the two instruments to tilt

are used in calibration.[7] Above their resonance frequencies, both instruments respond in first order to tilt because the passive elements (mass or pendulum) cannot respond with sufficient speed, so they remain virtually stationary while the outer sensor plates oscillate about them.

7. Filtering and Recording of Data

For geophysical purposes, the quartz fiber accelerometers have broadband response. In the open loop system, the region of high gain extends from DC to the resonance frequency.

The open loop bandwidth is thus about 1 Hz. Such bandwidth is sufficient for simultaneous investigations of earth tides, free oscillations of the earth, and long period teleseisms. Very often, however, it is not convenient to use the same data record to study all three phenomena. Tidal data appears cleaner, and is more easily analyzed, when earthquakes are removed from it. Study of teleseismic records is only hampered by apparent drift due to earth tides. Certain studies require higher gain than that available at the accelerometer output. For these reasons, the raw output of the accelerometer is modified by three active analog filters, which respond preferentially to tides, free oscillations, and teleseisms. Because they modify the accelerometer output before it is recorded, these devices are called prefilters.

Each of the three prefilters is an electronic circuit which uses one or more fedback operational amplifiers to set its response. Each has a full scale output of ±10V. The tidal prefilter simply attenuates high frequency signals, while the normal mode and seismic prefilters both have gainful response at certain frequencies.

The tidal prefilter is a double-pole lowpass filter. Its cut-off frequency can be made 5.75 cph (slow) or 57.5 cph (fast) by means of a switch. For tidal investigations, the lower cutoff frequency is used. Since the highest tidal frequency of usual interest is that of the triurnal tide, or 0.125 cph, the slow cutoff frequency gives the tidal prefilter nearly unity gain and zero phase shift over the entire tidal band.

In calibration and testing of the instrument, the response near DC is of major interest. The tidal prefilter is used during calibration to observe DC levels while averaging out fluctuations due to microseismic ground noise.[10] To avoid long waiting periods, the time constant is set to fast for such work.

For studying the normal modes of free oscillation of the earth, a gainful bandpass filter is used. Its passband is variable, having a lower knee frequency of 1 cph and an upper knee frequency of 30,60, 120 or 180 cph. The gain in the passband is 40db above the DC level. On the high side of the passband, the response falls 40db/dec. On the low side, it falls 40db/dec to 0.1 cph and is constant thereafter. An input attenuator sets the DC level. When the attenuation is zero, the gain at DC is unity.

The normal mode prefilter is usually run with no input attenuation and the upper knee frequency set at 30 cph. This configuration provides sufficient gain and bandpass for studies of the lower frequency normal modes. Increasing the upper knee frequency includes more of the normal mode band in the gainful region. At the highest setting, long period seismic signals are included in the bandpass. This setting allows all seismic signals with periods greater than 20 sec to be observed with nearly the same gain. Unfortunately, large Rayleigh waves and ground noise tend to saturate the prefilter electronics when its bandwidth is this large. This is the reason the input attenuator is provided. It allows a compromise between gain and bandwidth to be made. The nature of this compromise depends on the size of events to be observed and the level of ground noise at the instrument site.

The reason for the relative attenuation below 0.1 cph is the large amplitude of the tidal signals. Peak-to-peak tidal accelerations can be as high as 3×10^{-7}g, while normal modes and seismic waves typically produce accelerations of order 10^{-9}g. Tidal signals at the lock-in amplifier output are thus near IV peak-to-peak. If amplified significantly, these signals saturate the prefilter. Phase shifts due to the changing gain of the prefilter near tidal frequencies displace and distort the tidal signals. This precludes use of the normal mode prefilter output for tidal studies or tidal calibration.

The seismic prefilter is a peaked bandpass filter. Its peak is fixed at 100 second periods, while its half power points are at 60 and 200 second periods. At high frequencies, its response falls as ω^{-7}, or 140db/dec, while at low frequencies its response dies as ω^{2}, or 40db/dec. The peak gain is set by the input attenuator, which has six positions, and can be varied from 60 to 5830. Normally, the attenuator is set for a peak gain of 621.

The high peak gain and the rather narrow bandwidth of the seismic prefilter are quite useful in observing long period teleseisms. They permit measurement of seismic signals as low as 10^{-10}g in amplitude. The sharp rolloff of the response at high frequencies reduces interference due to microseismic signals,[10] while the rolloff at low frequencies eliminates the tides. The seismic prefilter is used primarily for detection of distant teleseismic events.

The accelerometers have flat responses to acceleration over the bandpasses of the prefilters. Thus, the shape of the composite response at the output of each prefilter is determined by the response of the prefilter itself. The gain level is determined by the DC gain of the accelerometer. The exact form of the response to acceleration at each prefilter output is calculated by multiplying the prefilter response function by the appropriate accelerometer response. The resultant total response functions are plotted along with the accelerometer response for the open loop system in Figure 7.

FIGURE 7

Composite responses to acceleration of open loop instrument and three prefilters, with response at position sensor output shown for comparison. All response magnitudes are plotted relative to open loop DC gain of accelerometer.

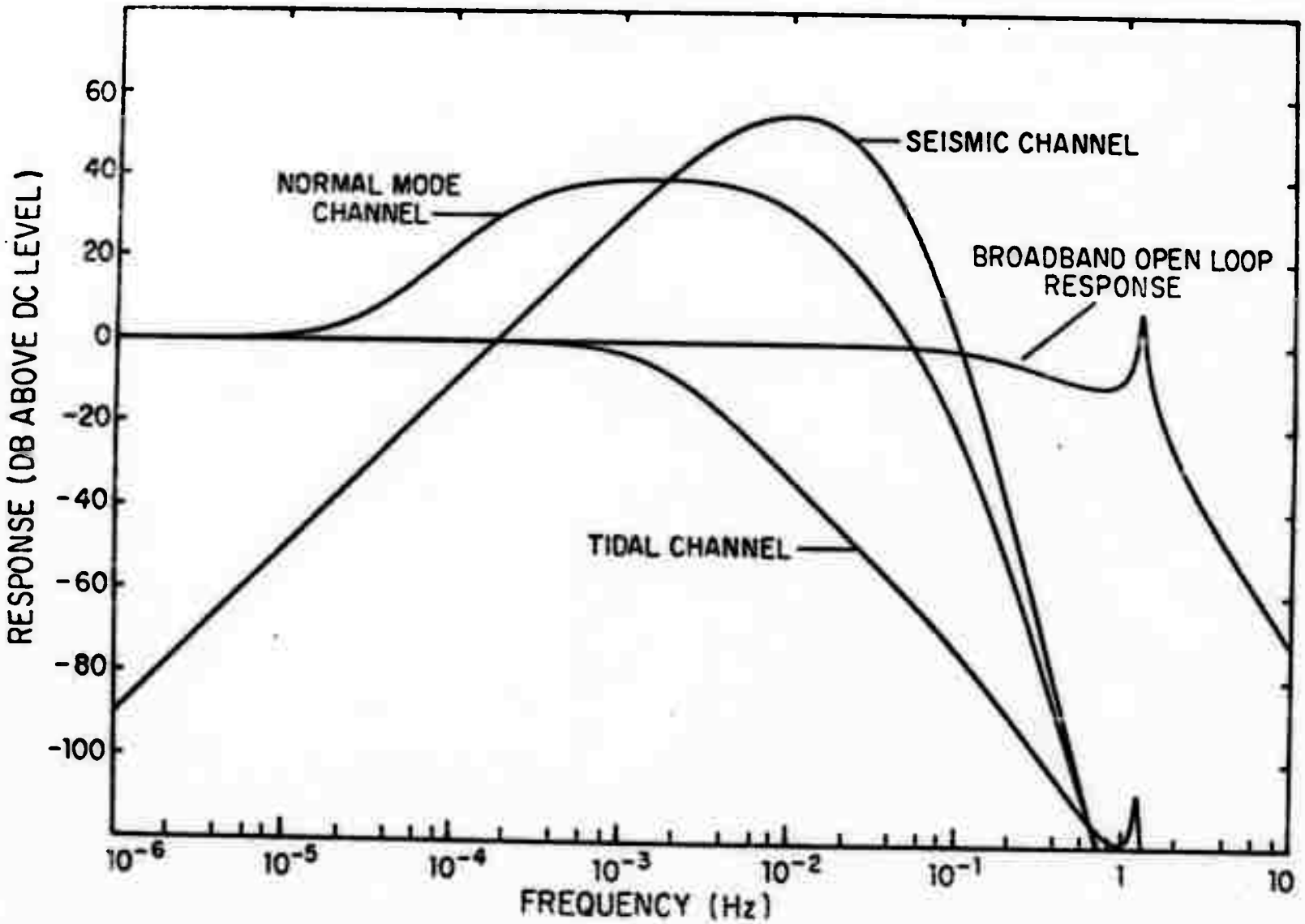
RESPONSE (DB ABOVE DC LEVEL)
60
40
20
0
-20
-40
-60
-80
-100
NORMAL MODE CHANNEL
SEISMIC CHANNEL
BROADBAND OPEN LOOP RESPONSE
TIDAL CHANNEL
10^{-6}
10^{-5}
10^{-4}
10^{-3}
10^{-2}
10^{-1}
1
10
FREQUENCY (Hz)

The output of each prefilter is recorded digitally on magnetic tape with a resolution of ±16384 digitizer counts per ±10 volts. In the cases of the normal mode and seismic prefilters, the outputs with ±10V full scale,

are used for digitizing. Although various sampling intervals are available, the typical interval is 1 second, so that the digitizer Nyquist frequency is 1/2 Hz. Part of the function of the prefilters is to provide plenty of attenuation above the Nyquist frequency to eliminate aliasing of energy in the digitizing process. As Figure 7 shows, the response of each prefilter at the Nyquist frequency is down at least 80db from its peak response. Such attenuation is sufficient to eliminate aliasing for all practical purposes.

It is impossible to overemphasize the importance of digital recording of data. Once a digital tape recording is made, all the computational power of high speed electronic computers is readily available. This puts the mathematical tools of modern data analysis within easy reach. In particular, digital filtering and fast-Fourier transformation allow quick and quantitative determination of the spectral content of various signals. Cross-correlation aids in establishing a relationship of cause and effect. And high-resolution computer plots provide a simple and accurate means of displaying results.

Unfortunately, many geophysicists have realized too late that the difference between digital and analog records is not merely quantitative. The dynamic range of digital records is as high as the digitizer resolution, usually $\sim 10^4$. Due to the width of the pen and the servo dead band, the dynamic range of a chart recorder is seldom much larger than 200. This lower resolution allows much of the information in small signals to be buried in the pen width. Once lost in a chart record, such information can never be recovered. In addition, the effort and expense involved in digitizing even large signals from analog records is often prohibitive.

Chart records are valuable as diagnostic tools and catalogues of events, but digital records are indispensable for quantitative work. Without direct digital records, the analysis presented here and elsewhere[5,7] could not have been attempted.

8. Noise

There are three sources of noise in quartz-fiber accelerometer systems: Brownian motion of the mass or pendulum, fluctuations of the fiber temperature, and spurious signals in the sensor and pre-filter electronics. Reduction in noise from the latter two sources is largely a function of the effort expended in perfecting the temperature controller and electronic systems. For all accelerometers the Browian noise level represents an intrinsic limit to signal detection. It depends on the construction and operating temperature of the mechanical accelerometer, but is otherwise invariable.

In the quartz-fiber accelerometers, Brownian noise is produced by collisions of gas molecules with the mass or pendulum, random motions of electrons in the damping plates through the fringe fields of the damping magnets, and fluctuations in the crystal structure of the mass or pendulum assembly. Because these random phenomena are uncorrelated in time, their effects can be expressed as an equivalent input acceleration with a flat spectrum. The constant power spectral density $P_a(\omega)$ of the Brownian acceleration noise depends on the mechanical parameters of the accelerometer and the absolute temperature of the immediate environment. The formula is[7]

$$P_a(\omega) = \frac{L^2}{C_m^{\,2}} \frac{\omega_0}{QI} 4K_BT \qquad (8.1)$$

where L, C_m, ω_0, Q, and I are as in equations 6.3 and 6.4,

$K_B = 1.38 \times 10^{-23}$ joule/°K is Boltzmann's constant, and T is the absolute temperature.

Except for the geometrical factor L^2/C_m^2, formula 8.1 applies to all similar accelerometers. The Brownian noise power varies inversely as the free period $T_0 = 2\pi/\omega_0$, the moment of inertia I, and the quality factor, Q. As shown by equation 6.6, the DC gain of the accelerometer depends on the square of the free period. Thus, a large free period provides both high gain and low noise. For this reason,

geophysical accelerometers have traditionally been designed with masses that can only be described as gargantuan. In the quartz fiber accelerometers, the free period is made sufficiently large by using a weak restoring device, and the moment of inertia is made rather small. Thus unwieldy size and weight are avoided. The Q of the accelerometer, which is still left as a free parameter, is made large enough to reduce Brownian noise to an acceptable level. In practice, the Q is determined by fringe fields of the damping magnets and not by the residual pressure in the hard vacuum can. If operation in areas with low site noise is contempleted, the Q can be raised by increasing the damping magnet spacing and thus reducing all damping. Otherwise, careful work is required to maximize the Q of the fundamental mode while minimizing the Q's of all the unwanted modes. Normally, Q's

of the order of 20 set the Brownian noise level at about $10^{-24} g^2$/cph, which is sufficiently low for most geophysical observations.

Calculations of the Brownian noise levels are readily made from formula 6.1. The necessary instrumental parameters for typical vertical and horizontal accelerometers are given in Table 1. Normally, the temperature is T = 313°K. The power spectral densities of Brownian acceleration at the inputs are listed in Table 2.

TABLE 2

Vertical (Q3)	Horizontal (H1)
$P_a = 2.1 \times 10^{-24} g^2$/cph	$P_a = 8.5 \times 10^{-25} g^2$/cph
$= 7.4 \times 10^{-21} g^2$/Hz	$= 3.0 \times 10^{-21} g^2$/Hz

From these values, the noise levels at any point in the accelerometer electronics due to Brownian noise at the input may be calculated. Over the bandwidth of flat response, the power spectral density of fluctuations at the position sensor output are determined by multiplying the numbers in Table 2 by the square of the DC accelerometer gain. This gain, which is taken as unity in Figure 7, is determined by static tilt calibration of the instrument.[7] For typical vertical and horizontal accelerometers the power spectral density of fluctuations at the position sensor output are given in Table 3.

TABLE 3

Vertical (Q3)	Horizontal (H1)	
$P_v(\text{sens}) = 8.2\times10^{-11} v^2/\text{cph}$	$P_v(\text{sens}) = 2.3\times10^{-12} v^2/\text{cph}$	(V1.3)
$= 2.9\times10^{-7} v^2/\text{Hz}$	$= 8.0\times10^{-9} v^2/\text{Hz}$	

Of course, these values apply only below the resonance peak in the open loop response, *i.e.*, in the region of flat response.

Since the prefilters have appreciable gain only in the region of flat response, the accelerometer's resonance peak and the filtering in the phase sensitive detector can be ignored for the purpose of calculating fluctuations at the prefilter outputs. Each prefilter is considered subject to white noise at its input. The power spectral density at the output is obtained by multiplying the input density by the square modulus of the prefilter response function. The output spectrum thus assumes the shape of the squared filter response. By integrating the output spectral density over frequency, the mean square value of voltage fluctuations at the prefilter output is obtained. The mean square and RMS fluctuations at the three prefilter outputs are given in Table 4 for both the vertical and horizontal accelerometers.

TABLE 4

Fluctuations at Prefilter Outputs Due to Brownian Noise

	Tidal Prefilter		Normal Mode Prefilter with No Input Attenuation Upper Knee Frequency				Seismic Prefilter with Peak Gain at 621
	FAST T_t=10sec	SLOW T_t=100sec	30 cph	60 cph	120 cph	180 cph	
Vertical Accelerometer							
$\langle V^2 \rangle$ (volts)^2	3.63×10^{-9}	3.63×10^{-10}	1.65×10^{-5}	3.16×10^{-5}	5.34×10^{-5}	6.73×10^{-5}	1.48×10^{-4}
V_{RMS} mv	.06	.019	4.1	5.6	7.3	8.2	38
Horizontal Accelerometer							
$\langle V^2 \rangle$ (volts)^2	1.00×10^{-10}	1.00×10^{-11}	4.56×10^{-7}	8.72×10^{-7}	1.47×10^{-6}	1.86×10^{-6}	4.08×10^{-5}
V_{RMS} mv	.01	.0032	0.68	0.93	1.2	1.4	6.4

In addition to Brownian noise at the input, there are several sources of spurious signals in the accelerometers. The most common of these is Nyquist noise in resistors. Also, time-varying magnetic fields in the environment can produce large and meaningless signals if ground loops are present. These are the standard ills to which all electronic equipment is prey. Special evils occur in electronics designed for use at low frequencies. One of these is 1/f noise, which is common in DC amplifiers. At the extremely low frequencies involved in geophysical observations, temperature coefficients of components, particularly those of diode and transistor junctions, are another source of noise.

In the position sensor circuitry, the vicissitudes of low frequency work are avoided through the use of phase sensitive detection. The preamplifier and leading stages of the lock-in-amplifier operate at 16 KHz , so that only Nyquist noise and ground loops are significant. Theoretically, Nyquist noise in the 100MΩ resistor across the preamplifier input constitutes the essential limitation of the sensor electronics.

According to the Nyquist formula, the power spectral density

of random voltage fluctuations in a resistor is 13.

$$P_v = 4K_BTR \tag{8.2}$$

where $K_B = 1.38\times10^{-23}$ joule/°K is Boltzmann's constant, T is the absolute temperature, and R is the resistance. At the controller temperature of 313°K, the noise power density produced by the 10^8 ohm resistance is about

$$P_v \approx 1.7\times10^{-12}(\text{volts})^2/\text{Hz} \tag{8.3}$$

Although this noise power is rather formidable by itself, it is considerably attenuated at 16 KHz. The reason is that this resistor and the sensor capacitor act as an RC lowpass filter for the Nyquist noise. The effective capacitance to ground of this filter is that of the two halves of the sensor in parallel. The effective lowpass cutoff frequency ω_n is calculated to be $\omega_n \approx 1.4\times10^2$ Hz.[7]

All the experimental information in the sensor signal is contained in a small bandwidth about the reference frequency of 16 KHz. Synchronous detection shifts this bandwidth nearly to DC and Nyquist noise outside this bandwidth is eliminated by the filtering in the lock-in-amplifier. Thus, the only Nyquist noise important at the output is that near 16 KHz. At this frequency, the lowpass filter has an attenuation of

$\frac{1.4\times10^{2}}{10^{5}} = 1.4\times10^{-3}$ in amplitude. The noise power at the preamplifier input at 16KHz is reduced by the square of this factor. With the 4 db noise figure of the preamplifier in the present circuit taken into account, the effective Nyquist noise at the preamplifier input is

$$P_v(\text{in}) \simeq 8.7\times10^{-18}\ (\text{volt})^2/\text{Hz} \tag{8.4}$$

throughout the experimental bandwidth. At the output of the phase sensitive detector, the corresponding noise power density in the region of flat response is

$$P_{v\,(\text{sens})} = C_L^2\, P_v(\text{in}) = 8.7\times10^{-10}(\text{volt})^2/\text{Hz} \tag{8.5}$$

Here C_L, the DC gain of the preamplifier and phase sensitive detector, is taken as 10^4, a typical value. Comparison of the above value with values in Table 3 shows that the noise level at the position sensor output due to Nyquist noise is at least an order of magnitude below that due to Brownian motion. Thus, Nyquist noise presents no problems in practice.

There are, however, other types of electronic noise in the sensor circuitry. Noise originating in the mixer, or detector, of the phase sensitive detector can be appreciable. The level of this noise was reduced by lock-in amplifier modifications suggested

by the manufacturer.[7] In the prefilters, which operate at frequencies near DC, 1/f noise and fluctuations in temperature and supply voltage present problems.

Measurement of electronic noise in all the instrument systems is accomplished quite simply. The drive signal to the outer plates of the sensor capacitor is removed and all the electronic circuits, including the temperature control system, are left in normal operating configuration. Then the various prefilter outputs are recorded as usual. In this manner, noise from all electronic sources is observed, while Brownian noise and ground noise are eliminated. Root-mean-square values of the voltage fluctuations at the prefilter outputs with drive removed have been computed from the digitized data. They are as follows:

Normal mode prefilter (30 cph)	Seismic prefilter with peak gain at 621	
V_{out}(RMS) ≅ 5 mv	V_{out}(RMS) ≅ 18 mv	(8.6)

These values, of course, are the same for both the vertical and horizontal accelerometers, as the electronic systems are the same.

The criterion for optimization of the electronic systems is that output fluctuations due to electronic noise from all sources be smaller than those due to Brownian motion in the accelerometer. If this is achieved, then further reduction in the electronic noise is superfluous. Comparison of results 8.6 with Brownian noise estimates in Table 4 shows that this condition is nearly achieved in the vertical instrument. Fluctuations of the seismic prefilter output due to Brownian motion are more than twice as large as those due to electronic noise. At the normal mode prefilter output,

fluctuations from the two sources are nearly equal. In the horizontal instrument, which has a lower Brownian noise level, the optimum condition is not attained. The amplitude of electronics noise is a factor of 3 too large at the seismic prefilter output, and nearly an order of magnitude too large at the modal prefilter output. Horizontal ground noise, however, is so large that the electronics noise level has never been observed with drive applied.

9. Torsional Mode Data

In the past, the torsional free oscillations of the earth generated by large earthquakes have been measured with both horizontal accelerometers and strain meters.[1,3] Compared to the spheroidal modes, the torsional modes of the earth involve larger fractional shear energies. Because shear motion is more dissipative than compression,[2] the torsional modes have lower Q . Spheroidal fundamentals typically have Q's near 300, while the toroidal fundamentals have Q's of about 150. In addition, due to local tilting of the ground, horizontal ground noise at the surface in the normal mode band is relatively high.

Because of the higher horizontal noise level at surface sites and the generally lower Q values, torsional oscillations are observed at surface sites to decay into the noise more rapidly than spheroidal ones. Thus, observation of torsional modes requires large initial excitation if adequate spectral resolution for separation and identification of modal lines is to be obtained.

Since its maiden run in early April, 1971, the horizontal accelerometer has been operating nearly continuously in the open loop configuration. For most of this time, it was deployed at a surface site (vault depth 10 ft.) at the Elliott Field Station (32.88°N, 117.1°W) about 13 miles northeast of San Diego, California. While the instrument was at this station, no particularly large events occurred. Such is the capriciousness of nature, however, that there were two major events during the few days required to transport the

instrument to Wallace, Idaho, for tests in the Star Mine to determine the depth dependence of earth noise. Thus, no observations of strong excitation of torsional modes were obtained.

To illustrate the quality of data available from the horizontal accelerometer, records of the normal mode prefilter output for two events of intermediate magnitude are shown in Figures 8 and 9. Relevant parameters for these events are shown in Table 5.

TABLE 5

Parameter	Adak Earthquake (Figure 8)	Chilean Earthquake (Figure 9)
Origin Time	06:08:27.3 GMT	21:00:40.9 GMT
Origin Date	May 2, 1971	June 17, 1971
Epicenter	51.4°N, 177.2°W	25.5°S, 69.2°W
Location	Adak Island Region	Chile
Source-received distance Δ	46.8°	73.8°
Incidence Angle α	93.1°	90.7°
Magnitude	$M_s = 7.1$	$m_b = 6.3$
Depth	43 Km	93 Km

Except for the incidence angle α and source-receiver distance Δ, which were calculated from the epicentral locations, the information is as reported in the National Oceanographic and Atmospheric Administration's Preliminary Determinations of Epicenters. The incidence angle α is the smallest angle between the great circle path from the

FIGURE 8

Normal mode prefilter data from open loop horizontal accelerometer at Elliott Station for Adak earthquake of May 2, 1971. Vertical scale applies only to signals in 1-30 cph passband of prefilter. Start time of record is 06:12:30 GMT May 2, 1971. Note body wave arrivals at beginning of record and high noise level throughout. Low frequency noise is probably due to local ground tilt

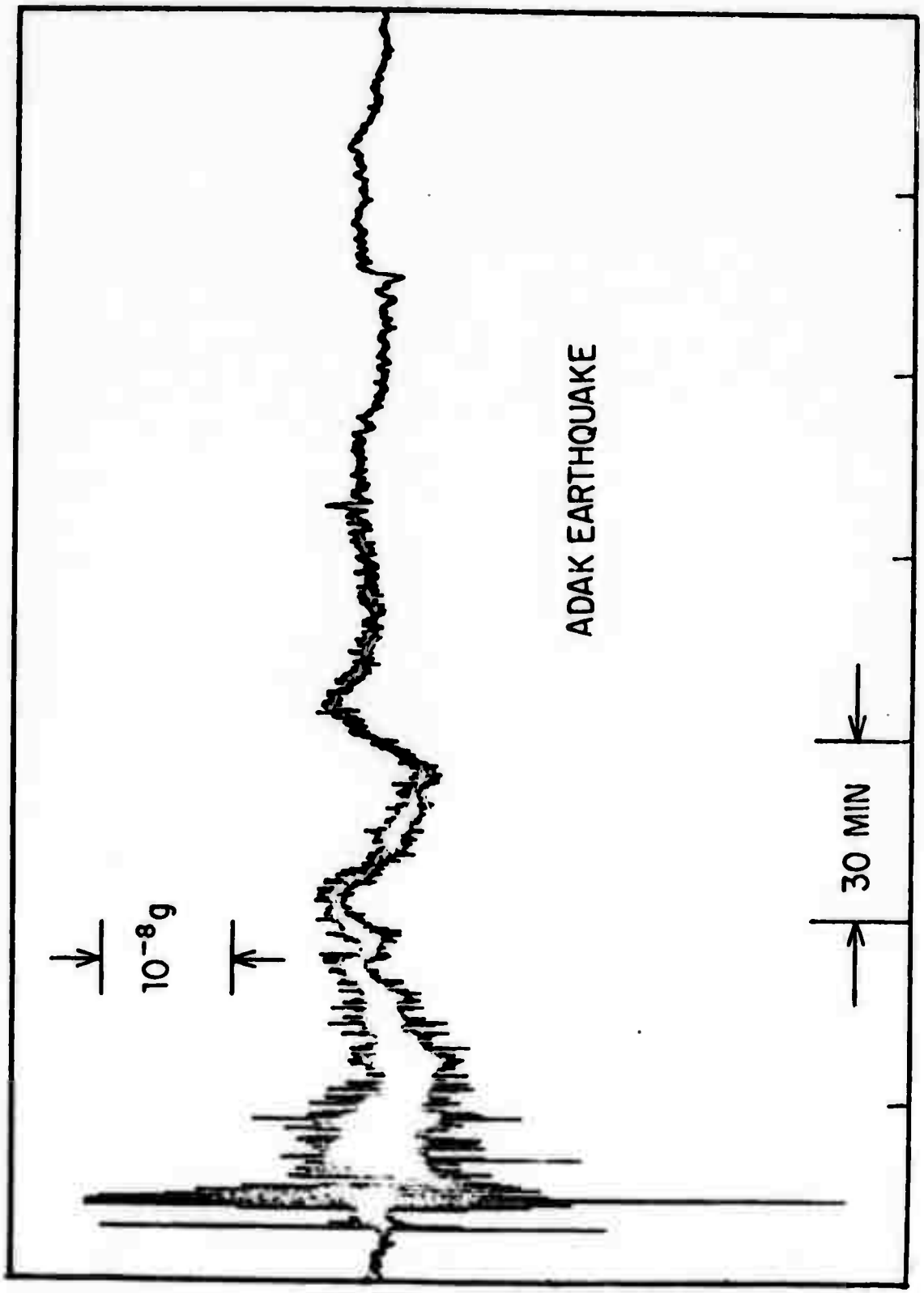
10^{-8}g
30 MIN
ADAK EARTHQUAKE

FIGURE 9

Normal mode prefilter data from open loop horizontal accelerometer at Elliott Station for Chilean earthquake of June 17, 1971. Vertical scale applies only to signals in 1-30 cph passband of prefilter. Start time of record is 21:14:50 GMT June 17, 1971. Note large body wave arrivals at beginning of record and passage of Love wave packets G1 and G2 .

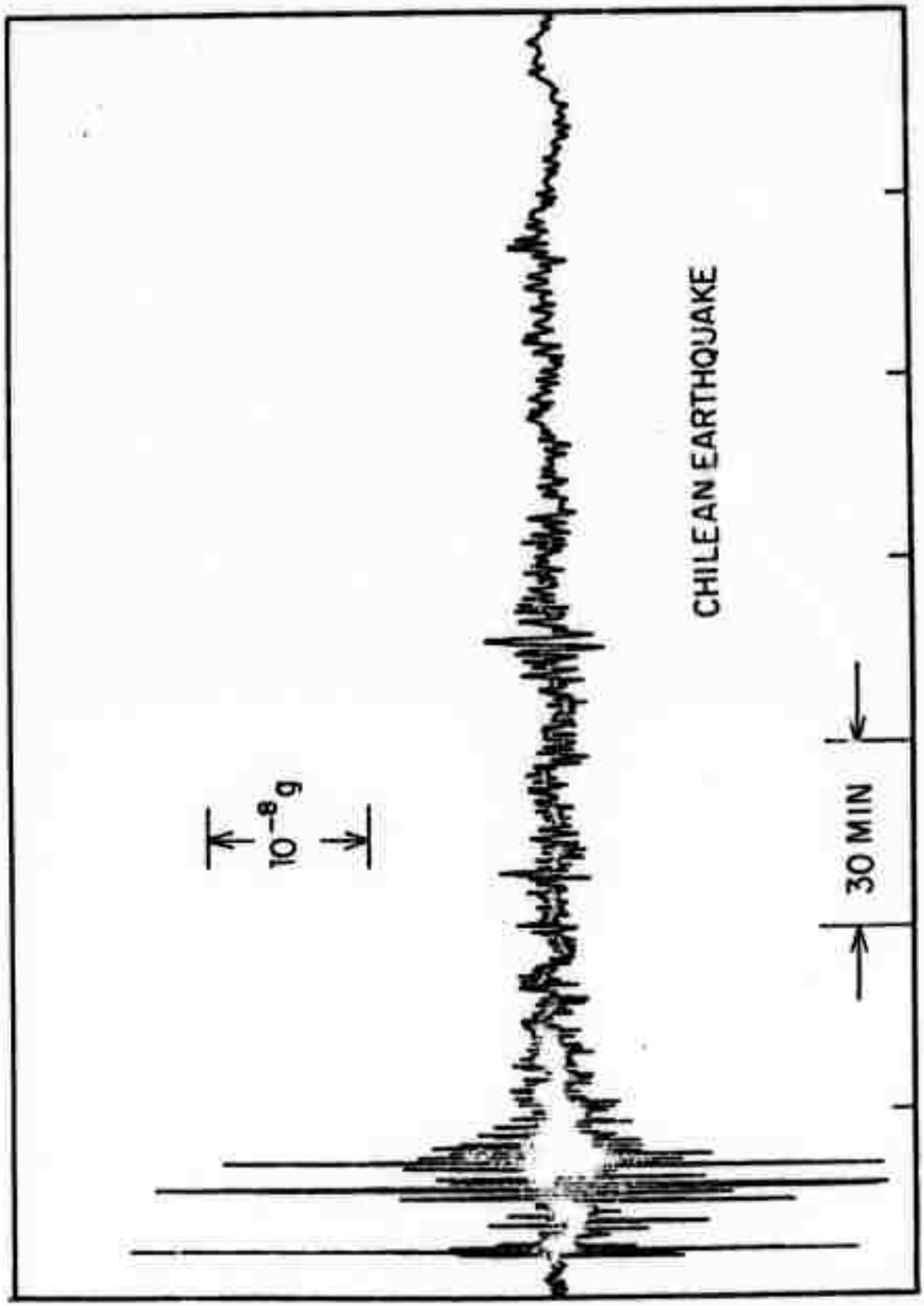
10^{-8} g
30 MIN
CHILEAN EARTHQUAKE

epicenter to Elliott Station and the direction of maximum sensitivity of the horizontal instrument. For these events, the horizontal accelerometer was oriented N45°E.

The figures for both of the events show excitation of surface waves which last for several hours. In neither record, however, is significant energy observed to travel completely around the earth. Since the incidence angle α is close to 90° for both events, the horizontal motion observed is due to transversely polarized Love waves, rather than longitudinally polarized Rayleigh waves. Thus the observed disturbances are interpreted in terms of torsional free oscillations of the earth, rather than spheroidal oscillations, which are also seen on horizontal instruments.[15]

Figure 10 shows a Fourier power spectrum of 10 hours of the modal prefilter record for the Chilean earthquake. The running mean of the ambient spectrum is plotted for comparison. Below 15 cph, the signal-to-noise ratio is close to unity. Above this frequency, definite structure appears in the earthquake spectrum with up to a 20 db signal-to-noise ratio. Certain lines in the spectrum are identified as fundamental torsional modes of free oscillation on the basis of theoretical eigenfrequency calculations.[8] Although collective motion of the earth as a whole is not really excited by this small earthquake, interpretation of the disturbances in terms of a superposition of modes is still possible. The relatively high frequency at which the spectrum emerges from the noise is evidence of the rapid decay of the motion.

FIGURE 10

Spectra of Chilean earthquake and of ambience from normal mode prefilter output for horizontal accelerometer at Elliott Station. Earthquake spectrum is taken from 10 hour record of prefilter output, of which section shown in Figure 9 is initial part. Ambient spectrum is derived from record of prefilter output of equal length beginning 06:24:59 GMT April 30, 1971, in which there was no visible earthquake. Trace shown is running mean of ambient spectrum over 1 cph interval. Boxcar time windows are used for both spectra. Certain toroidal modes of earth are tentatively identified from theoretical calculations of eigenfrequencies. Bumpiness of running mean of ambient spectrum is due to high horizontal noise level.

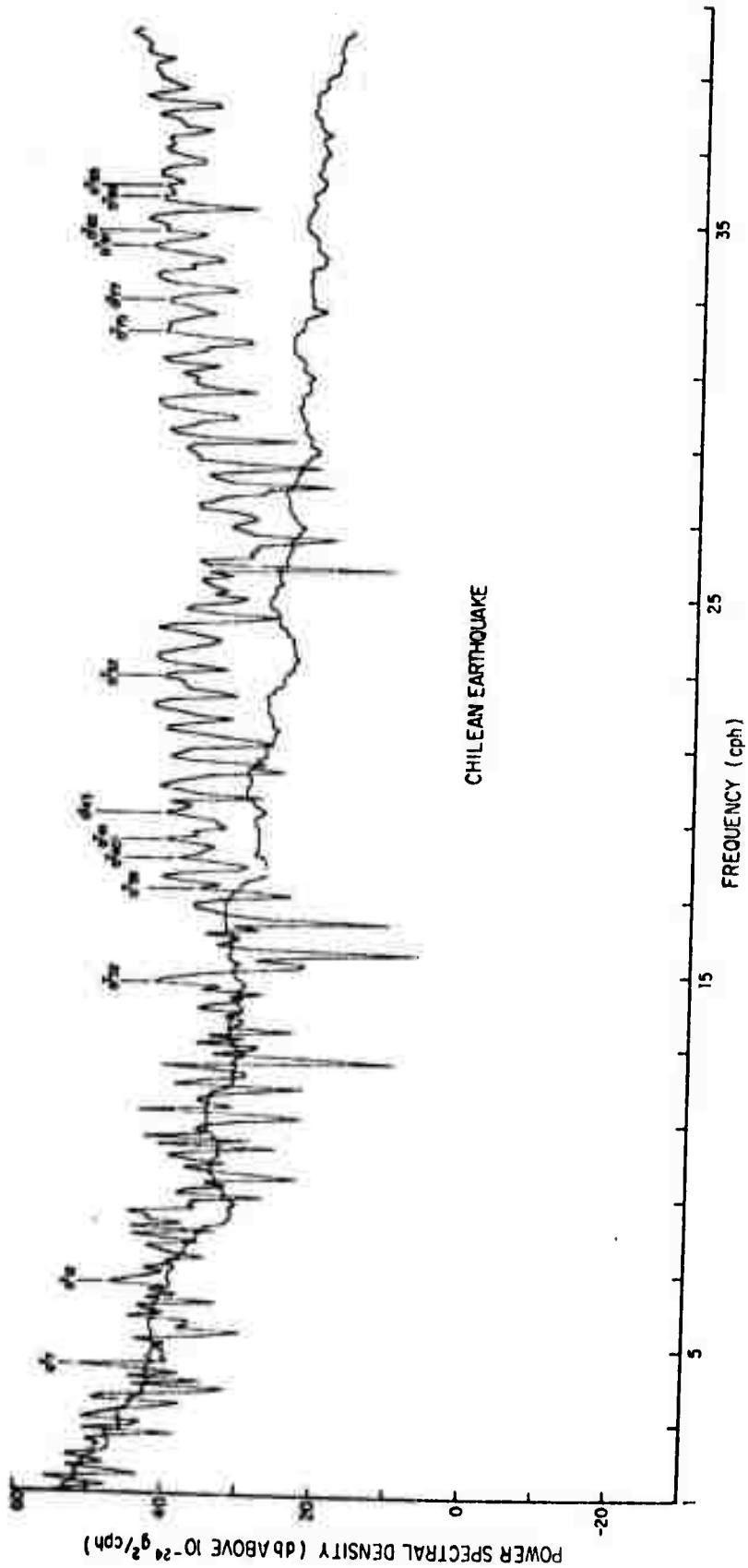
CHILEAN EARTHQUAKE
FREQUENCY (cph)
5
15
25
35
POWER SPECTRAL DENSITY (db ABOVE 10-24 g2/cph)
-20
0
20
40
60

10. Teleseismic Detection with both Horizontal and Vertical Accelerometers

As pointed out in section 9, horizontal accelerometers at surface sites are subject to a rather high noise level due to short-range tilting of the ground. Since the amplitude of horizontal displacement in Rayleigh waves is only about 2 to 3 times that of vertical displacement, the signal-to-noise ratio for Rayleigh waves is higher for vertical accelerometers. Thus, for Rayleigh wave detection the vertical accelerometer is the preferred instrument. Nevertheless, the horizontal instrument is quite useful for seismic monitoring. Due to their horizontal polarization, Love waves, which provide a valuable secondary source discriminant, are not observed with vertical instruments. In addition, due to the definite horizontal polarization in both Rayleigh and Love waves, the horizontal accelerometer is sensitive to the direction of wave arrival. Thus, two horizontal instruments can be used to estimate the direction of a source.

In early April, 1971, the prototype horizontal quartz fiber accelerometer was deployed at the Elliott Station along with a vertical accelerometer The two instruments were placed side-by-side in the surface vault and both were run in the open-loop configuration. For comparison with a laser strain meter at the same site,[4] the horizontal was oriented N45°E. Outputs from both instruments were recorded digitally on magnetic tape at a sampling interval of 1 second.

Although data from all three prefilters were continuously

recorded for both instruments, only records from the seismic prefilters are of interest here. The acceleration response of the horizontal instrument at the seismic prefilter output is plotted relative to the DC open loop gain in Figure 7. In the seismic band below the resonance frequencies of both instruments, the response of the vertical accelerometer at its seismic prefilter output has the same shape, but the gain level is different.

The DC open loop gain of each instrument for this run has been carefully measured. For the vertical accelerometer, it has been determined by tilt calibration and by a fit of the theoretical earth tides to the tidal prefilter output. The result is

$$G_0(\text{vert}) = (6.25 \pm 0.06) \times 10^6 \text{ volts/g} \qquad (10.1)$$

where g is the local acceleration of gravity. At this gain, peak-to-peak tidal acceleration, or about 3×10^{-7}g, amounts to one tenth of the full scale range of ± 10v at the detector output. For the horizontal, the DC open-loop gain has been determined by tilt calibration and checked against design calculations. It is

$$G_0(\text{hor}) = (1.95 \pm 0.05) \times 10^6 \text{ volts/g} \qquad (10.2)$$

Due to a difference in the attenuators at the two seismic prefilter outputs for this run, 0 db for the horizontal seismic prefilter in Figure 7 is 2.83×10^6 volts per g of acceleration or per radian

of tilt. For all the other outputs of the horizontal, 0 db is 1.95×10^6 volts/g as above. Thus, at its seismic prefilter output, the equivalent acceleration response of the horizontal is a factor of 2.2 less than that for the vertical.

Figure 11 shows the response of the vertical to ground displacement at the seismic prefilter output. It is computed using the standard seismic approximation in which only kinematic acceleration is considered. Since the horizontal instrument measures both kinematic acceleration and tilt, interpretation in terms of ground displacement is not possible for it. The response at its seismic prefilter output is best obtained from Figure 7.

The upper two traces of Figures 12 and 13 are computer plots made from simultaneous recordings of the seismic prefilter output for both instruments. Trace (a) is the horizontal seismic prefilter output, and trace (b) the vertical. The figures show the noise levels at various times of night, as well as seven distant earthquakes. These two examples are representative of a much larger body of data , part of which has been reported elsewhere.[5]

Careful inspection of these records shows that the noise from the horizontal instrument is concentrated at frequencies slightly below those of seismic interest. In fact, most of the horizontal noise can be removed from the records by digital filtering. The lower two traces in Figures 12 and 13 show the result of the application of a highpass convolution filter to the data of the upper two traces. This highpass filter, whose response is shown in Figure 11, has a -3 db break point at a

FIGURE 11

Response to ground displacement at seismic prefilter output of open loop vertical accelerometer (scale at left), and response of digital highpass filter (scale at right). Seismic prefilter output for horizontal instrument is not readily interpreted in terms of ground displacement. Small bump in highpass filter response is first sideband. Highpass filter response is essentially unity at periods shorter than 45 seconds.

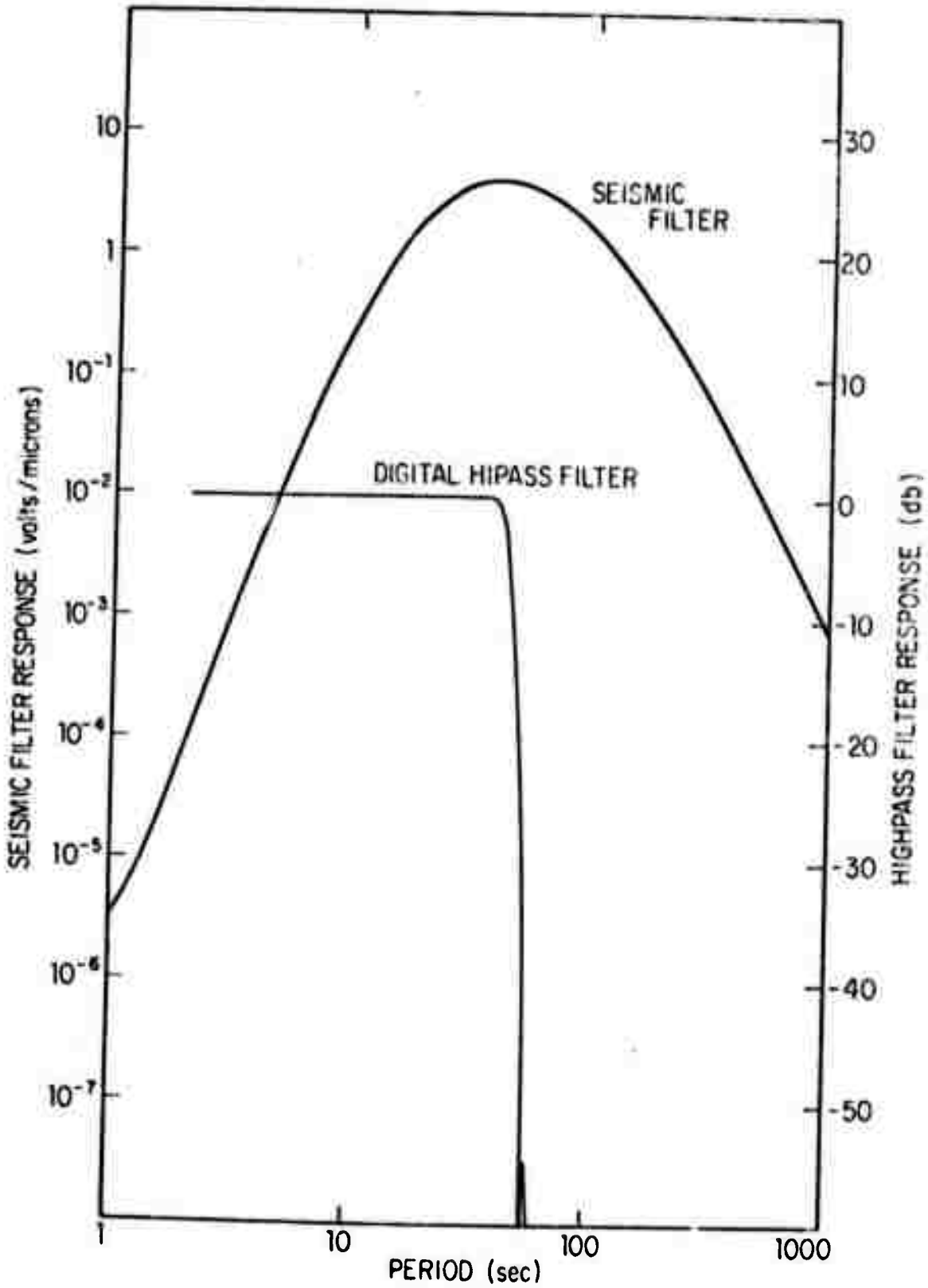
SEISMIC FILTER
DIGITAL HIPASS FILTER
SEISMIC FILTER RESPONSE (volts/microns)
HIGHPASS FILTER RESPONSE (db)
PERIOD (sec)
10
1
10^{-1}
10^{-2}
10^{-3}
10^{-4}
10^{-5}
10^{-6}
10^{-7}
30
20
10
0
-10
-20
-30
-40
-50
1
10
100
1000

FIGURE 12

Computer plots of horizontal and vertical seismic prefilter outputs for Event 4 of Table 6. Traces (a) and (b) are raw outputs of horizontal and vertical seismic prefilters, respectively. Traces (c) and (d) are the results of application of the digital filter of Figure 11 to traces (a) and (b).

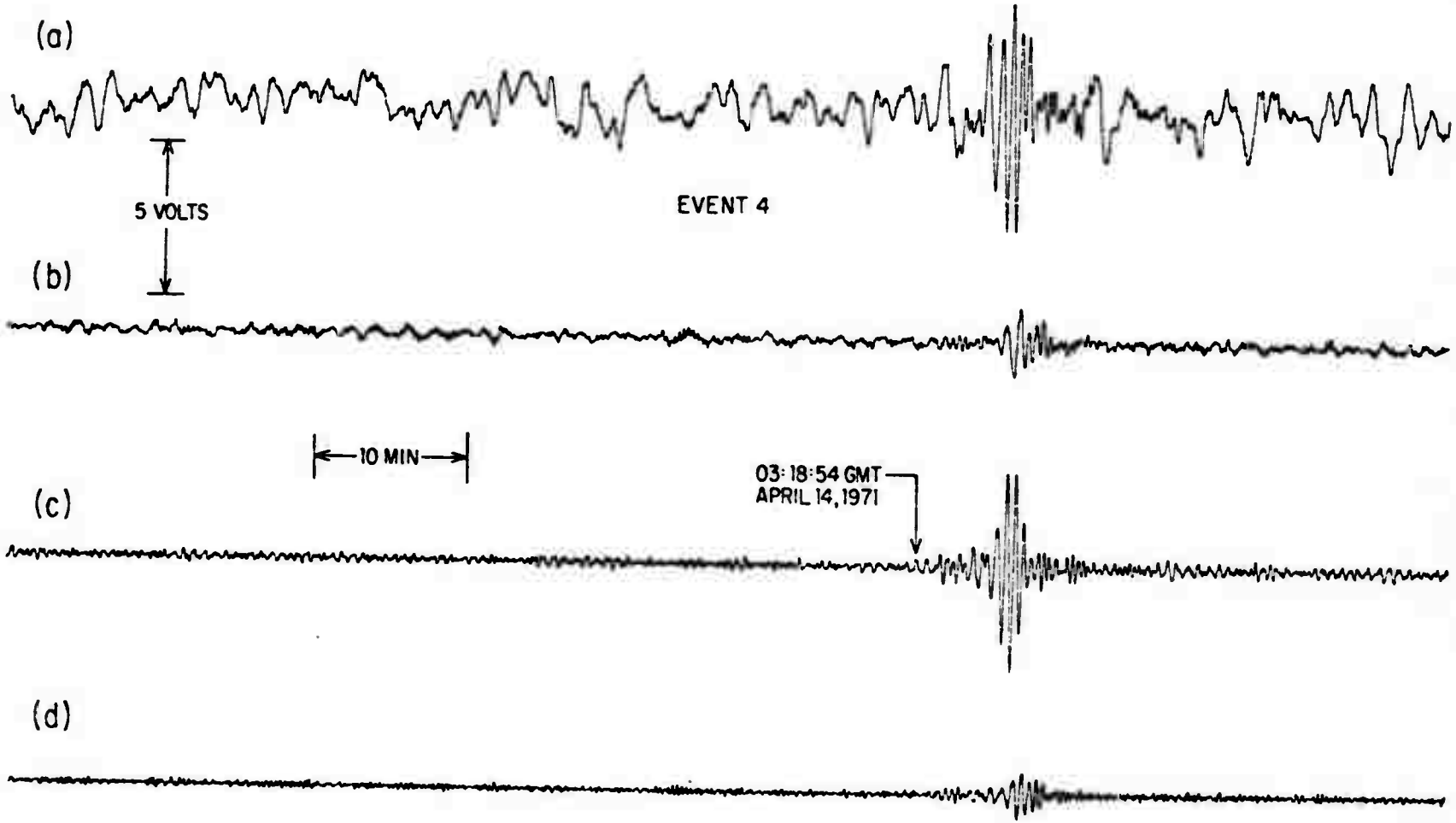
(a)
5 VOLTS
EVENT 4
(b)
10 MIN
03:18:54 GMT
APRIL 14, 1971
(c)
(d)

FIGURE 13

Computer plots of horizontal and vertical seismic prefilter outputs for Event 5 of Table 6. Traces (a) through (d) are as in Figure 12.

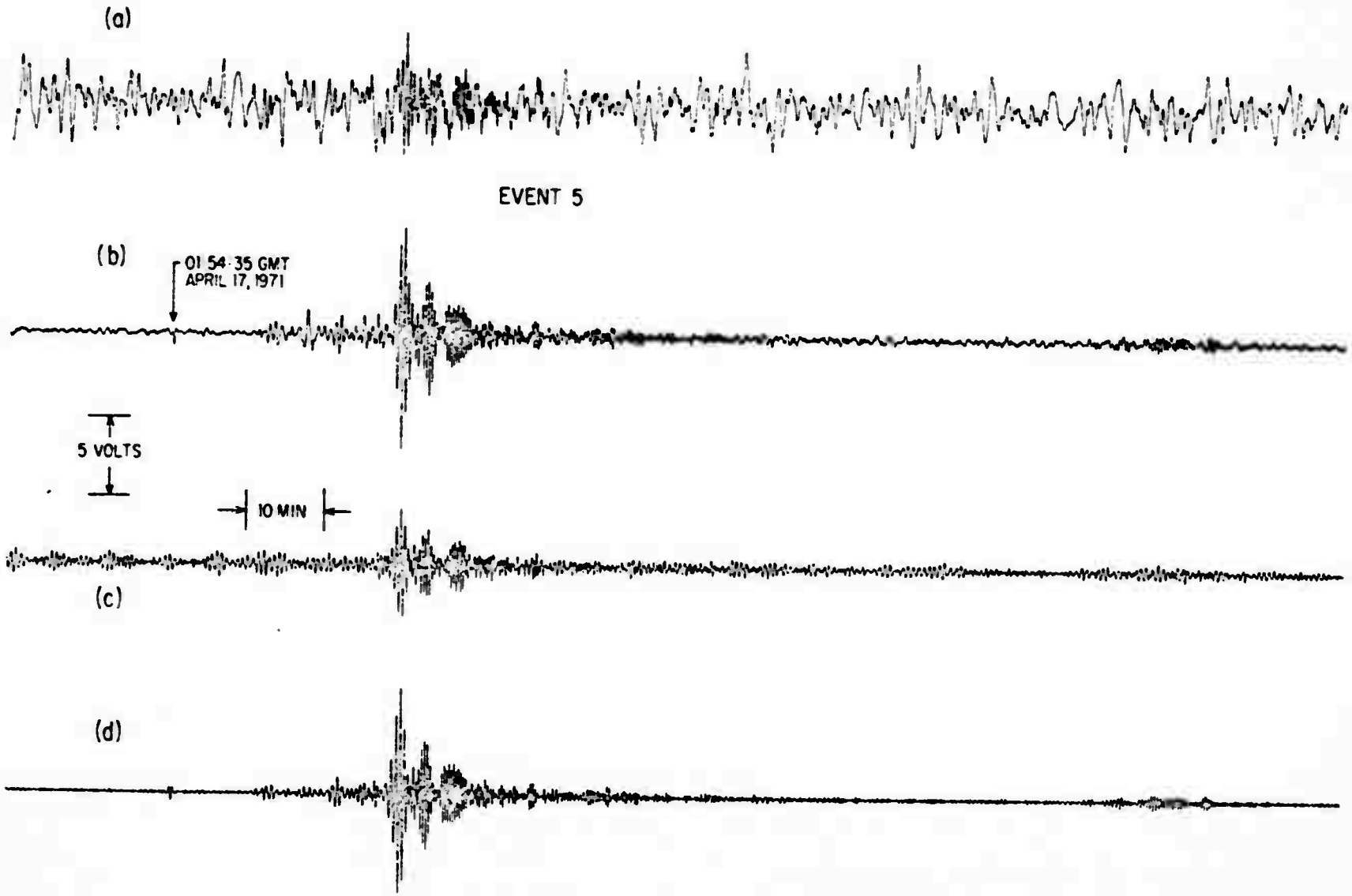
(a)
EVENT 5
(b)
01 54 35 GMT
APRIL 17, 1971
5 VOLTS
10 MIN
(c)
(d)

period of 45 seconds and is down 20 db at 50 seconds. After digital filtering, the peak-to-peak horizontal noise (trace (c)) is reduced by nearly an order of magnitude, yet the seismic signal is unaffected by the filtering. The signal-to-noise ratio for the vertical record is also improved by digital filtering, as shown in trace (d).

The surface site at Elliott Station is subject to considerable acoustic and high frequency ground noise from a nearby air base and a highway. However, noise in the seismic band is relatively low, at least for the vertical. The horizontal noise is much higher and varies with weather and the time of day. If the output of the horizontal is interpreted in terms of acceleration, and if the difference in DC gain between the two instruments is taken into account, the vertical and horizontal noise levels can be compared. At night, the horizontal noise is a factor of 6 to 15 greater in equivalent acceleration than the vertical. During midday, this factor is augmented by as much as another factor of three, especially during windy and variably cloudy days. When the weather is calm and uniformly overcast, as on foggy days, the daytime horizontal noise is as low as it night. This variation in the horizontal noise level is due to the fact that the noise derives from short-range pressure and temperature fluctuations.[9,18]

Noise originating in the instrument electronics has been measured by removing the reference signal as explained in section 8. The seismic prefilter output for either instrument with no reference makes a straight line on the scales of either of Figures 12

and 13. The effects of Brownian motion have been calculated for each instrument for this run in the manner of section 8. At the outputs of the seismic prefilters, the voltage fluctuations due to Brownian noise have an amplitude of 38 mv for the vertical and 3.5 mv for the horizontal.* As Figures 12 and 13 show, this is at least an order of magnitude down from the noise observed. Coherence measurements with a second horizontal will be made to determine total instrumental noise levels. At present, the preliminary noise measurements and calculations above, as well as the variation of the horizontal noise with environmental conditions, lead to the conclusion that the observed noise is predominantly real earth motion.

Table 6 gives the identification and parameters of the events, which occurred on April 14 and April 17, 1971. The angle α in the table is the smallest angle between the great circle path connecting the epicenter to the station and the line of maximum sensitivity of the horizontal. When this angle is near 90°, only transversely polarized Love waves are observed by the horizontal. When it is close to zero, only Rayleigh waves, which are longitudinally polarized, are seen.

*For the horizontal, this number is slightly different from that given in Table 4 because different prefilter attenuation was used for these observations.

TABLE 6

The Events Shown in Figures 12 and 13

Event	Origin Time and Day (GMT)	Epicenter and Location	Depth (km)	Mag. m_b	Mag. M_s	Mag. $M_s(30°)$	Distance Δ(deg)	Angle α (deg)
4	03:09:02 4/14/71	14.1°N, 91.5°W Guatemala[1]	119	4.8	3.3	3.3	30	78
5	01:41:20.1 4/17/71	6.3°S, 154.7°E Solomon Islands[2]	72	5.7	5.3	4.5	92	39

NOTES: Parameters M_s, $M_s(30°)$, and α are described in text.

[1] Source = Large Aperture Seismic Array in Montana.

[2] Source = National Oceanographic and Atmospheric Administration - Preliminary Determination of Epicenter.

The origin times, locations, epicenters, body wave magnitudes and depths of the events are as given in the L.A.S.A. or N.O.A.A. P.D.E. reports. The source-receiver distance Δ and the angle α, are computed from the reported epicenters.

Both the surface wave magnitudes M_s and $M_s(30°)$ are calculated from the vertical records in Figures 12 and 13, using the calibration implicit in Figure 11. The method is described in detail elsewhere.[7,14] The surface wave magnitude $M_s(30°)$ is the magnitude computed by setting the source-receiver distance arbitrarily to 30°. It is useful in estimating the effectiveness of instrumentation for seismic monitoring of underground nuclear explosions. Detection capability of the present instrumentation is examined in detail elsewhere.[5, 7, 14]

Figure 12 shows Event 4, whose seismic waves arrived at an angle of 78° to the horizontal's axis of maximum sensitifity. Strong Love waves are observed, so that the signal-to-noise ratio is appreciably larger in the horizontal records. Figure 13 shows Event 5, whose seismic waves arrived at an angle of 39° to the horizontal's axis of maximum sensitivity. No Love waves were observed for this event, and the signal-to-noise ratio was 6 times larger on the vertical. There is an apparent decrease of the horizontal-to-vertical polarization ratio of the Rayleigh waves with increasing period in this record.

Although the new wide-band horizontal accelerometer is noisy at this surface site, the noise is not in the frequency region of seismic interest. It can be removed by digital filtering. The digitally filtered horizontal records then become a powerful adjunct to the vertical records for purposes of seismic detection. Both the theoretical power of Love-waves as a source discriminant and an augmented signal-to-noise ratio for events producing Love waves are now available.

ACKNOWLEDGEMENTS

This research was supported by the Advanced Research Projects Agency of the Department of Defense and was monitored by the Air Force Office of Scientific Research under Contract No. F44620-71-C-0128.

LIST OF REFERENCES

1. Alsop, L. E., G. H. Sutton, and M. Ewing. Free oscillations of the earth observed on strain and pendulum seismographs, *J. Geophys. Res.*, *66*, 631, 1961.

2. Anderson, D. and C. Archambeau. The anelasticity of the earth, *J. Geophys. Res.*, *69*, 2071-2084, 1964.

3. Benioff, H., F. Press and S. Smith. Excitation of the free oscillations of the earth by earthquakes, *J. Geophys. Res.*, *66*, 605-619, 1961.

4. Berger, J. and R. H. Lovberg. Earth strain measurements with a laser interferometer, *Science*, *170*, 296-303, Octobed 16, 1970.

5. Block, B. and J. Dratler, Jr. Teleseismic detection with wide band vertical and horizontal accelerometers, *Nature Phys. Sci.*, *232*, No. 28, 33-37, July 12, 1971.

6. Block, B. and R. D. Moore. Tidal to seismic frequency investigations with a quartz accelerometer of new geometry, *J. Geophys. Res.*, *75*, No. 8, 1493-1505, March 10, 1970.

7. Dratler, J., Jr. *Quartz Fiber Accelerometers and some Geophysical Applications*, doctoral thesis, IGPP, University of California at San Diego, September, 1971.

8. Gilbert, F. Normal mode eigenfrequency calculations, to appear in *Methods of Computational Physics*.

9. Haubrich, R. A. and G. S. MacKenzie. Earth noise, 5 to 500 millicycles per second, *J. Geophys. Res.*, *70*, 1429-1440, 1965.

10. Haubrich, R. A. and K. McCamy. Microseisms: coastal and pelagic sources, *Reviews of Geophysics*, *7*, No. 3, 539-571, August, 1969.

11. Heyl, P. R. and G. S. Cook. The value of gravity at Washington, *Journal of Research of the National Bureau of Standards, 17,* No. 6, 805-839, December, 1936.

12. Hoffman, W. F. *A Pendulum Gravimeter for Measurement of Periodic Annual Variations in the Gravitational Constant,* Appendix 1, doctoral thesis, Palmer Physical Laboratory, Princeton University, January, 1962.

13. Johnson, J. B. Thermal agitation of electricity in conductors, *Physical Review, 32,* 97-113, July, 1928.

14. Prothero, W., J. Dratler, Jr., J. Brune and B. Block. Surface wave detection with a broad band accelerometer, *Nature, 231,* No. 80, May 24, 1971.

15. Richter, C. F. Elasticity and elastic waves, Chapter 16, *Elementary Seismology,* W. H. Freeman and Company, San Francisco, 1958.

16. Romberg, F. E. An inverted-pendulum seismometer element for horizontal motion, *Annales Geophysique, 18,* No. 4, 394-396, 1962.

17. Simon, I., A. G. Emslie, P. F. Strong and R. K. McConnell, Jr. Sensitive tiltmeter using a diamagnetic suspension, *Review of Scientific Instruments, 39,* No. 11, 1666-1671, November, 1968.

18. Sorrells, G. G. A preliminary investigation into the relationship between long period seismic noise and local fluctuations in the atmospheric pressure field, *Geophys. J. Roy. Astr. Soc.,* in press.

19. Sorrells, G. G. and Z. A. Der. Long period seismic noise and atmospheric pressure variations, Teledyne Geotech Technical Report Number 70-12, Garland, Texas, 1970.